UNIVERSITY OF CALIFORNIA SAN DIEGO

Studies on the role of innate and adaptive immune signaling in pain processing: Tools, Techniques and Translation

A dissertation submitted in partial satisfaction of the requirements for the degree Doctor of Philosophy

in

Biomedical Sciences

by

Matthew Adam Hunt

Committee in charge:

Professor Tony Yaksh, Chair
Professor Camillla Svensson, Co-Chair
Professor Maripat Corr
Professor David Gonzalez
Professor Yury Miller

2020

The Dissertation of Matthew Adam Hunt is approved, and is acceptable in quality and form for publication on microfilm and electronically:

_____

_____

_____

_____
Co-Chair

_____
Chair

University of California San Diego

2020

DEDICATION

I dedicate this work to my family and friends who have helped me along the way, my mentors who have guided me, and to the projects that have failed or challenged me. Especially to my wife, who put her life on hold to fly across the world to come live and work with me and whom is represented in all three of the above categories, and to our new baby boy (who hopefully waits until I'm present to join us!) I can't wait to see what our future holds…

EPIGRAPH

But, Mousie, thou art no thy-lane,
In proving foresight may be vain;
The best-laid schemes o' mice an' men
Gang aft agley,
An' lea'e us nought but grief an' pain,
For promis'd joy!

-Robert Burns

TABLE OF CONTENTS

LIST OF ABBREVIATIONS

ATP	Adenosine triphosphate
CAIA	Collagen antibody induced arthritis
CGRP	Calcitonin gene related peptide
CIA	Collagen induced arthritis
CII	Type II collagen
CIPN	Chemotherapy induced peripheral neuropathy
CNS	Central nervous system
DAMPS	Damage associated molecule patterns
DRG	Dorsal root ganglion
FcγR	Fc gamma receptor
FuDR	Fluorodioxyuracil
GFAP	Glial fibrillary acid protein
HMGB1	High-mobility group protein 1
HPRT	Hypoxanthine Phosphoribosyltransferase 1
IA	Intra articular
IHC	Immunohistochemistry
IKK	IκB kinase
IPLT	Intraplantar
IRAK	IL-1 receptor-associated kinase
IκBα	NF-κB inhibitory protein
KO	Knockout
LPS	Lipopolysaccharide
LTA	Lipoteichoic acid
MapKKK	mitogen-activated protein kinase kinase kinase
MHC-II	Major histone compatibility complex
myd88	myeloid differentiation primary-response protein 88
NF-κB	Nuclear factor kappa B
NGF	Nerve growth gactor
NMDA	N-methyl-d-aspartic acid
OCT	Optimum cutting temperature
OEC	Open ended catheter
PAMPS	Pathogen associated molecular patterns
PBS	Phosphate buffered Saline
PFA	Paraformaldehyde
PMVC	Paired multi valve catheter
PRRs	Pattern recognition receptors
SGC	Satellite glial cell
SLA	Stereolithography
TAK1	transforming growth factor β-activated kinase 1
Tgfβ	Transforming growth factor beta
TIRAP	TIR-domain-containing adaptor protein
TNF	Tumor necrosis factor
TRAF6	tumor necrosis factor receptor-associated factor 6
TRAM	IR-domain-containing adaptor molecule)
TRIF	(TIR-domain-containing adaptor protein inducing beta interferon [IFN-β])
TrkA	Tropomyosin receptor kinase C

LIST OF FIGURES AND TABLES

ACKNOWLEDGMENTS

Chapter 2 is currently in preparation for submission as: Matthew A. Hunt, Alex Bersillini Farinotti, Diana Nascimento, Katalin Sandor, Gilson Dos Santos, Lauriane Delay, Mary Corr, Camilla I. Svensson, Tony L. Yaksh. IRF7 as a mediator between innate and adaptive immune signaling in DRG neurons. The dissertation author was the primary researcher and author of this material.

Chapter 3 is currently in preparation for submission as: Matthew A. Hunt, Harald Lund, Lauriane Delay, Juliana Navia, Sara Hunt, Gilson Dos Santos,Tony L. Yaksh. Three dimensional study of macrophages in the DRG: Tools and techniques. The dissertation author was the primary researcher and author of this material.

Chapter 4 is currently in prepration for submission as: Matthew A. Hunt, Sara A.C. Hunt, Joanne Steinauer, Tony L. Yaksh. Characterization of a Poly Valve Catheter for Intrathecal Delivery. The dissertation author was the primary researcher and author of this material and a patent application has been preliminarily filed for the PMVC.

VITA

Education

2012 Bachelor of Science, University of California San Diego

2014 Master of Science, University of California San Diego

2020 Doctor of Philosophy, University of California San Diego

Fellowships

2019 T32 Rheumatic Disease

Publications

Lu, P. , G. Woodruff, Y. Wang, L. Graham, M. Hunt, D. Wu, E. Boehle, R. Ahmad, G. Poplawski, J. Brock, L. S. Goldstein, and M. H. Tuszynski. 2014. 'Long-distance axonal growth from human induced pluripotent stem cells after spinal cord injury', *Neuron*, 83: 789-96.

HUNT, M. , LU, P. & TUSZYNSKI, M. H. 2017. Myelination of axons emerging from neural progenitor grafts after spinal cord injury. *Experimental Neurology,* 296**,** 69-73.

Hunt, M. A. , D. S. M. Nascimento, A. Bersellini Farinotti, and C. I. Svensson. 2018. 'Autoantibodies Hurt: Transfer of Patient-Derived CASPR2 Antibodies Induces Neuropathic Pain in Mice', *Neuron*, 97: 729-31.

Poplawski, G. H. D. , R. Lie, M. Hunt, H. Kumamaru, R. Kawaguchi, P. Lu, M. K. E. Schäfer, G. Woodruff, J. Robinson, P. Canete, J. N. Dulin, C. G. Geoffroy, L. Menzel, B. Zheng, G. Coppola, and M. H. Tuszynski. 2018. 'Adult rat myelin enhances axonal outgrowth from neural stem cells', *Sci Transl Med*, 10.

Yaksh, T. L. , M. A. Hunt, and G. G. Dos Santos. 2018. 'Development of New Analgesics: An Answer to Opioid Epidemic', *Trends Pharmacol Sci*, 39: 1000-02.

Bersellini Farinotti, Alex, Gustaf Wigerblad, Diana Nascimento, Duygu B. Bas, Carlos Morado Urbina, Kutty Selva Nandakumar, Katalin Sandor, Bingze Xu, Sally Abdelmoaty, Matthew A. Hunt, Kristina Ängeby Möller, Azar Baharpoor, Jon Sinclair, Kent Jardemark, Johanna T. Lanner, Ia Khmaladze, Lars E. Borm, Lu Zhang, Fredrik Wermeling, Mark S. Cragg, Johan Lengqvist, Anne-Julie Chabot-Doré, Luda Diatchenko, Inna Belfer, Mattias Collin, Kim Kultima, Birgitta Heyman, Juan Miguel Jimenez-Andrade, Simone Codeluppi, Rikard Holmdahl, and Camilla I. Svensson. 2019. 'Cartilage-binding antibodies induce pain through immune complex–mediated activation of neurons', *The Journal of Experimental Medicine*, 216: 1904-24.

Ana M. Moreno, Fernando Alemána, Glaucilene F. Catroli, Matthew Hunt, Michael Hu, Amir Dailamy, Andrew Pla, Sarah A. Woller, Nathan Palmer, Udit Parekh, Daniella McDonald, Amanda J. Roberts, Vanessa Goodwill, Ian Dryden, Robert F. Hevner, Lauriane Delay, Gilson

Gonçalves dos Santos, Tony Yaksh, and Prashant Mali. 2020. 'Long-lasting Analgesia via Targeted in situ Repression of NaV1. 7 in mice', *Science Translational Medicine (Accepted)*

Matthew A. Hunt, Alex Bersillini Farinotti, Diana Nascimento, Katalin Sandor, Gilson Dos Santos, Lauriane Delay, Mary Corr, Camilla I. Svensson, Tony L. Yaksh. IRF7 as a mediator between innate and adaptive immune signaling in DRG neurons. (In preparation)

Matthew A. Hunt, Harald Lund, Lauriane Delay, Juliana Navia, Sara Hunt, Gilson Dos Santos,Tony L. Yaksh. Three dimensional study of macrophages in the DRG: Tools and techniques. (In preparation)

Matthew A. Hunt, Sara A.C. Hunt, Joanne Steinauer, Tony L. Yaksh. Characterization of a Poly Valve Catheter for Intrathecal Delivery (In preparation).

Presentations

***M. A. HUNT,** Lu, P. , Tuszynski,M. H. , Society for Neuroscience Poster Presentation: "De-novo myelination of grafted neural progenitor cells in the adult cns". 310. 30/H29 Chicago, IL: 2015

***M. A. HUNT**[1], A. B. FARINOTTI[2], D. S. M. NASCIMENTO[2], K. SANDOR[2], T. L. YAKSH[1], C. I. SVENSSON[2]; Society for Neuroscience Poster Presentation:"Linking toll like Receptor ac tivation to Fcγ receptor mediated pain. " 572. 15/ X4 San Diego, CA: 2018

Invited Oral Presentations:

M. A. HUNT, T. L. Yaksh. "3D imaging and anlysis of the DRG" *Anesthesiology Grand Rounds* Nov 2019

M. A. HUNT, M. Corr, C. I. Svensson, T. L. Yaksh. "Linking the innate and adaptive immune systems through IRF7" *Rheumatology Orthopedics Seminar Series* Sep 2019

M. A. HUNT, M. Corr, C. I. Svensson, T. L. Yaksh. "Linking TLR activation to Fcγ Receptor mediated pain " *Rheumatology Grand Rounds* Oct 2020

ABSTRACT OF THE DISSERTATION

Studies on the role of innate and adaptive immune signaling in pain processing: Tools, Techniques, and Translation

by

Matthew Adam Hunt

Doctor of Philosophy in Biomedical Sciences

University of California San Diego, 2020

Professor Tony Yaksh, Chair
Professor Camilla Svensson, Co-Chair

It is appreciated that in certain conditions, the acute wounding can lead to a chronic pain state. The principal focus of this dissertation is to address the innate and adaptive immune signaling in the primary afferent and dorsal root ganglion. In addition, this work pointed to the importance of dorsal root ganglion (DRG) macrophages, to which I developed novel approaches to assess macrophage function. Finally, these studies aimed towards development of therapeutics with spinal and DRG action, which elucidated the importance of the spinal route of delivery and the current problems presented in his approach. With regard to the initiating aim, the studies contained herein point to the ability of TLR4 to drive the upregulation of Fc gamma

receptors in the DRG. This work identified interferon regulatory factor 7 (IRF7) as an important link between TLR4 activation and the expression *Fcgr1*. The results presented here indicate that IRF7 may represent a potential therapeutic target for preventing/treating painful autoimmune conditions. In the second phase, the importance of DRG macrophages, led to the development of new techniques to study and quantify them in the DRG. I show the power of our techniques with two proof of principle experiments in which we observe macrophage activation in the DRG following intrathecal LPS and following treatment with a chemotherapeutic (cisplatin) that leads to a painful polyneuropathy. Here, I show that we can classify and study novel sub-populations of macrophages in-situ, which coupled to an artificial intelligence learning algorithm permitted systematic 3D analysis of macrophages, revealing a potent activation by innate immune signaling. These techniques enable rapid data acquisition with reduced user input. Finally, in order to address the problems associated with driving intrathecal drug distribution, a problem faced by the implementation of intrathecal therapeutics such as viral vector mediated therapeutics, we developed a novel intrathecal catheter delivery system, the paired multi-valve catheter (PMVC), with which we can increase the regional rostrocaudal distribution of intrathecal injectate through a multiple valve system. I show here that using the PMVC over traditional catheters enables us to use up to 100 fold lower titer of viral vector (AAV9), while achieving better distribution throughout the entire neuraxis. In short, these three linked sets of studies point to novel therapeutic targets (IRF7), the role of innate and adaptive immune signaling in the DRG macrophages and an approach by which such intrathecal therapeutics may be more homogenously delivered along the neuraxis.

CHAPTER 1 INTRODUCTION

1.1 GLOBAL SIGNIFICANCE

Nociception, as noted by Sherrington[1, 2], is the physiological and behavioral response to an insult that either causes tissue damage or has the potential to do so. Pain reflects in addition, the aversive emotional component that is the amalgamation of the nociceptive input and higher order contributions of learning and memory. If the pain inducing stimuli is acute, then the sensation of pain is proportional to the intensity of the stimulus, and once removed, the perception of pain ceases. In this way pain is a protective response, it signals impending or potential damage and modifies our behavior to avoid further injury. However, following tissue damage or inflammation, the pain state can persist long after the insulting stimuli are removed. Pain, when chronically perceived in the absence of harmful stimuli, ceases to serve a protective purpose, and becomes a pathological disease state[3]. The generally accepted definition of chronic pain is that which persists for greater than 3-6 months[4].

Chronic pain afflicts as many as 1 in 5 people worldwide, and in the US, represents the most expensive major clinical diagnosis, with patient care estimated to cost $560-$635 Billion annually [5]. Chronic pain is so pervasive that its effects are not only exerted on patients, who experience a markedly decrease quality of life, but also by their family and caregivers[6]. This is because chronic pain negatively impacts all aspects of life including but not limited to: negatively affecting mood, increasing anxiety and depression, negatively affecting patient's ability to enjoy leisure activities, impacting their capacity for work, and hindering the ability to sleep[7].

Currently, treatment for chronic pain is often limited to severely addictive analgesics such as opioids that induce tolerance (*tachyphylaxis*) with extended periods of use. This property necessitates incremental dose escalation and is accompanied by the development of dependence and an addicted state. Not infrequently these characteristics of opioid action are ultimately responsible for a high incidence of lethal opioid overdose[8, 9]. The US alone is responsible for

86% of all opioid use worldwide, causing the US government to declare that there is currently an "opioid epidemic"[10]. As such, understanding the mechanisms responsible for chronic facilitated pain states and development of novel, safer analgesics, represent a great unmet clinical need.

1.2 MECHANISMS OF PAIN

Under non-pathological conditions, pain is associated with the activation of populations of peripheral sensory nerve fibers, the terminals of which express specialized sensors that are activated by strong mechanical, chemical, or thermal stimuli[11]. These afferents, referred to here as "nociceptors", are pseudounipolar neurons, which have their soma located in the DRG. A single process extends from the soma (the glomerulus) and bifurcates into two branches, one that projects to periphery where it senses the environment, and the other that extends into the spinal cord where the nociceptors then synapse onto second order neurons in outer portion (lamina I and II) of the dorsal horn[12]. The DRG is a surprisingly complex structure which lies outside of the blood brain barrier and which, aside from the soma of the primary afferent and the afferent axon, displays dense concentration of glial like cells (to be discussed below) and an extensive vascularity.

Nociceptors are classified via their size and conduction velocity: slowly conducting un-myelinated C fibers[13], or larger diameter myelinated Aδ fibers[14], as well as their ability to transduce signals in response to types of noxious stimuli: mechanical, thermal, and chemical[15, 16]. Under non-pathological conditions nociceptive neurons are silent. Upon strong noxious stimuli, they initiate action potentials at a frequency directly proportional to the intensity of the stimulus[13]. Under non-pathological conditions, the alerting function of these nociceptors initiating a pain sensation serves a beneficial purpose to initiate escape/ withdrawal. Perception of pain teaches us to avoid harmful behaviors, such as touching a hot stove and may serve to alert us of potentially unknown and detrimental problems, such as inflammation from a bacterial infection. Pain also aids in our ability to heal by increasing our sensitivity to the site of injury, which reduces furthering

potential damage during the healing process. The importance of the ability to sense pain may be best exemplified by the detrimental effects observed in those who lack it. Patients with congenital insensitivity to pain often present with unintended self-mutilation, undiagnosed and untreated bone fractures, and or joint deformities, ultimately resulting in high incidence of early death[17].

As emphasized above, activation of nociceptors alone, leading to sensation, is only one component of the pain state. Pain is associated with an unpleasant, aversive, state with strong negative reinforcing properties. Such associations ultimately occur in diencephalic and telencephalic centers and can be greatly modified by excitatory and inhibitory circuitry arising from centers associated with learning and memory[18].

The above commentary reveals the importance of the afferent pathways through which signaling to higher order systems occur. An important characteristic of these ascending systems is that the input-output function of the afferent-spinal processing systems is subject to modification at several ascending linkages including, at the primary afferent terminals, in the DRG, in the dorsal horn of the spinal cord, at the level of ascending second order neurons and/or at any number of locations in brain. These modification can occur locally (such as in the DRG components including satellite cells, macrophages) and in the dorsal horn though local excitatory and inhibitory neuronal (inter-neuronal) and non-neuronal (astrocyte and microglia) cells as well as by descending (bulbospinal) pathways[19]. As such several mechanisms exist in which pain signaling can go awry and lead to chronic and pathological phenotypes.

1.2.1 Transient persistence of the acute pain state

Though complex, much is known about how the beneficial, acute pain, can transition into a pathological, chronic pain. Since early descriptions in the 1960's by Mendel and Wall, it has been appreciated that sustained activation of C fibers results in a progressive enhancement of discharge of the second order neuron. This is known as wind-up[20], and is the result of temporal summation of the second order neurons induced by high frequency activation of C fiber

(nociceptors) . This enhanced response is accompanied by post-synaptic modifications which further enhances the responsiveness to C fiber input, a phenomenon that persists for minutes to hours[21]. Much like the plasticity involved in learning and memory, this central sensitization occurs when repetitive high frequency stimuli result in sustained glutamate release from the presynaptic terminal, which in turn depolarizes the post-synaptic neuron sufficiently to remove the magnesium block from the NMDA ionophore channel, resulting in a robust influx of calcium[22]. NMDA receptor activation can also coincide with increased AMPA receptor trafficking, further increasing the post-synaptic response to pre-synaptically released neurotransmitters[23]. Sustained primary afferent activation can also lead to increased intracellular signaling cascades, which ultimately activates kinases that phosphorylate neuronal membrane receptors and channels, enhancing their activity[24]. All of the above result in an enhanced sensitivity to aversive stimuli, a state referred to as central sensitization. Such sensitization yields an increased response of the second order neuron to a given nociceptive stimulus, resulting in enhanced output, which mediates a transiently increased pain response (e. g. hyperalgesia). Thus, wind up and its associated facilitatory cascade will often resolve when the acute injury resolves.

1.2.2 Chronicification of the post injury pain state

Chronic pain conditions can often be categorized as either inflammatory or neuropathic pain[25]. Inflammatory pain can be explained by a peripheral injury leading to activation of the afferent-second order circuits outlined above as well as local immune cells, which release factors that facilitate and initiate a cascade of migration and activation of further immune cells. Immune cells release a large number of pain-enhancing lipids, chemokines and cytokines, which include but are not limited to: prostaglandins, Il-1β, TNF, IL-6, Bradykinin and histamine, which can exert their effects both directly and indirectly on the primary afferents[26].

The link between inflammation and pain dates back to the 1st century AD, and many of the mechanisms responsible for inflammation mediated nociception have been mapped out [27]. A

barrage of cytokines, growth factors, lipids, and proteases are released peripherally and centrally (spinally) in response to injury or immune signals [27-29]. In the periphery, these active factors can initiate ongoing traffic in small (nociceptive primary afferents) and sensitize these terminals such that they respond at lower stimulus intensities. In addition, such ongoing afferent traffic can lead to a state of central sensitization. An example of this phenomena is the flinching behavior produced by the intraplantar (IPLT) injection of formalin into the rodent paw. This induces a flinching of the injected paw, exhibiting an early phase reflecting robust afferent activation by formalin acting though a specific terminal channel transient receptor potential ankyrin 1 (TRPA1) and then a second phase that is considered to represent a state of spinal facilitation generated by the robust conditioning afferent input mediating the phase 1 response [30]. Such central facilitation, as reviewed above, typically reflects ongoing depolarization of second order spinal nociceptive neurons, increased intracellular calcium, and the activation of a downstream signaling involving the activation of a variety of kinases, which phosphorylate membrane channels and receptors[31, 32], activate intracellular enzymes such as phospholipases[33], activation of a variety of transcription factors reflective of inflammasome activation[34, 35] and altered protein synthesis[36]. The net effect of these changes is to produce a behaviorally defined pain phenotype referred to as hyperalgesia or an increased sensitivity to non-aversive stimulation (e. g. tactile allodynia: sensitivity to light touch). Of note, many of these pain states resolve with the resolution of the injury, however, as reviewed below, such afferent conditioning can lead to profound and persistent changes in nociceptive processing.

In contrast to the phenomena associated with tissue injury and inflammation, damage to the nerve can lead to so called neuropathic pain states[37]. Neuropathic pain states can arise in disease states such as diabetes mellites, multiple sclerosis, and in rare channelopathies, as well as following spinal cord injury or chemotherapy[38-41]. Such nerve injuries often display a common profile which include an ongoing pain state (dysesthesia) and amplified response to light touch (mechanical allodynia) and cold[42]. Assessment of the mechanisms underlying the pain state

frequently reveal the appearance of ongoing traffic in the peripheral nerve and neuronal soma, mediated by profound changes in the expression of channel and receptor subunits in the primary afferent and the activation of non-neuronal cells in the spinal cord (astrocytes and microglia) and macrophages and satellite cells in the DRG[43]. The study of these neuropathic pain states, has benefited from the development of rodent models generating nerve injury though the use of metabolic alterations[44], chemical toxins[45-47], and even biologic infections[48] and these models show clear parallels to the systemic response observed in the human patient.

1.2.3 Non-neuronal cells

There are nearly 10x more glial cells in the human CNS than neurons, and yet they were long thought of as simply the glue that held the CNS together, agents of the blood brain barrier, or the native first responders to foreign proteins or infection. However, we have come to appreciate they are far more diverse and with yet more important purposes[49, 50]. In the CNS there are two types of glial cells: macroglia, and microglia. Macroglia, including astrocytes and oligodendrocytes, are derived from the same neuroepithelial cells as neurons[51]. Unlike, neurons and macroglia, microglia, come from erythromyeloid precursors, which migrate from the yolk sac to the neural tube via blood circulation during early perinatal development[52, 53].

Astrocytes are the most abundant glial cells in the CNS and provide many supportive roles, including forming the BBB, cleaning up debris following injury and forming protective barriers, recycling of neurotransmitters, maintenance of extracellular ion concentration, as well as modulation of synaptic transmission[54]. Astrocytes are large complex cells, which exist in lattice throughout the CNS[55, 56]. Depending on their location of origin astrocytes have been shown to respond differentially to stimuli[57], which may be due to heterogeneous expression of surface receptors[58]. Activation of astrocytes, known as astrogliosis has been well studied and characterized, but was often overshadowed by microgliosis. However, animal models developed in which astrogliosis and microgliosis could be separated and studied independently have helped

to elucidate the function and mechanisms of astrogliosis and how it relates to pain[59, 60]. Increases in the astrocyte marker glial fibrillary acid protein (GFAP) in the spinal cord have been correlated to nerve injury[61]. Astrocytes are interesting among glia in the spinal cord in that they express receptors for pain related neurotransmitters including Substance P[62], calcitonin gene-regulated peptide (CGRP)[63], glutamate[64] and adenosine triphosphate (ATP)[65]. This likely indicates that substantial peripheral nociceptor activation, and subsequent release of the neurotransmitters mentioned above with synaptic overflow, would result in activation of astrocytes, and indeed this is what is observed. Further, blocking astrogliosis with antagonists for the glutamate ionophore N-methyl-D-aspartate (NMDA) has been shown to reduce hyperalgesia in models of neuropathic pain[66].

Microglia are often described as brain-resident macrophages and as such represent the immune system of the CNS, which has otherwise been thought of as being immune privileged[67]. Microglia are highly dynamic cells that have been shown to modify synapses, and to aid in synaptic pruning during CNS development[68]. Following injury, or pathogenic infiltration into the CNS, microglia become activated, increasing expression of Ionized calcium binding adaptor molecule 1 (Iba1) and major histocompatibility complex II (MHC-II), changing their morphology, and rapidly proliferating[69]. This response is termed microgliosis, and occurs not only in response to direct damage of the CNS parenchyma, but also if there is damage to the peripheral nerve indicating that communication of a far of injury signal with the local spinal environment occurs[70]. Further microgliosis has been shown to be a contributing factor to development of chronic neuropathic pain states, and blocking activation of microglia with drugs like minocycline, can prevent chronic hypersensitivity following peripheral nerve injury[71, 72]. Microgliosis occurs rapidly, within 24 hours post peripheral nerve injury and persists for upwards of 3 months[73-75]. This activation has been shown to occur in models of diabetic neuropathy[76], models of bone cancer[77], following intrathecal injection of viral proteins[78], and in models of chemotherapy induced neuropathy[79]. While microglia and microgliosis have been extensively studied in the

CNS, as will be discussed below, much less attention has traditionally been placed on peripheral macrophages, notably those which are present in the DRG. Only recently have peripheral macrophages, located in the DRG, come to be viewed as important regulators of primary afferent driven hyperalgesia and allodynia[43]. Following nerve injury, changes in DRG macrophage functional types have been shown to occur[80]. Activation of DRG macrophages following injury, or during inflammatory states likely mimics microgliosis in the CNS, and direct communication between DRG neuronal soma and DRG macrophages has recently been described[81]. As will be reviewed in the next section, a robust presence of glial like cells are observed in the DRG and are almost certainly involved in the regulation of afferent excitability.

1.3 THE DORSAL ROOT GANGLION

The DRG was long thought of as a simple structure containing the cell bodies (soma) of the primary afferent that provide the trophic support (e. g. protein synthesis) for the extensively ramified afferent axons. It is now appreciated that the DRG represents an important niche environment that controls, integrates, and modulates the signals carried by the afferent axon, and which DRG neurons themselves serve as *ectopic* generators of spinofugal and spinopetal sensory traffic. I will review this composite system in the following sections.

1.3.1 Components of the DRG

Examination of the DRG reveals the complexity of the constituents: the soma, the glia, the vasculature and sympathetic innervation.

i) Soma: The afferent axon and cell body, where in the cell body of the afferent axon is connected to the main axon by a long and sinuous glomerulus. This glomerulus is capable of carrying a conducted potential to and from the axon and to transport products synthesized in the soma to the afferent axon. This property emphasizes that afferent activity is capable of activating

the soma and that the soma if activated can generate an “ectopic” potential activating a sensory action potential to the spinal cord and to the periphery.

ii) The satellite cell is the homologue of the neuraxial astrocyte and displays robust staining for GFAP. These cells lie in intimate proximity to the neuronal soma, investing it.

iii) Macrophages, bearing functional similarity to the CNS resident microglia (which stain for IBA1) occupy a large fraction of the extracellular DRG volume. These cells frequently lie in very close contact with the DRG vasculature.

iv) Vasculature of the DRG is robustly present in the afferent cell body rich portion of the DRG. Unlike neuraxial vessels, these in the DRG do not possess tight junctions, e. g. reflecting the fact that the DRG lies outside the blood brain barrier.

v) Postganglionic sympathetic afferents, typically labeled by tyrosine hydroxylase, provide sympathetic innervation to the DRG vasculature and contact the afferent soma. This post ganglionic innervation is consistent with the assertion that the DRG lies outside the blood brain barrier and its vasculature and sympathetic innervation is comparable to other peripheral vascular beds.

1.3.2 Embryogenesis and development

Neurons and glia within the DRG and PNS originate from neural crest cells, which developmentally, are located dorsal to the neural tube, and then migrate ventrally [82, 83]. During development neuronal fate is controlled by the transcription factors neurogenin 1 and neurogenin 2[84]. Neurogenesis in the DRG occurs in 3 waves, the first mainly produces large-diameter proprioceptors that express tropomyosin receptor kinase C (TrkC), and mechanoreceptors that express tropomyosin receptor kinase B (TrkB), the second mainly consist of small diameter neurons that express tropomyosin receptor kinase A (TrkA) and may be mechanoreceptors, nociceptors, or thermoreceptors, and a third later phase, that mainly produces TrkA positive

nociceptors as well as some additional neuronal subtypes[85, 86]. Along with neurons, the DRG has two types of glial cells, schwann cells and satellite glial cells, which are both derived from the neural crest cells, the same tissue of origin as DRG neurons[86, 87]. Early on during embryogenesis, the arteries from the dorsal trunk branch off and extend into the developing DRGs, eventually forming a loose blood nerve barrier that is highly permeable to circulating agents[88]. Finally there are DRG macrophages, which are derived from early erythromyeloid progenitors in the yolk sac which then migrate to the developing DRG and become resident macrophages[89, 90].

1.3.3 Non-neuronal cells in the DRG

Schwann cells come in two varieties, myelinating and non-myelinating. Myelinating Schwann cells act similarly to oligodendrocytes in the CNS, except that they myelinate a single axon, which helps to increase conduction velocity by enabling saltatory conduction. In contrast, non-myelinating Schwann cells will form a “Remak bundle”, ensheathing multiple small, otherwise non myelinated, axons (C fibers).

Satellite glial cells are similar in morphology to Schwann cells, but remain within the DRG[91],[92]. Several satellite glial cells (SGC) form a laminar ensheathment around each neuronal soma, with the distance between SGCs and neuronal soma being only 20nm[92]. SGCs can adhere to one another and form gap junctions and express receptors involved in pain processing including, CGRP[93], purinergic receptors[94, 95], Substance P[96], TNFα[97], IL-1β[98] endothelin-B[99] and NMDA Receptors[100]. As DRG soma can locally secrete their neuroactive substances, the expression by the SGCs of the above receptors and their tight investment, it is envisioned that SGC can be influenced by the activation of the neuron via paracrine signaling[101]. Further the SGCs and soma have been shown to express gap junctions further enabling crosstalk between these cells[102].

Macrophages in the DRG, through our findings (currently unpublished), represent as much as 5% of the total volume of the DRG and yet have only recently become of major

interest. Macrophages play many roles in the peripheral nervous system. Following injury to the peripheral axon, macrophages will help clear the debris in a process known as Wallerian degeneration[103, 104]. Macrophages are known to respond to inflammatory signals in the DRG and have been shown to display activation which parallels that of microglia in the CNS and are robust secretors of a variety of cytokines and chemokines[105].

1.4 IMMUNE SYSTEM AND PAIN

As briefly described above, the immune and nervous systems are deeply intertwined. So much so that afferent neurons (nociceptors) are, in essence, sensors of immune response. Again, if we think of pain as a protective mechanism, then in the case of a pathogen, our ability to sense and identify the pathogens location, is equally as important as is our ability to defend against and neutralize it[106]. The sensory afferents innervate every tissue in the body and provide near instantaneous input to the CNS regarding the peripheral milieu to which they project. Thus, in the event of a pathogen, the PNS can recognize a present threat via innate immune signaling pathways. More recently the importance of adaptive immune signaling pathways were also established. The peripheral afferent not only acts to sense pathogens, but also can help direct and mount the immune response. This is because DRG neurons, as described above are characterized by a bifurcating axon, which enables them to both send action potentials orthodromically towards the spinal cord, as well as antidromically, towards the peripheral terminals. During sustained activation of primary afferents, antidromic action potentials (generated from the spinal dorsal horn and DRG as well as from the ramified peripheral dendritic tree of the sensory axon) can lead to neurotransmitter release in the periphery. CGRP and substance P both cause vasodilation by directly acting on smooth muscle and vascular endothelial cells, ultimately leading to plasma extravasation and edema[107-109]. Antidromic activation of sensory neuron terminals, and subsequent release of neurotransmitters as well as additional

signaling molecules, also act on a plethora of innate immune cells, which act to conduct and mobilize an immune response.

1.4.1 Innate immune system

An innate immune system is common to nearly all multicellular life and is composed of physical/anatomical barriers, such as skin and epithelial surfaces as well as immune cells that can recognize and identify foreign agents and mount a response to remove them. In the event of a pathogen, innate immune cells act as the first line of defense and attempt to identify, isolate, and phagocytose the pathogen(s). Pathogens, such as bacteria, often express molecules that have a distinguishable pattern, and as a defense mechanism, immune cells have evolved to express receptors that can recognize many of these pathogen-associated molecular patterns (PAMPs)[110, 111]. Most PAMPs, such as lipopolysaccharide (LPS, forming a component of the cell wall of the gram negative bacteria)), are necessary for survival of the particular pathogen, and thus are largely immutable, and always present whenever the pathogen is. As such recognizing these molecules is a strong protective mechanisms of the host immune system. Host immune cells will constitutively express these pattern recognition receptors (PRRs) that when activated, induce an inflammatory response, whereby immune cells become activated and can destroy and remove the pathogen[112]. More recently it was postulated, and then discovered, that upon tissue damage cells can release factors containing damage associated molecular patterns, which have similar molecular patterns to PAMPs and thus can also activate PRRs, and elicit innate immune removal and isolation of damaged cells and debris[113-116]. PRRs include c-type lectin receptors (CLRs), Toll-Like receptors (TLRS), Rig-I-Like receptors RLRs) , AIM2-like Receptors (ALRs), and Nod-like receptors (NLRs)[117].

TLRs are one of the largest groups of PRRs, and are conserved from *C.elegans*, all the way up to mammals[112, 118]. There are a total 12 different TLRs that have been identified in mammals and they all share some basic features. TLRs are all integral membrane glycoproteins

that contain a variable number of leucine rich repeats, and cytoplasmic domains homologous with the interleukin1 receptor known as Toll/IL-1R (TIR) domains. TLRs generally will recognize a class of PAMP/DAMP, for instance TLR1,2, and 6 all recognize lipids, while TLR7-9 all recognize nucleic acids [112]. TLR1,2,4-6 are all found on the cell surface, while TLR3,7-9 are usually observed intracellularly in endosomes[119]. Upon binding to PAMPs or DAMPs TLRs will recruit adapter molecules, MyD88, TRIF, TIRAP, and or TRAM. In the case of TLR4 LPS binding leads to activation of two different pathways, one MyD88 dependent, and the other MyD88 independent. In the MyD88 dependent pathway, TLR4 dimerizes and MyD88 forms a complex with I RAK (IL-1 receptor-associated kinase)[120], which sets into motion a signaling cascade that ultimately activate phosphorylate NF-κB causing it to translocate from the cytoplasm to the nucleus[121]. In the MyD88 independent pathway IκB kinases are activated by TRIF, which activates NF-κB downstream, but unlike the myD88 dependent pathway IRF3 is activated, which induces expression of the IFN-β and the IFN inducible genes[122-124]. TLRs are expressed by dendritic cells, macrophages, B cells, and some T Cells in the immune system[125], as well as DRG sensory neurons[126, 127].

1.4.2 Adaptive immune system

As the name innate immune system insinuates, the PRRs, found on innate immune cells are germline-encoded, meaning their ability to detect foreign agents are finite and fixed. In contrast the adaptive immune system can produce antibodies capable of recognizing novel pathogenic or foreign proteins throughout one's life. However, the contribution of the adaptive immune system to pain signaling is far less clear than that of the innate immune system. We are only starting to parse out mechanisms linking the adaptive immune system and pain. There are many autoimmune diseases with associated pain components such as Rheumatoid Arthritis, Celiac's Disease, Guillain-Barré syndrome, and Crohn's disease among many other.

As inflammation is so intimately linked with pain, it is perhaps expected that autoantibodies, leading to destruction of tissue and release of cytokines would cause pain through inflammatory mechanisms. However, inflammation and pain, often in a paradoxical seeming fashion, can have an apparent disconnect. This has been observed in conditions such as Rheumatoid Arthritis[128] and complex regional pain syndrome (CRPS)[129].

One mechanism through which the adaptive immune system could initiate or mediate a hyperalgesic state is upon generation and production of autoantibodies that directly bind to primary afferent epitopes and alter their excitability. This was recently shown in patients with chronic inflammatory demyelinating polyradiculoneuropathy, where it was determined that antibodies against the paranodal regions of primary afferents were detected[130]. In a serum transfer model, CASPR2 antibodies isolated from patients with Morvan's syndrome were determined to bind to neuronal soma in the DRG and alter the distribution of voltage gated calcium and potassium channels, ultimately leading to hyperexcitable primary afferents[131, 132]. An indirect, action of autoantibody induced pain has also been observed and recently elucidated as the result of autoantibody/autoantigen bound in immune complex activating FcγRs on neurons[133, 134] in models of rheumatoid arthritis.

1.5 RHEUMATOID ARTHRITIS

Rheumatoid arthritis is a chronic autoimmune disease characterized by inflammation, swelling, stiffness and pain of the joints. Worldwide RA affects as many as 5 in every 1000 adults, with a 2-3 times greater prevalence among women than men. While RA can present at any age, the peak incidence of clinical manifestation and diagnosis is observed in individuals in their 60's[135]. Patients with RA experience substantial decrease in physical function and pain, which results in reporting a marked decrease in quality of life[136]. More than half of RA patients (50-70%) test positive for serum antibodies that recognize citrullinated peptides (ACPAs), or the rheumatoid factor (RF)[137, 138]. Serum positive patients also often exhibit more severe joint damage as well as

a higher mortality rate compared to serum negative RA patients[139-141]. It's estimated that a heritable/genetic cause for RA is observed in roughly 40-60% of seropositive patients[142]. Studies into genetic mutations commonly observed among RA patients have pointed to genes relating the immune system including with single nucleotide polymorphisms in HLA genes showing the greatest risk[143, 144].

RA likely represents a group of more specific diseases that all have been placed under an umbrella of similar manifestations/features. As such, there are no specific tests to determine RA and rather it is diagnosed based on a common pattern of symptoms and serum profiles[145].

1.5.1 RA pathophysiology and pain

While disease modifying antirheumatic drugs such as methotrexate often can remediate the inflammatory aspects of RA, they often fail to adequately address the aspect of the disease that patients report as their important symptom, pain[146-148]. This highlights the disparity described above between inflammation and pain in RA. RA patients also often report pain prior to the clinical manifestation of the disease. This along with circulating autoantibodies being found up to 10 years prior to diagnosis in patients further indicates that pain states in RA may often come from non-inflammatory origins[149]. RA pathophysiology is complex, which is reflected by the heterogeneous pathologies observed in patients.

Patients, seropositive with autoantibodies, which target epitopes present in cartilaginous tissue and joint structures often display more severe RA symptoms and have higher rates of mortality[139, 150]. These hallmarks of RA include erosion of synovial membranes and destruction of articular cartilage, which can be debilitating for patients[151]. The autoantibodies can be IgG, IgA, or IgM and often have altered glycosylation states that increase their ability to bind to Fc receptors[152, 153]. Either in immune complex or alone, RA autoantigens can elicit immune response via activation of macrophages and/or activation of osteoclasts[154]. The latter of which explains why RA patients often experience bone loss. Synovial inflammation in RA patients is indicative of

immune cell over-activation. In fact the immune response is so robust that macrophages, monocytes, dendritic cells, mast cells, T cells and B cells have all been shown to play a role in the inflammatory phase of RA[155, 156].

Under normal circumstances the synovium is relatively void of cells but becomes hyperplastic in response to a massive barrage of cytokines such as TNF, TGFβ, and IL-(1,6,10,12,15,18,25) among others. In the earlier stages macrophages and synovial fibroblasts become activated in response to PAMPs and DAMPs and ramp up their production and release of cytokines[157, 158]. The destructive nature of the cytokine barrage in the joint is mitigated somewhat by drugs targeting TNF and IL-6, which have become common place in treatment regimes[159]. Once the inflammatory machinery in the joint is started, the synovial space becomes occupied by invading immune cells, which cause osteoclast production[160] and activation[161], resulting in bone erosion. While bone erosion is underway a destructive and concerted catabolic activation of chondrocytes destroy joint cartilage[162].

1.5.2 Animal Models of RA

Many of the strides we have made towards understanding and treating RA, have come about through the use of numerous animal models. One of the earliest and most robust animal models is the collagen induced arthritis model (CIA). CIA was developed in rats in the 1970s and subsequently has been used in various mouse strains[163, 164]. In the CIA model, animals are immunized with type II collagen from various sources, often delivered in complete Freund's adjuvant. Following induction animals begin developing antibodies against type II collagen[165], and roughly 20-25 days after injection animals develop polyarthritis, mimicking human RA , with synovitis and infiltration of immune cells, as well as bone erosion and cartilage destruction in the joints[166].

The collagen antibody induced arthritis model (CAIA), is similar to CIA, but instead of inoculation with type II collagen itself, animals are given a cocktail of antibodies produced against

type II collagen[167]. The CAIA model developed first as a serum transfer model, in which serum was isolated from arthritic mice inoculated with chick type II collagen, injected into naïve mice, which in turn became arthritic[168]. Even IgG alone isolated from CIA mice and transferred to naïve mice render these animals arithtic[168]. This observation was incredibly important in that it showed that autoantibodies alone, regardless of other disease factors, could induce the hallmark pathologies observed in RA. In subsequent work monoclonal antibodies targeting the triple helical portion of type II collagen were characterized and developed into a 4 antibody cocktail that is commonly used today in order to induce arthritis in the CAIA model[169]. While the innate and adaptive immune contributions can be isolated from one another in the CAIA model, an innate immune stimulus, such as LPS, is usually delivered one week after cocktail injection in order to "synchronize" the onset of symptoms[169].

The K/BxN model of RA is a mouse model first developed through an apparent failed experiment. A mouse strain with transgenic T cell receptor (KRN), which failed to exhibit the intended phenotype, were crossed with the non-obese diabetic (NOD) mouse strain, and the resulting offspring developed pronounced joint inflammation[170]. These K/BxN mice develop severe and spontaneous synotivitis, bone erosion, and cartilage destruction[171]. K/BxN mice develop autoantibodies against glucose-6-phosphate isomerase (G6PI), which is ubiquitously expressed but with high concentrations in the joints specifically. It's been shown that the formation of G6PI-immune complexes (IC) is necessary for initiation of K/BxN arithitis[172]. Circulating G6PI immune IC binds to the activating FcγRs on neutrophils and mast cells, eliciting vasodilation, and ultimately increases vascular permeability of the joints, enabling infiltration of immune cells and G6PI IC[173]. Importantly serum from K/BxN mice can be transferred to naïve mice of various strains, and induce the same RA-like phenotypes, similar in fashion to the experiments discussed with the CAIA model.

1.6 PAIN IN RESPONSE TO ANTIBODIES IN IMMUNE COMPLEX

1.6.1 Section primer

Here I will give an overview of the findings from our 2019 paper that lay the basis for chapter 2 of my dissertation. While I worked on this paper and am a co author, I did not feel it was appropriate to include it in full.

1.6.2 Brief overview

Specific autoantibodies had been shown to cause hypersensitivity of nociceptive neurons, leading to neuropathic pain through direct targeting of neuronal surface channels[132, 174]. In our paper, “Cartilage-binding antibodies induce pain through immune complex–mediated activation of neurons” we showed that autoantibodies can induce hypersensitivity in nociceptive neurons, indirectly, via formation of immune complexes and their subsequent binding to local neuronal FcγR’s (Figure 1-1). In the paper we show that *Fcgr* mRNA is expressed in the soma of DRG neurons, and is transported to the terminals, where it can be locally translated. This was supported by observation of FcγRI and FcγRIIB protein being observed in protein gene product 9.5 (PGP9. 5) positive fibers in the skin, even though it was apparently absent in the DRG neuronal soma via histology. Further, accumulation of *Fcgr* mRNA was observed in nerve fibers following ligation of the sciatic nerve. Importantly, we showed that type II collagen antibodies in immune complex (CII-IC) could directly stimulate DRG neurons in culture, resulting in release of CGRP. And that mice lacking the common gamma chain on non-immune cells did not develop pain in the early stages of CAIA, indicating that the pain is likely from neuronal FcγRs. This can explain the presence of a pain phenotype in the absence of any inflammatory state. As described above, RA patients often experience pain prior to clinical manifestation of the disease and continue to experience pain following treatment that resolves joint inflammation. This work indicates that FcγR’s and their downstream signaling represent potential therapeutic targets for the treatment of pain in RA patients.

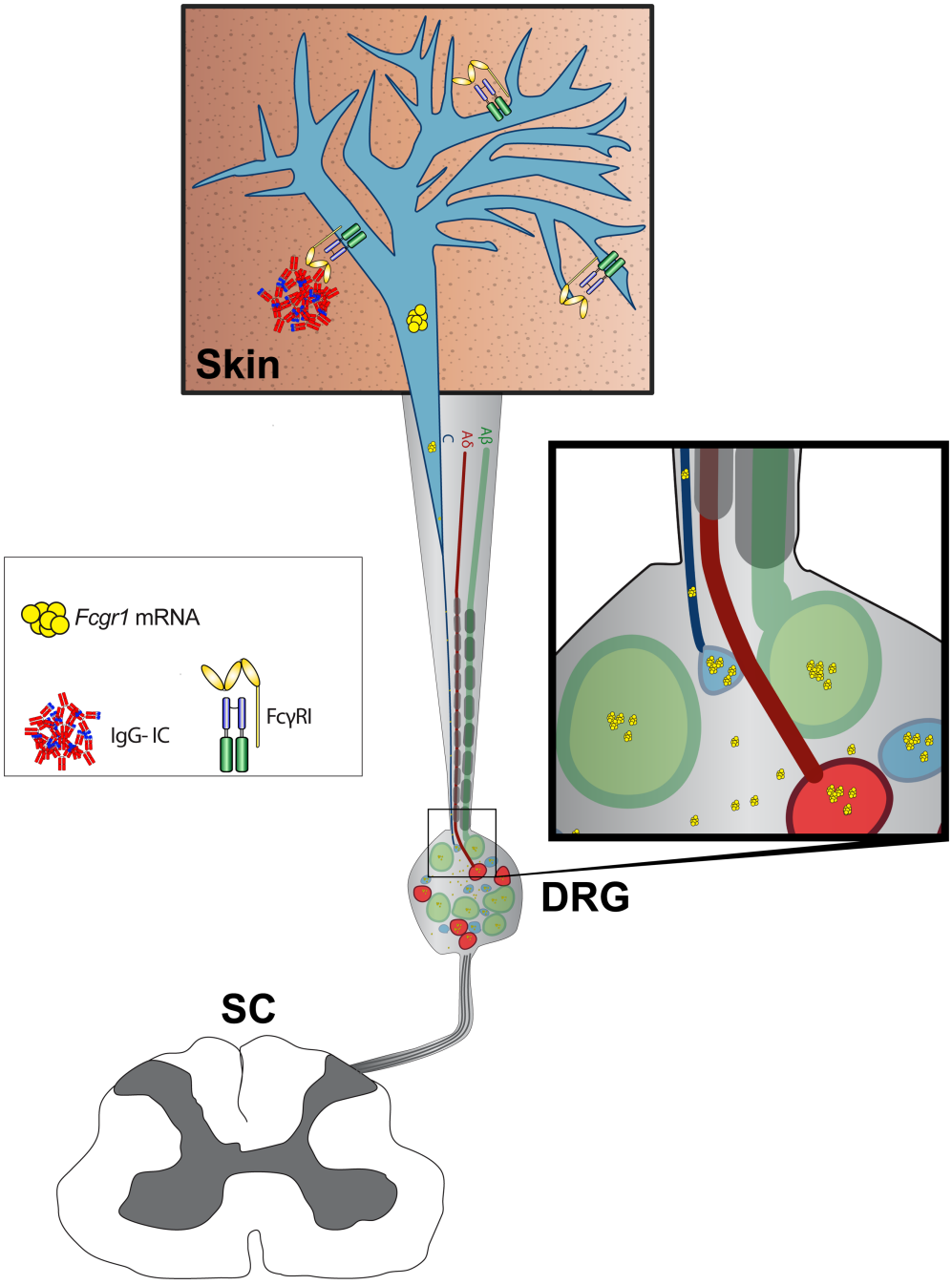

Figure 1-1: Graphical Abstract of Bersellini Farinotti et al. 2019: Neurons in the dorsal root ganglion express Fcgr1 mRNA which is transported down the primary afferent to its terminals, where it is translated into functional protein. Immunoglobulins and antigens in immune complex, such as CII-IC, can bind directly to neuronal FcγRI and induce pain like behaviors mice.

CHAPTER 2 IRF7 AS A MEDIATOR OF INNATE AND ADAPTIVE IMMUNE SIGNALING IN DRG NEURONS

2 BACKGROUND / INTRODUCTION

Autoantibodies have been shown to cause pain via direct binding to nociceptive neurons [175, 176] as well as through activation of FcγRs via formation of immune complex. Interestingly RA patients often complain of joint pain prior to clinical manifestation of the disease and prior to a diagnosis[177]. However, circulating autoantibodies may be present for months or even years prior to the clinical manifestation of the disease[178]. Similarly, in the collagen antibody induced arthritis model (CAIA), mice are given a cocktail of antibodies directed against type II collagen and then given an injection of LPS to synchronize the RA-like phenotype among the mice. However, prior to LPS injection, mice develop pain in the absence of inflammation. This pain state was shown to be depended upon neuronal FcγRs[133]. Here we were interested in whether an innate immune stimulus, such as LPS, could amplify the primary sensory afferent neurons response to antibodies in immune complex through the activating FcγRs.

2.2 MATERIALS AND METHODS

2.2.1 Animals

All animal experiments were carried out according to protocols approved by the Institutional Animal Care and Use Committee of UC San Diego. Mice were housed with up to 4 littermates per cage, and given food and water ad libitum, in a temperature-controlled facility with 12 hour light dark cycles. Wild type C57/Bl6 mice were purchased from (Harlan, Indianapolis, IN) and IRF7 functional knockout mice, mutant B6;129P2-*Irf7*^{tm1Ttg} (*Irf7*$^{-/-}$) mice, were generated by Tadatsugu Taniguchi[179], obtained from RIKEN (RBRC01420) and then bred at UCSD after backcrossing for 10 generations on the B6 background.

2.2.2 Intrathecal drug administration

Mice were anaesthetized with 2-3% Isoflurane, and the respiratory rate was monitored via observation. Stock LPS (50µL aliquots at 2mg/ml stored in -20°) was diluted (10µL stock/ 90µL saline) to a final concentration of 0. 2µg/µL. TLR2 agonist LTA was diluted to 0. 05µg/µL in saline and TLR5 agonist FLAst was diluted to 0. 2µg/µL (Invivogen, San Diego, Califronia). Each animal received 5µL injections intrathecally. Injections were performed as follows: A 25µL Hamilton syringe affixed to a 30g needle via polyethylene tubing PE10 was first flushed with sterile water and then loaded with 5µL of LPS. The 30g needle was then inserted between L4-L5 intervertebral-space until a tail twitch was observed. The injection was performed slowly, during which, any compression of the air bubble within the tubing was be observed and noted as an indication of impeded flow.

2.2.3 Behavioral tests

Mechanical withdrawal thresholds were assessed using an adapted up-down method of the von Frey test of Dixon[180] modified by Chaplan[181]. In this method, animals were placed in Plexiglas cages on wire-mesh floor and a series of calibrated nylon von Frey hairs (Stoelting Co.) ranging from 0. 04 to 2g (0. 04, 0. 07, 0. 16, 0. 4, 0. 6, 1, 1. 4g) was used to calculate the 50% withdrawal threshold. Mechanical values for the left and right hind paws were calculated and averaged to produce a single data point per time of measurement.

2.2.4 Cell culture experiments

All DRGs were dissected from mice following perfusion with ice cold saline. freshly collected DRGs from each mouse were placed in 1.5ml of HBSS and stored in 5ml ependorph tubes on ice until ready for dissociation. 20 minutes prior to dissociation 1.5 ml of HBSS was mixed with 90µl Papain, 3µl NaHCO3 and 1mg L-Cystine, and then mixed with the 1.5ml of HBSS containing the DRGs. DRGs were then incubated for 30 minutes at 37°C on a shake plate. DRGs

were then spun at low speed for one minute and the solution was carefully aspirate away. DRGS were then incubated in 3ml of HBSS containing 6mg collagenase and 13mg dispase for 30 minutes at 37°C on shake plate. Cells were again spun down at low speed and solution was carefully aspirated away. Finally DRGS were washed in 2ml of warmed media composed of 500ul F12 with 10% FBS, Penicillin/streptomycin in 50ml conical HBSS without Ca /Mg (GIBCO, cat. no. 14170) , then spun down again and aspirated, before adding 2.5 ml of media and triturating until completely dissociated. Dissociated cells were then plated on uncoated plastic 6 well plates for 1 hour to let non-neuronal cells adhere. Non-attached neurons were then collected, counted, and replated on laminin and poly-D-lysine (PDL) coated 24 or 12 well plates. Media contained FuDR in order to inhibit proliferation of any residual non-neuronal cells, as well as nerve growth factor (NGF) to support DRG neurons. Media was changed on days 2, 5 and 7. On day 5 NGF was removed from the media. On day 7 neurons were stimulated with LPS (100ng/ml)

2.2.5 RNA extraction

Freshly collected DRGs were immediately frozen in dry Ice and stored at -80°C until ready for RNA extraction. DRGs were placed in 2ml screw top Eppendorf tubes. 500µL of Qiazol (Qiagen) was added to each tube along with 3-5 3mm steel beads. 8 samples at a time were then placed into a Biospec Mini Beadbeater-8 set to homogenize and run for 2 cycles of 1 minute each. Between cycles samples were placed on ice. 100 µL of chloroform was then added to each sample and they were shaken briskly for 15 seconds. Following a 15min centrifugation at 14,000 RPM, 200 µL of the aqueous phase was collected and transferred to new 1. 5ml Eppendorf tubes. 6µL of glycoblue (diluted 1:10 in RNase free water) was added to each tube. RNA was precipitated out by adding 250µL of isopropanol and stored overnight at -20. The following day samples were centrifuged for 10min at 14,000 RPM. The fluid was carefully aspirated away without disturbing the RNA pellet. The pellet was then washed in 250µL of 4M LiCL. Spun down at 14,000 RPM for 10 min at 4°C and the solution was aspirated away without disturbing the pellet. Finally, Samples

were washed in 75% Ethanol spun for 10 min at 4°C at 14,000 RPM and let air dry for 10 minutes. The pellet was finally dissolved in 22µL of TE buffer and quantified using a Nanodrop 2000.

2.2.6 qPCR

cDNA was made from fresh 125µg of RNA using super script IV VILO (ThermoFisher) following manufacturers protocol. Taqman probes used are displayed in table 2-1. Probes were mixed with cDNA following manufacturers protocols, and all experiments were done with HPRT-VIC as the housekeeping gene. All qPCR was run on biorad cfx96 touch (BioRad) or quant studio 3 (Applied Biosystems). Data was analyzed using ddCT method and statistics performed comparing fold changes over control condition.

2.2.7 Nano String

RNA is hybridized to 3' complementary biotinylated capture probes as well as 5' reporter probes directly tagged with fluorophore barcodes for identification. Non-target transcripts are then removed using magnetic beads containing capture probe complimentary nucleic acids, and then non-target bound capture probes are removed using magnetic beads containing complimentary nucleic acids to the transcript targets. Samples are then Run through the nCounter Digital Analyzer, which outputs barcode counts for direct quantification without cDNA library prep (Nano String technologies, Seattle WA).

2.2.8 Histology

Mice were transcardially perfused with ice cold saline followed by 4% PFA and post-fixed in 4% PFA for 24 hours. DRGs were dissected and cryoprotected in 30% sucrose at 4° C for 2 days and then embed in OCT. DRG sections were cut using a cryostat at 14µm and directly mounted onto glass positive charged microscope slides. Tissues were washed quickly with water and then permeabilized with PBS + 0. 25% Triton and then blocked with 5% donkey serum.

Primary antibodies (TrkA, Cell Signaling; IRF7, SantaCruz Biotechnology; IB4-594, Invitrogen) were diluted in blocking solution and then incubated for 24hrs at room temperature. Slides were then washed in PBS and then incubated with secondary antibodies overnight in blocking solution. Tissues were then washed in PBS, cover slipped, and imaged on a confocal microscope (Zeiss LSM800).

2.2.9 Data analysis

Data analysis was performed using nSolver Analysis Software (nanostring technologies, Seattle WA). Data was first assessed for quality control and then normalized. Changes gene expression in response to TLR agonists were first determined as -fold change over IT vehicle control samples and significance was determined using false detection rates less than $p<0.05$ to be statistically significant. Hierarchical clustering was used to infer and visualize relationships between conditions. Gene Ontology and network analysis was used to determine potential mechanisms responsible for TLR agonist induced *Fcgr* expression changes.

2.3 RESULTS

2.3.1 LPS increases *Fcgr1* and *Fcgr4* expression in the DRG

In the CAIA model LPS is used to initiate and synchronize the onset of arthritis [182]. Pain in the CAIA model has been shown to be dependent upon the activating FcγRs [134, 183]. Since a large spike in allodynia is observed following administration of LPS, we hypothesized that LPS may act to increase the expression of the activating FcγRs. Following IP injection of LPS (25µg in 100µL of injection saline) we observed an increase in lumbar DRG expression of the activating *Fcgr1* and *Fcgr4* (figure 2-1 A, C). In order to minimize off target effects, including making the animals sick, we opted to switch to intrathecal LPS, as we could reach the DRGs and administer a much smaller dosage to the mice. In order to choose the optimal time point to collect DRGs we first did a time course study and found that 6 hours following IT-LPS had the greatest increase in

genes of interest (Figure 2-2 A-D). In order to explore the mechanisms of how TLR activation, an innate immune stimulus, could lead to increased sensitivity to an adaptive immune response we assessed the ability of different TLR agonists, administered intrathecally, to stimulate expression of *Fcgrs* mRNA in the DRG. Following intrathecal administration of the agonists outlined in table 2. 2 (LTA-TLR2, LPS-TLR4, and FLAst-TLR5) we collected DRGs and use the Nanostring pan cancer immune profiling panel. Intrathecal injection of TLR4 agonist LPS and, to a lesser extent, TLR5 agonist FLAst, elicited an increase in expression of *Fcgr1*, *Fcgr2b* and *Fcgr4* mRNA (Figure 2-3 A-C).

2.3.2 Identification of IRF7 as putative master regulator

Using the nSolver software we first assessed the overall data by running a principle component analysis (Figure 2-4 A), which showed that IT TLR agonists grouped very tightly together, indicating that the data was strong. In comparing the gene expression to naïve control mice, we first looked at hierarchical clustering of major pathways and observe that the greatest change was in the TLR4 agonist group, which received intrathecal LPS. We also observed here that IFN signaling was the largest change from naïve control of any of the pathways analyzed. We used the ingenuity pathway analysis software to predict a potential mechanism through which activation of TLRs could lead to increased expression of the *Fcgrs.* To do so we took each gene of interest (*Fcgr1*, *Fcgr2b* and *Fcgr4*) and identified all known or predicted transcription factors, then identified all direct, or indirect pathways linking back to each of the TLR receptors of interest (TLR2, TLR4 and TLR5). We could then overlay the expression data from the Nano String results and observe changes in these newly generated pathways. The results for *Fcgr1 Fcgr2b* and *Fcgr4* are shown in Figures 2-5, 2-6 and 2-7 respectively. Because our previous work had indicated that FcγRI was the major contributor to pain in our rodent RA models we first focused on a potential mechanism linking TLR activation to increased *Fcgr1* activation. IRF7 prominently stood out as a potential master regulator, and in looking at our previous results with LPS, *Irf7* mRNA increases

significantly in the DRG in each and every time point (Figures 2-1,D; 2-2,B). Indeed *Irf7* in the Nano String data also showed to be significantly increased following IT LPS and not other TLR agonists (Figure 2-3,D). We wanted to explore other potential TLR4 agonists that may cause increases in expression of *Irf7* and *Fcgr1*, and chose to test morphine, as well as hmgb1. Morphine acting as a TLR4 agonist on neurons has been used to describe the phenomenon of opioid induced hyperalgesia[184]. To test morphine, we injected either 5µg or 15µg intrathecally into mice, to our surprise neither dosage of morphine led to an increase in expression of *Fcgr1* or *Irf7* (Figure 2-8, A-C). To further ask whether morphine acts as a TLR4 dimer on DRG neurons, we dissociated adult DRGs using a neuronal enrichment protocol, then stimulated with either LPS (100 ng/ml), morphine (10µM), or saline. After 1 hour we stained the cells and analyzed them via flow cytometry for the percent of dimerized TLR4. We observed that LPS induced dimerization significantly more than morphine, or saline treated DRG neurons, p = 0. 057 (Figure 2-8, D).

2.3.3 IRF7 in the DRG

In order to explore the role of IRF7 in the DRG we performed immunostaining on sectioned tissues. IRF7 was predominantly observed in neuronal nuclei in the DRG (Figure 2-9). IRF7 was present in small, medium and large diameter neurons (Figure 2-9,C). In order to assess whether IRF7 protein increase occurred in the DRG following TLR4 activation we injected mice with the endogenous TLR4 ligand dsHMGB1[185] (1µg/5µL). The number of IRF7 positive neurons in the DRG of mice injected with dsHMBG1 was significantly higher after 24 hours (Figure 2-9, D-E). We observed significant increase in the amount of both non-peptidergic, IB4(+) neurons (Figure 2-9,F) and peptidergic, TrKA(+) neurons 24 hours post IT injection of dsHMGB1 (Figure 2-9,G).

2.3.4 Functional IRF7 knockout prevents LPS induced upregulation of *Fcgr1 in vitro*

To assess the roll of IRF7 *in vivo* we first cultured DRG neurons from wild type C57/bl6 mice and those lacking functional IRF7 following neuronal enrichment protocols in order to remove any contribution from other cell types (Figure 2-10, A). Neurons were cultured with nerve growth factor (NGF), to stimulate their growth, as well as FuDR, to inhibit proliferation, both of which were removed 1 day prior to neuronal stimulation. Neurons cultured from wild type C57/bl6 mice stimulated with LPS (100 ng per ml) show a significant increase in expression of *Fcgr1, Fcgr2b* and *Irf7* mRNA, while neurons cultured from IRF7 functional knockouts stimulated with LPS, do not (Figure 2-10, B).

2.3.5 IRF7 deficiency prevents LPS induced upregulation of *Fcgr1 and Fcgr4 in vivo*.

We injected LPS (1µg LPS in 5µl of saline) intrathecally into mice. Intrathecal LPS caused rapid onset of hyperalgesia in both male and female wild type C57/bl6 mice (Figure 2-11, A-B). However, both male and female mice lacking functional IRF7 had a delayed onset of hyperalgesia (Figure 2-11 A,B). Though, initially delayed, the onset of hyperalgesia in IRF7 deficient mice became equivalent to wild type C57/Bl6 mice at 4 hours post IT LPS injection. This was consistent in both male and female IRF7 deficient mice (Figure 2-10). Female IRF7 deficient mice show slightly less, but not statistically significant, upregulation of *Fcgr1* mRNA following IT LPS, and reduced upregulation of Fcgr4 (Figure 2-12 A,C). Similarly IRF7 deficiency in male mice prevented LPS induced upregulation of Fcgr1, and Fcgr4 (Figure 2-13 A,C). While we did not observe any behavioral differences in response to IT LPS, we did however, observe sexual dimorphism in gene expression changes of *Fcgr2B*. Female mice deficient in IRF7 show a significantly larger increase in expression of *Fcgr2b* in response to IT LPS (Figure 2-12: B), while male mice deficient in IRF7 show significantly decreased upregulation of *Fcgr2b* mRNA (Figure 2-13 B).

2.3.6 IRF7 deficiency in mice reduces pain in a double hit model

Based on our previous conclusions that *Fcgr1* mRNA is produced in the DRG neuronal soma and then transported peripherally and locally translated in the joint, we hypothesized that TLR4 mediated upregulation of Fcgr1 would prime the nociceptive nerve endings in the joint, causing an increased allodynic response to any local antibodies in immune complex. To test this, we first injected LPS (1 µg in 5 µL) IT into male C57/Bl6 wild type, or IRF7 deficient mice. One week later we injected 2. 5 µL of CII-IC (200 µg/ml) intra-articularly into the right ankle and measured the resulting mechanical withdrawal thresholds. Both Wild type and IRF7 deficient mice display prolonged allodynia following IT LPS (Figure 2-14 A). At 1 hour following IA injection, wild type mice showed significantly more allodynia in their ipsilateral hindpaw compared to the uninjected hindpaw.

2.4 DISCUSSION

Here the preceding data presents a novel mechanism whereby an innate immune stimulus can prime DRG neurons, through an IRF7 dependent signaling pathway, making them hypersensitive to an adaptive immune response. Thus, IRF7 represents a potential therapeutic target for the treatment of pain in patients with autoimmune disorders such as RA, who often don't respond well to current pharmacological interventions[148]. Previously we showed that auto-antibodies in immune complex formation could bind directly to neuronal FcγR's and cause allodynia[133]. Here, we add to this previous work by showing that innate immune stimuli, both endogenous and exogenous, can elicit IRF7 dependent upregulation of *Fcgrs,* priming DRG nociceptive neurons and making them more sensitive to antibodies in immune complex.

For future studies, we are currently working on delivering IRF7 modifying therapeutics via AAV vectors, as well as knock down by antisense oligonucleotides. As IRF7 is very important for viral response in immune cells, we wish to specifically target spinal/DRG IRF7, for which intrathecal AAV-9 has a strong targeting propensity towards as well as ASOs.

One of the difficulties in this work was a lack of good antibodies for both IRF7 and FcγRI. For FcγRI we have tried many antibodies and have found one that works well for macrophages, but not well for neurons (Sino Biological). As for IRF7 the only antibody that we have found that worked is no longer produced (Santa Cruz Biotechnology, sc-9083), we used what was left sparingly, and have since tested nearly all commercially available mouse IRF7 antibodies with little to success.

Interestingly in the studies presented here, we did not observe any sexual dimorphism in allodynia following IT-LPS as previously published[186]. The only instance where we did observe significant sexual dimorphism was with *Fcgr2b* expression in IRF7 deficient mice. Here we observed that female mice given IT-LPS had a significant upregulation in *Fcgr2b* mRNA in the

DRG relative to wild type females given IT-LPS, whereas, male IRF7 deficient mice showed significantly less mRNA relative to wild type males given IT-LPS.

2.5 ACKNOWLEDGEMENTS

Chapter 2 is currently in preparation for submission as: Matthew A. Hunt, Alex Bersillini Farinotti, Diana Nascimento, Katalin Sandor, Gilson Dos Santos, Lauriane Delay, Mary Corr, Camilla I. Svensson, Tony L. Yaksh. IRF7 as a mediator between innate and adaptive immune signaling in DRG neurons. The dissertation author was the primary researcher and author of this material.

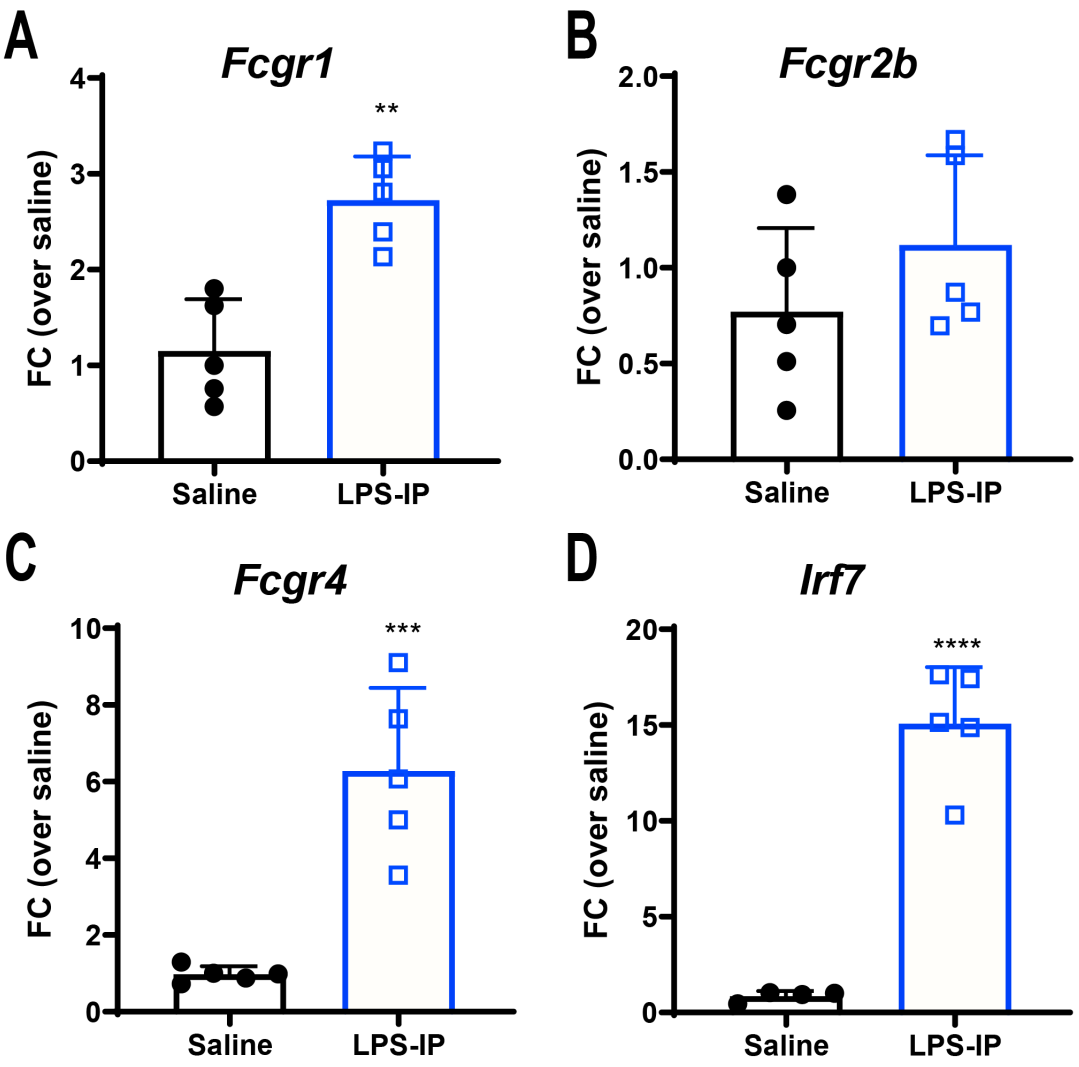

Figure 2-1 Lumbar DRG mRNA expression following IP LPS: Following IP LPS (25µg in 100µL) mRNA isolated from lumbar DRGs shows an increase in expression of Fcgr1 (A) Fcgr4 (B) and IRF7 (D)

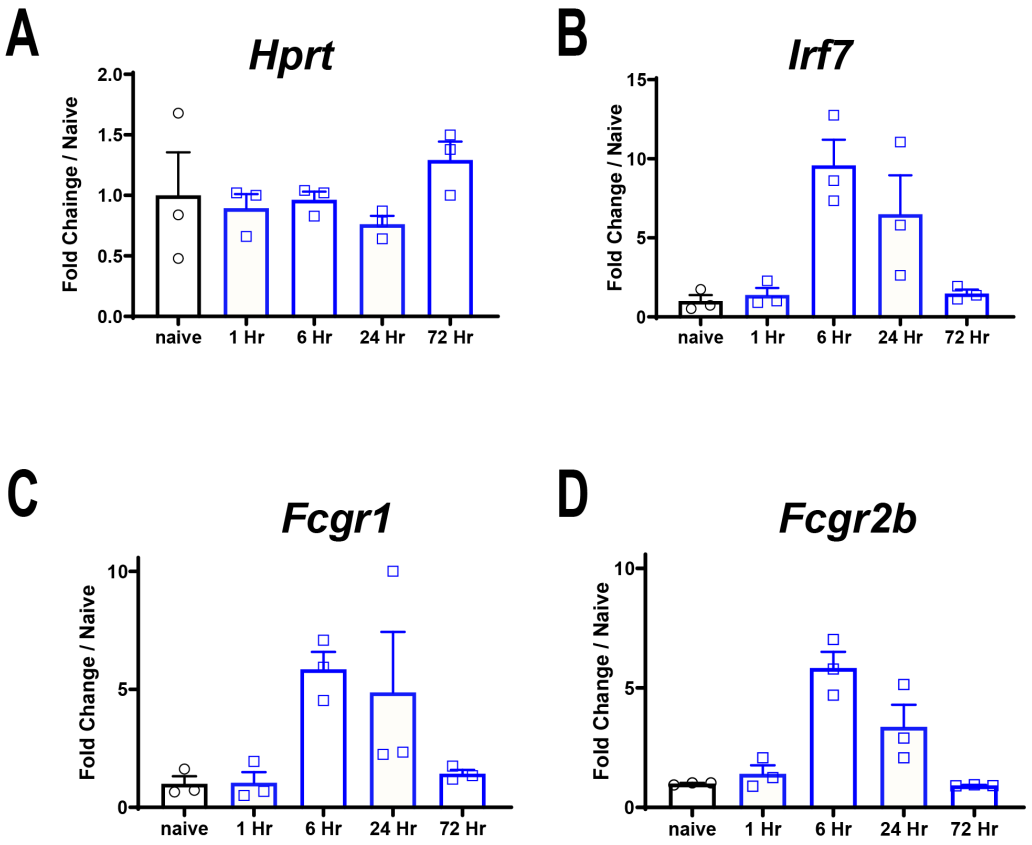

Figure 2-2 Lumbar DRG mRNA expression following IT LPS: mRNA expression following IT LPS (1µg in 5µL). A) No changes are observed in expression of the housekeeping gene Hprt. Peak expression is observed in IRF7 (B) Fcgr1 (C) and Fcgr2b (D) around 6 hours post IT LPS.

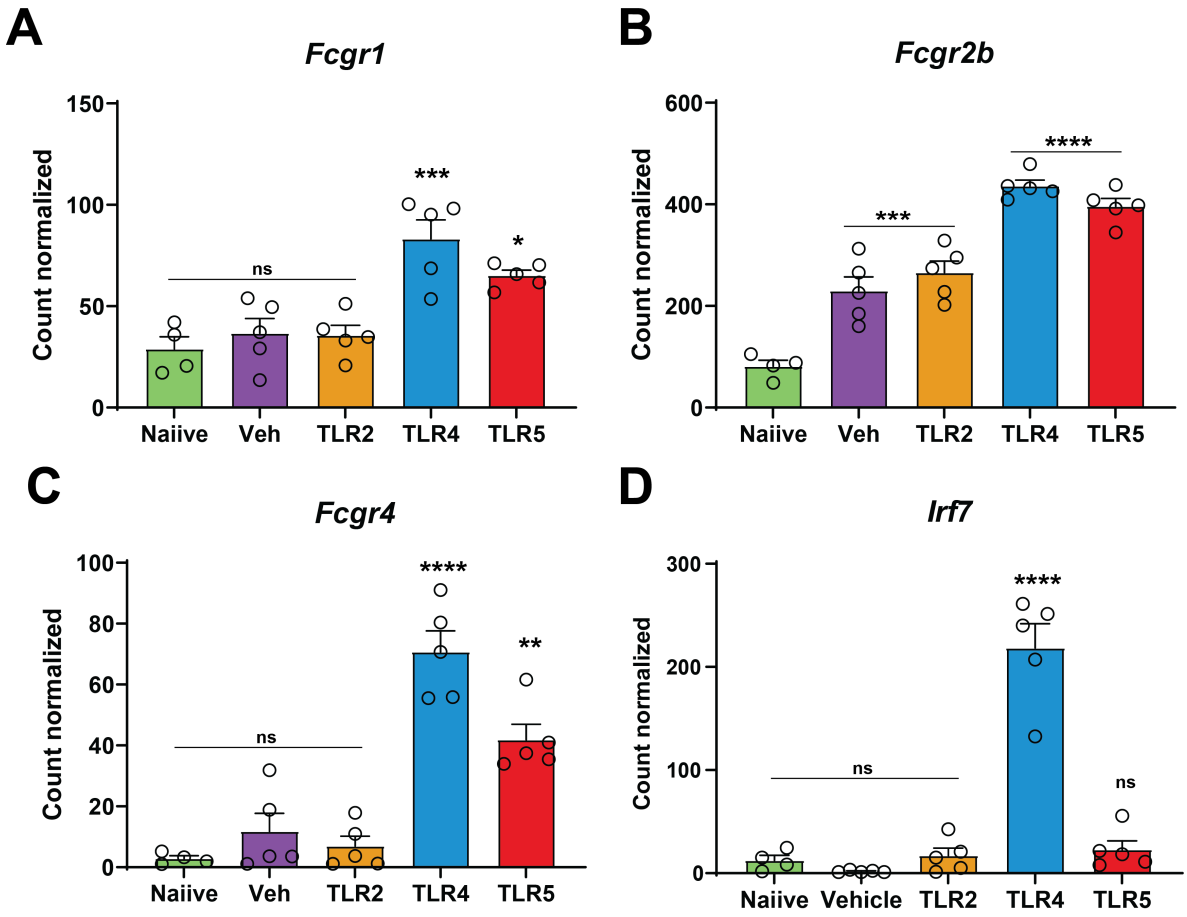

Figure 2-3 IT TLR Agonist effects on Fcgr expression: Normalized expression of Fcgr1 (A) Fcgr2b (B) Fcgr4 (C) and IRF7 (D) are shown following intrathecal injection of TLR agonists. All groups are compared to naïve via 1 way anova using Bonferonni correction and as * P<0. 05 **P<0. 01 ***P<0. 001 ****P<0. 0001

Table 2-1 List of taqman probes used for qPCR

qPCR PROBES			
Gene	**Probe ID**	**size**	**Dye**
Fcgr1	Mm00438874_m1	250 rxns	FAM-MGB
Fcgr2b	Mm00438875_m1	250 Rxns	FAM-MGB
Fcgr4	Mm00519988_m1	250 Rxns	FAM-MGB
Irf7	Mm00516793_g1	250 rxns	FAM-MGB
HPRT	Mm03024075_m1	360 rxns	VIC-MGB
P2rx4	Mm00501787_m1	250 rxns	FAM-MGB
Stat1	Mm00439518_m1	250 rxns	FAM-MGB
Stat3	Mm01219775_m1	250 rxns	FAM-MGB

Table 2-2 List of TLR agonists and intrathecal dose

Drug	IT Dose	TLR Target
Lipoteichoic Acid	0.25 µg	TLR2
Lipopolysaccharide	1 µg	TLR4
Flagellin (S.typhimurium)	1 µg	TLR5

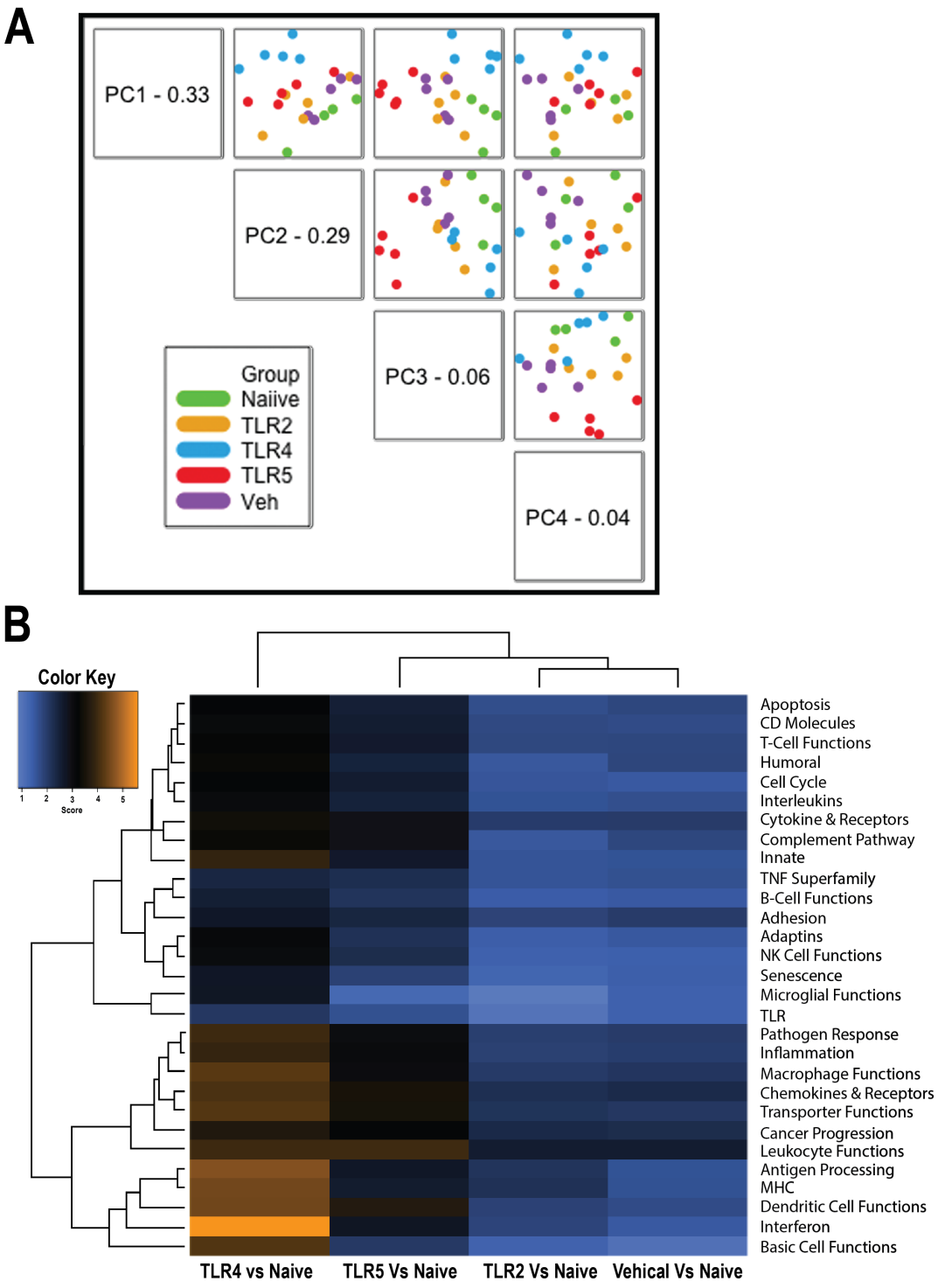

Figure 2-4 TLR agonist Nano String results: A.) Principle component analysis of individual samples is displayed showing tight clustering. B.) Hierarchical clustering analysis showing fold change over naïve of each group. Most of the change is observed in the group that received IT TLR4 agonists.

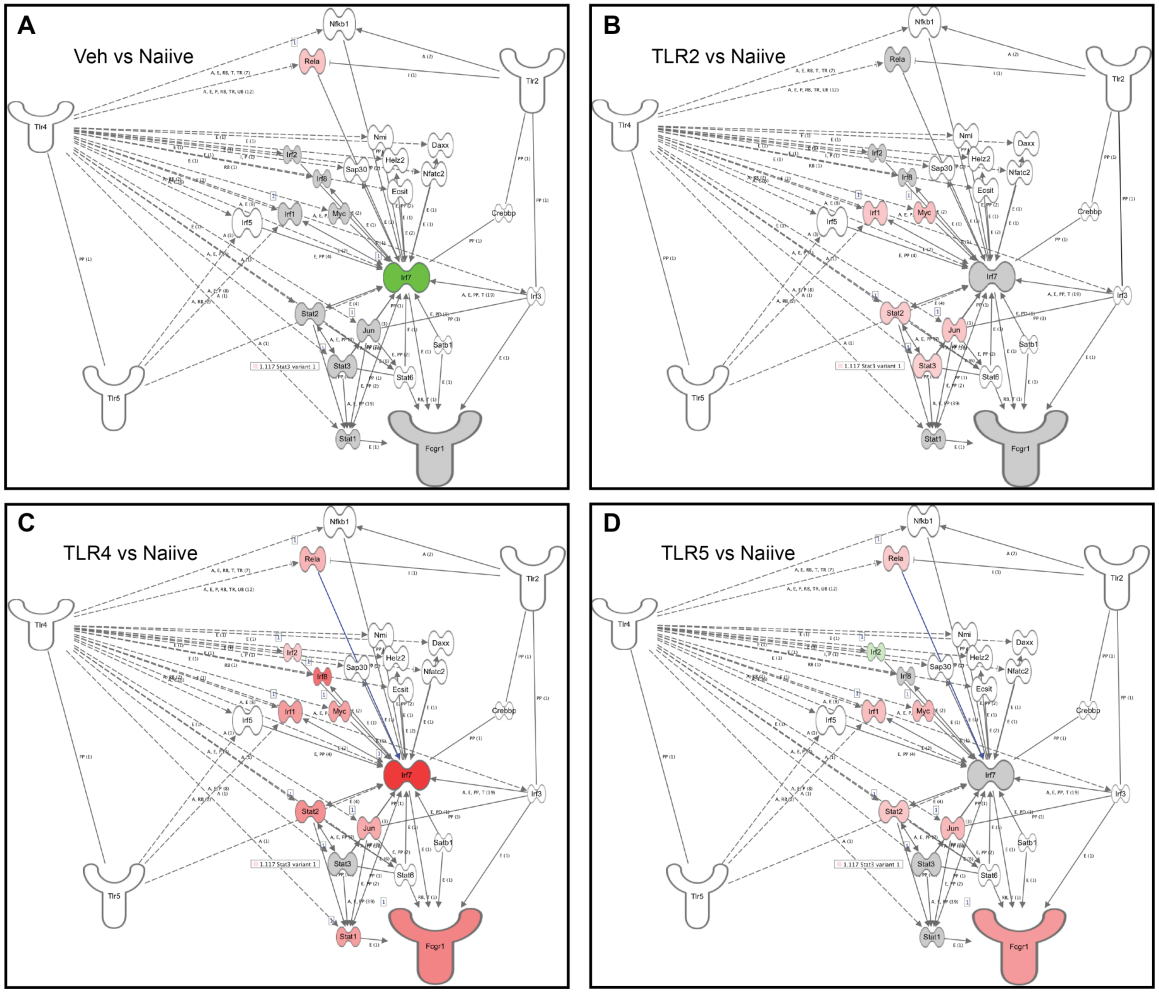

Figure 2-5 Predicted transcription factor pathways linking TLRs to Fcgr1: A.) Comparison of IT vehicle treated mice over naïve. B.) Comparison of IT LTA treated mice over naïve. C.) Comparison of IT LPS treated mice over naïve. D.) Comparison of IT FLA-st treated mice over naive. Red indicates significantly upregulated with bright red indicating a greater increase up to 5-fold. Green indicates significantly decreased expression with bright green representing 5-fold decrease. Grey represent genes that show significant change in at least one of the conditions. White represents either unchanged in any group or not assayed.

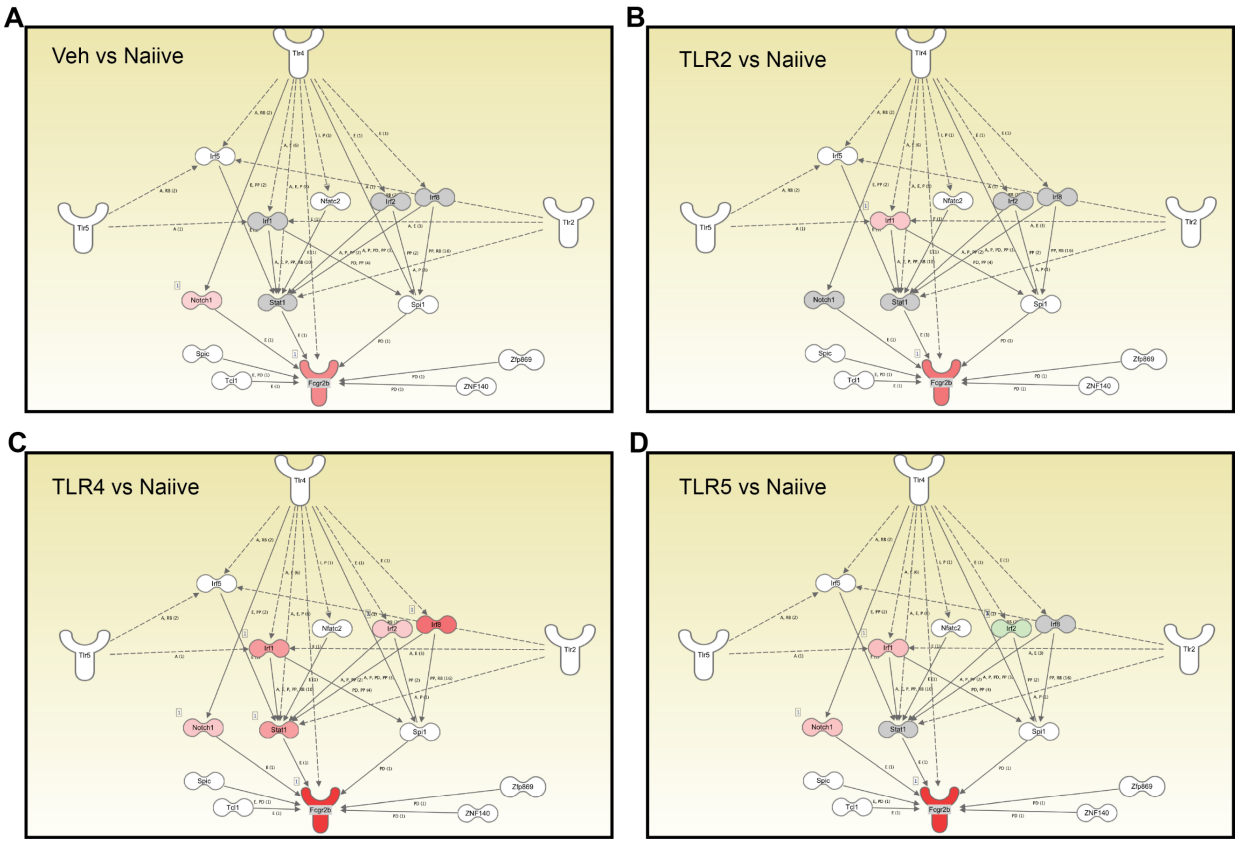

Figure 2-6 Predicted transcription factor pathways linking TLRs to Fcgr2b: Comparison of IT vehicle treated mice over naïve. B.) Comparison of IT LTA treated mice over naïve. C.) Comparison of IT LPS treated mice over naïve. D.) Comparison of IT FLA-st treated mice over naice. Red indicates significantly upregulated with bright red indicating a greater increase up to 5-fold. Green indicates significantly decreased expression with bright green representing 5-fold decrease. Grey represent genes that show significant change in at least one of the conditions. White represents either unchanged in any group or not assayed.

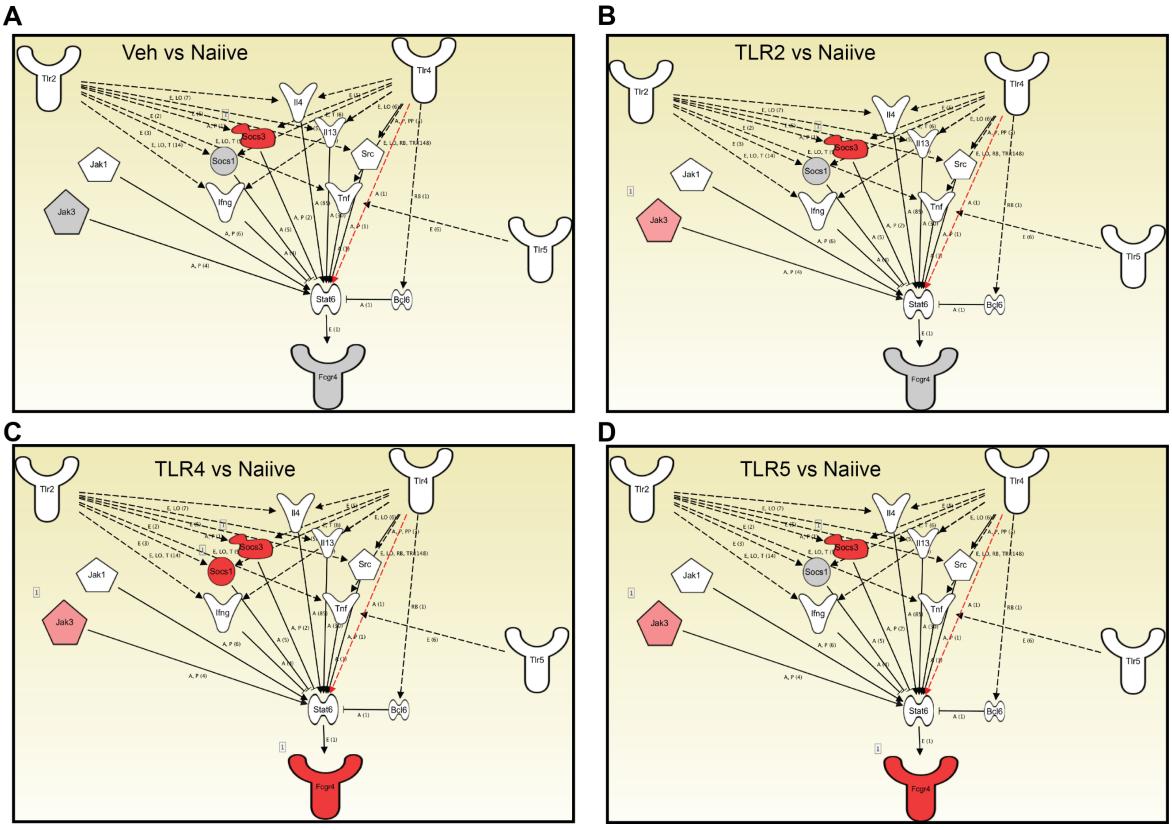

Figure 2-7 Predicted transcription factor pathways linking TLRs to Fcgr4: Comparison of IT vehicle treated mice over naïve. B.) Comparison of IT LTA treated mice over naïve. C.) Comparison of IT LPS treated mice over naïve. D.) Comparison of IT FLA-st treated mice over naice. Red indicates significantly upregulated with bright red indicating a greater increase up to 5-fold. Green indicates significantly decreased expression with bright green representing 5-fold decrease. Grey represent genes that show significant change in at least one of the conditions. White represents either unchanged in any group or not assayed.

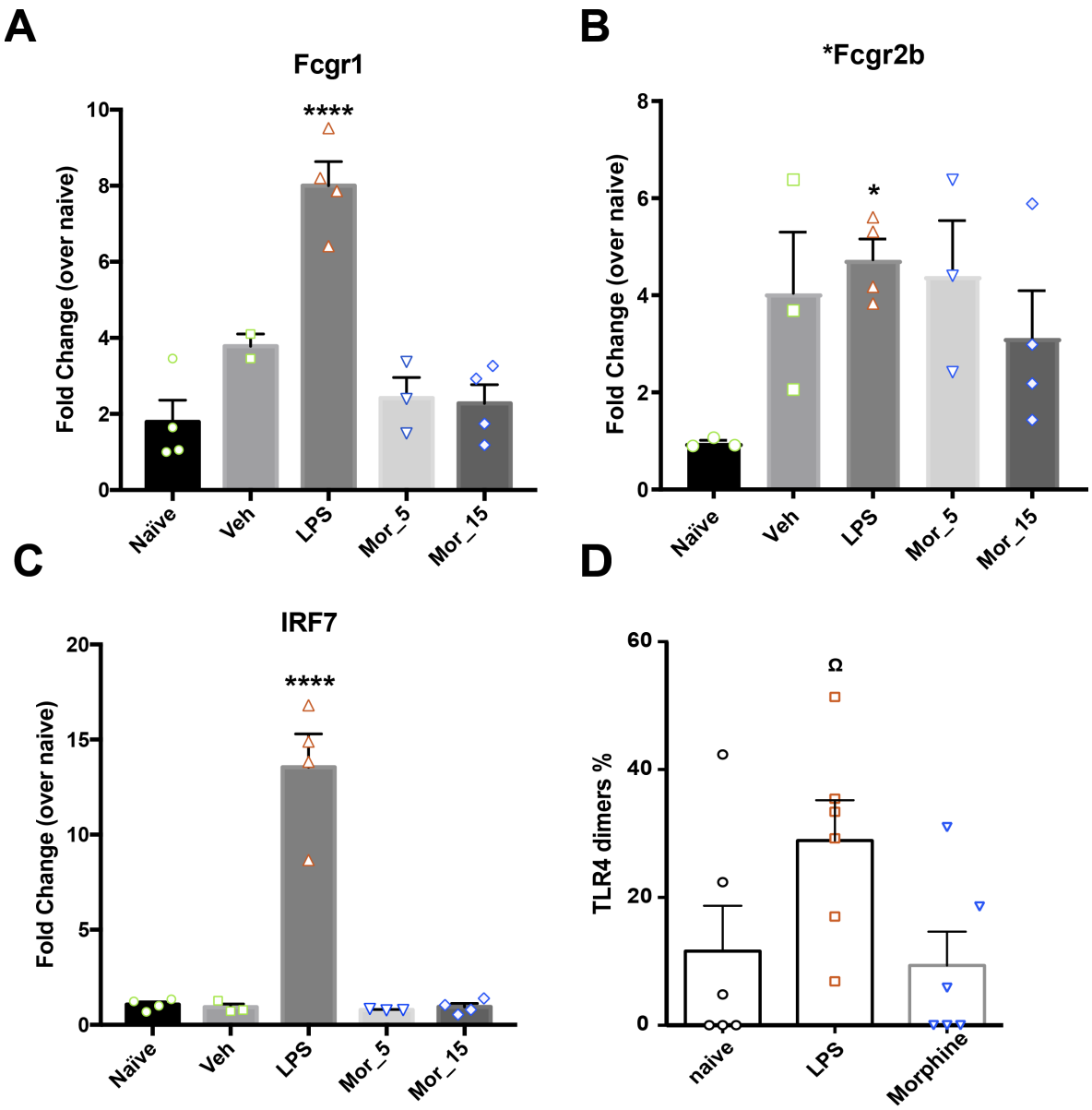

Figure 2-8 IT morphine does not alter mRNA expression in the DRG: Expression of Fcgr1 (A) Fcgr2b (B) and IRF7(C) are shown as fold change over naive. D.) Percent dimerization of TLR4 in cultured DRG neurons following via cytometry analysis stimulated with LPS or Morphine. All groups are compared to naïve via 1 way anova using Bonferonni correction and as * P<0. 05 **P<0. 01 ***P<0. 001 ****P<0. 0001, Ω p=0. 057

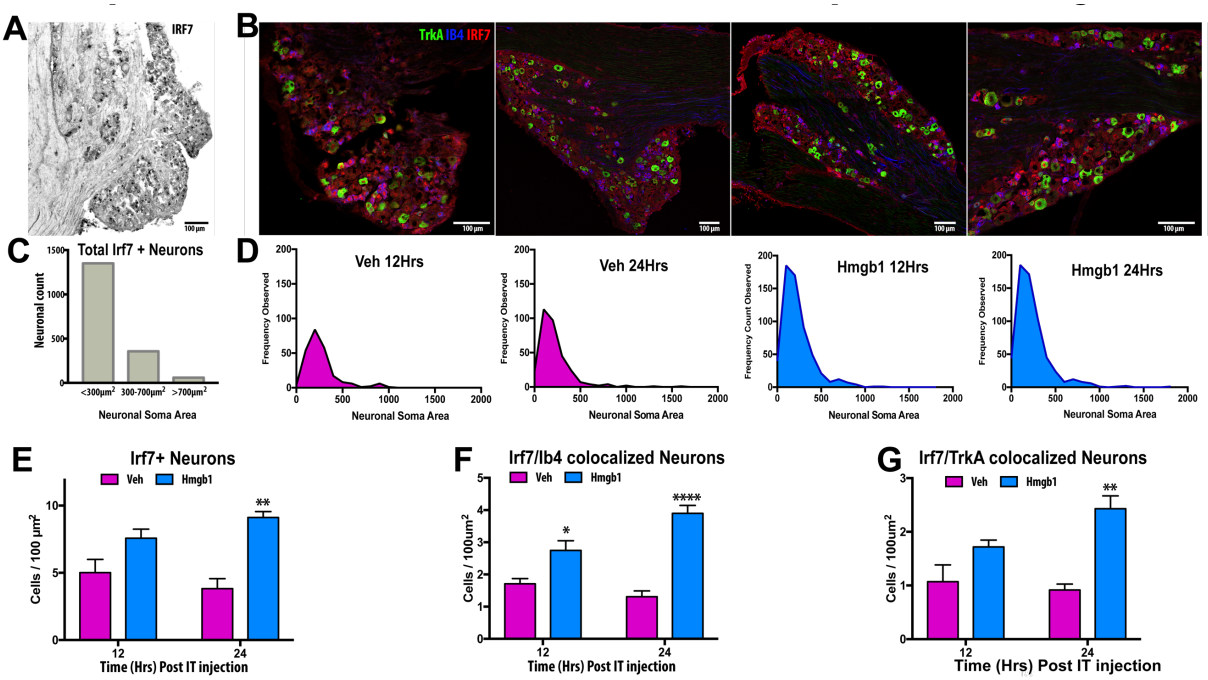

Figure 2-9 IRF7 in the DRG following IT dsHMGB1: Confocal images from C57/bl6 male mice show IRF7 staining nucleii within PFA perfused Lumbar DRG tissue (A). DRGs collected at 12 or 24 hours following intrathecal injection of endogenous TLR4 agonist dsHMGB1 (1μg/5μl) or vehicle control (n=3 per group) show IRF7 colocalizion with small soma Area, IB4(+) non-peptidergic and TrkA(+) peptidergic neurons, as well as some larger non-labelled nuclei (B,C). The total number of IRF7 (+) neurons per area significantly increase in Hmbg1 injected mice at 24 hours (E). The number of colocalized IRF7 and IB4 neurons significantly increase at 12 and 24 hours post injection (F), and IRF7/TrkA colocalized neurons at 24 hours(G).

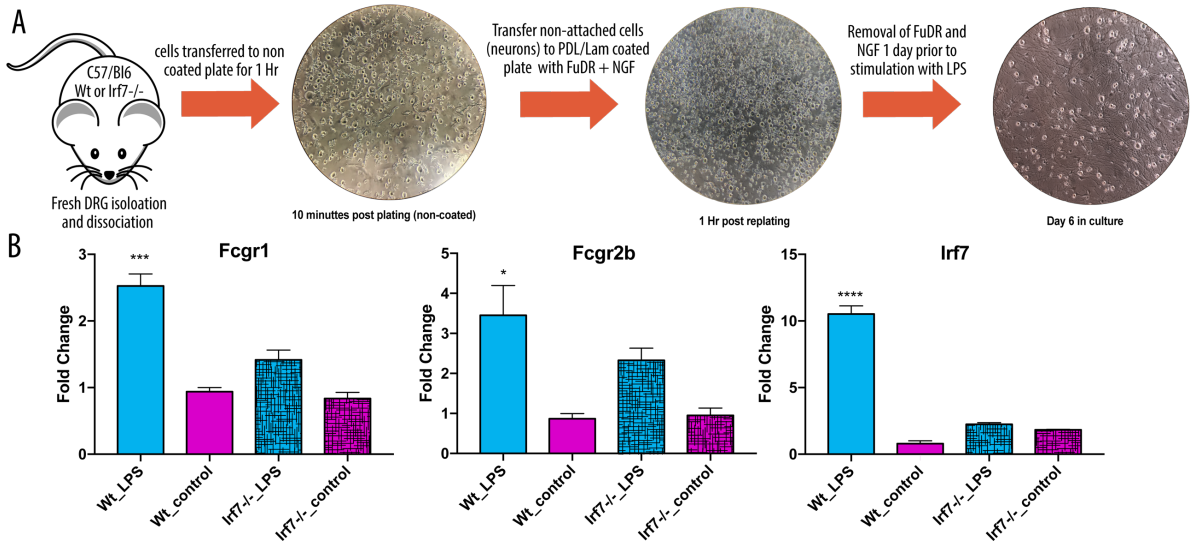

Figure 2-10 IRF7 KO in DRG neuronal cultures: A.) graphical outline of experimental time points highlighting the steps of primary DRG neuronal enriched cultures. B.) Expression of mRNA for Fcgr1 Fcgr2b and IRF7 following stimulation of cultured neurons.

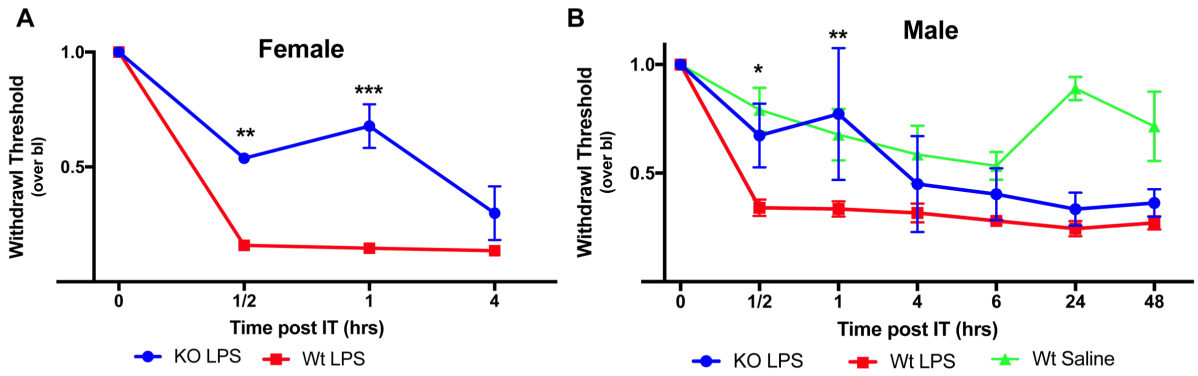

Figure 2-11 IRF7 functional knockout prevents early hyperalgesia following IT LPS: Mechanical withdrawal thresholds from female (A) and male (B) wild type C57/Bl6 and IRF7 deficient mice following IT LPS. * P<0. 05, ** P<0. 01

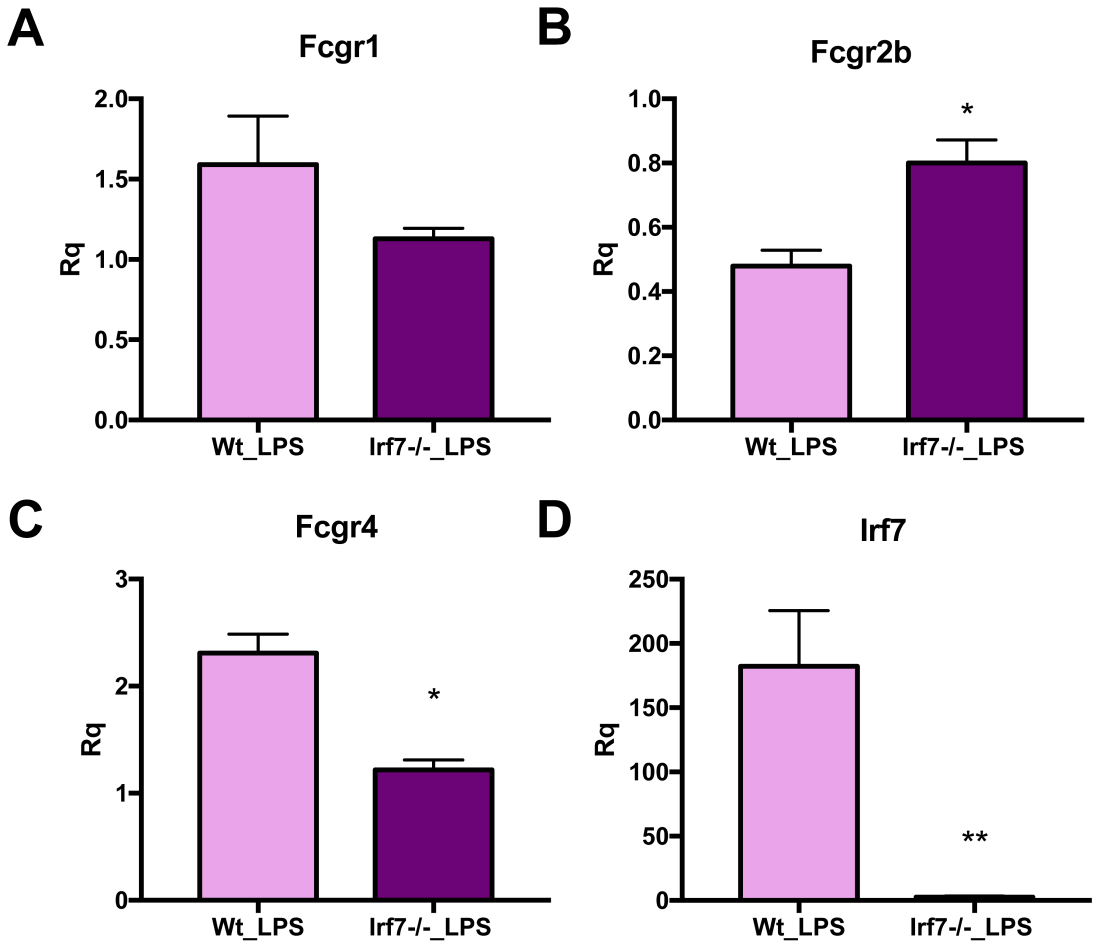

Figure 2-12 IRF7 functional KO in female mice following IT LPS: mRNA expression in the DRG of female wild type C57/Bl6 and IRF7 deficient mice 24 Hours after IT LPS. * P<0. 05 **P<0. 01

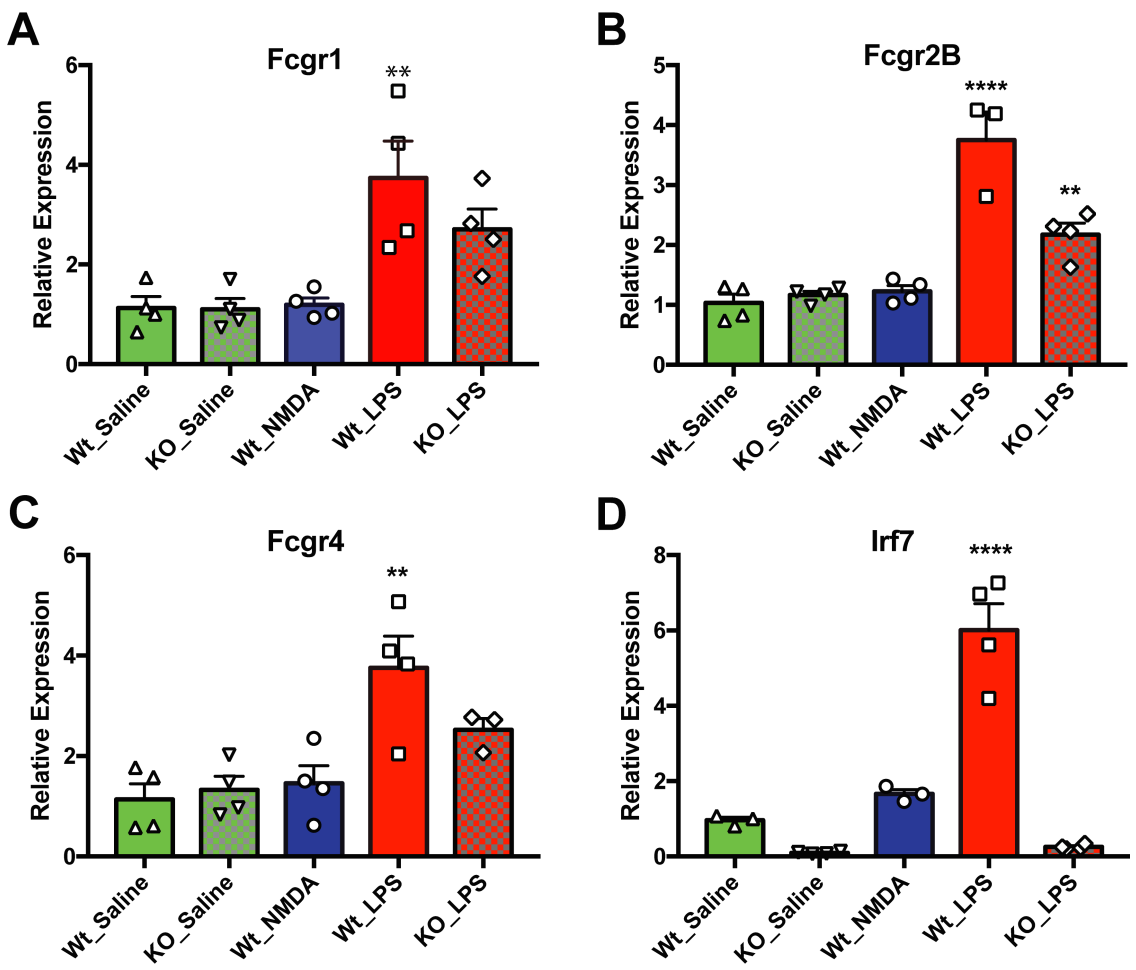

Figure 2-13 IRF7 functional KO in male mice following IT LPS: mRNA expression in the DRG of male wild type C57/Bl6 and IRF7 deficient mice 24 Hours after IT LPS, IT NMDA, or IT saline. A.) Fcgr1 B.) Fcgr2b C.) Fcgr4 and D.) IRF7. One way anova multiple comparisons using Bonferonni correction. Comparing each group to Wt Saline. ** P<0. 01 ****P<0. 0001

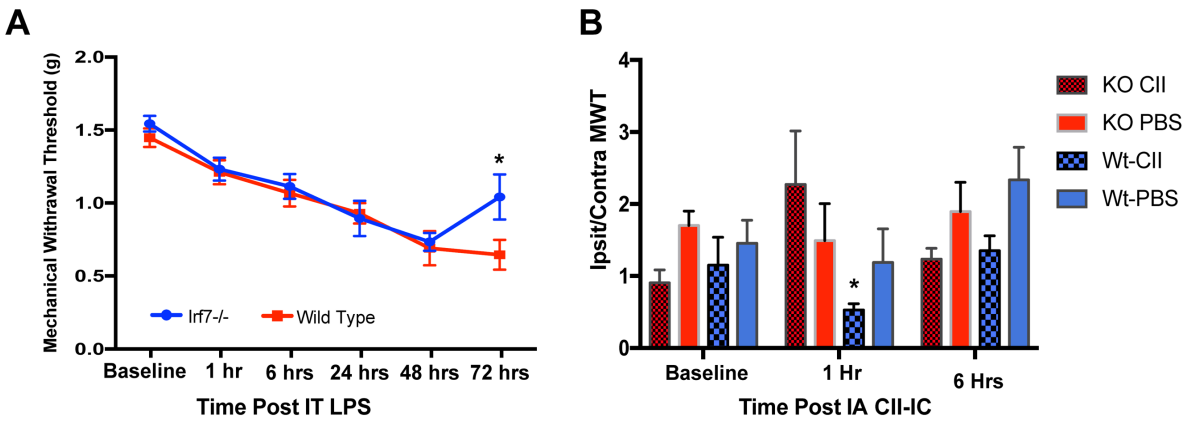

Figure 2-14 IRF7 functional KO reduces hyperalgesia following double hit: A.) mechanical withdrawal thresholds of mice following IT LPS. B.) Mechanical withdrawal threshold following intra-articular injection of CII-IC displayed as ipsilateral over contralateral paw. * P< 0. 05

CHAPTER 3: 3D MACROPHAGES AND MACHINE LEARNING

3. 1 INTRODUCTION

3.1.1 Rationale

The previous studies outlined above have pointed to the importance of the DRG macrophage in mediating changes induced by neuraxial innate immune signaling. This work encouraged me to focus in greater detail on the properties and characteristics of the DRG macrophage population. As will be noted further below, the use of standard macrophage analysis techniques with conventional histochemistry was found to be useful but limiting. DRG macrophages are morphologically complex and often display an amorphous structure. Accordingly, in analyzing such immunohistochemistry, the macrophage will often appear in and out of the plane of the section, making it difficult to count the number of macrophages. One approach was to undertake cell sorting. This however was labor intensive and restricted in the ability to analysis multiple epitopes or the geographic distribution of the macrophage, issues that became of increasing significance when I sought to assess their proximity to blood vessel. I concluded that addressing these issues would benefit from the use of whole mount immunohistochemistry with confocal microscopy. Immediately, I was faced with an enormous complexity in terms of the amount of data generated and to be analyzed. To that end I embarked on developing a machine learning algorithm which permitted an automated analysis of the 3-dimensional confocal images. Development of this methodology, while it took away for the initial primary focus of assessing innate and adaptive immune signaling has enabled the development of an exciting and very promising data set revealing functionality of the DRG macrophage that was hitherto unappreciated.

3.1.2 Complexity of the DRG Organization and its Analysis

We are currently at a really exciting and unique time from both histological and computational perspectives. In the past few years alone there have been a massive expansion in techniques for rendering large tissues, or even whole animals, transparent, enabling us to visualize proteins, cells, structures, tissues, or even entire systems in-situ. Computationally, the task of being able to identify, analyze, or even simply store high resolutions 3 Dimensional datasets, would not realistically have been feasible just 15 years ago. Further, recent advances in graphical processing units (GPUs) have drastically increased their capacity, decreased their price, and led to a large community of programmers among many different fields developing new tools that take advantage of their processing speed. In the work presented here we set out to use these new tools and techniques, as well as develop our own, with the goal of creating and optimizing a pipeline that we can use to better understand the complex organization of the dorsal root ganglion (DRG).

The sensory afferent transduces mechanical, chemical, thermal, stimulation from the exterior to the first order synapse in the dorsal horn. The cell body for the sensory axon lies within the DRG of the respective root. During embryogenesis the roots projecting from the soma to the dorsal horn and the nerve projecting from the soma to the peripheral target arise. During development the cell body moves away from the axon remaining connected by a long sinuous glomerulus, making the afferent a “pseudobipolar” neuron. Of note the glomerulus serves as the conduit by which products synthesized in the cell body are transported to the axon and from there to the central and peripheral terminals. In addition, the glomerulus is able to carry a conducted potential to the soma and therefore induce depolarization of the soma, and conversely, carry potentials from the soma to the axon where that depolarization travels to both the spinal and peripheral terminals. It has come to be appreciated that the DRG is a far more complicated systems than simply the soma and glomerulus for the primary afferent. Several points may be emphasized:

i. The cell-rich portion of the DRG is heavily vascularized. Of note is that the vasculature unlike that in the CNS does not display tight junctions, indicating that this tissue lies outside the blood brain barrier, which characterizes parenchymal tissue[187-189].

ii. Consistent with fact that the DRG lies outside the blood brain barrier, the DRG vessels receive postganglionic sympathetic innervation like other peripheral tissues[189].

iii. The soma of the afferent axon is surrounded by GFAP (+) cells with an astrocyte like phenotype which because this tissue lies outside the BBB are referred to not as astrocytes, but as satellite cells. Satellite glial cells communicate with the neuronal soma though GAP junctions[190].

iv. The DRG is heavily endowed with a population of monocyte derived cells, which because the DRG lies outside the BBB are defined not as microglia, but as macrophages. We now understand that the excitability of the afferent is strongly influenced by the excitability of the DRG afferent soma, the excitability of which is in turn altered by the influence of these macrophage and satellite cells. Accordingly, it has become increasingly apparent that that the primary afferent's excitability can be modified by changes in the local DRG environment, through interactions amongst glia and immune cells and neurons in the DRG[43].

Mouse DRG's are mostly spherical or disk shaped with a diameter around 500μm for the largest lumbar DRGs. Neuronal soma, fibers, satellite glial cells, macrophages, and blood vessels are densely packed into this small niche environment, which lacks archetypical or laminar organization. Thus, when sectioning DRGs one cannot know what cells or what parts of those cells will be in the section. With the diameter of DRG neuronal soma typically ranging anywhere from 15μm to 50μm[191] there is an extremely high likelihood that the section cut through parts of neuronal soma. As the DRG lacks any lamina or way to orient the tissue, this heterogeneous array always requires multiple sections to be analyzed to achieve a meaningful sample size. This problem is best exemplified by focusing on the macrophage. Macrophages in the DRG have a

complex morphology and no discernable orientation. In DRG sections, it becomes extremely difficult to identify single macrophages, as their processes may show up as disparate from their actual cell body as they pass in an out of the plane of sectioning. One way to overcome this limitation has traditionally been to dissociate tissue and isolate the tissue specific macrophages and then analyze them via flow cytometry. However, in doing so, we lose the cellular morphology and contextual information (e. g. arrangement within the DRG) that may be of interest in identifying sub populations which may be assumed by their size or the types of cells with which they may be in contact. Such discrimination has become increasingly noteworthy as macrophages have also recently been implicated as contributing to behavioral hypersensitivity as occurs in model of neuropathic pain[192]. As such we set out to find an improved methodology for studying macrophages in-situ in the DRG.

The DRGs relatively small size makes it ideal for a “whole-mount” methodology. The small size makes it amenable to staining, clearing, and imaging the entire tissue, without the need for sectioning, or embedding. Here we present methods I developed for processing the DRG, staining the tissue, enabling the use of high-resolution confocal microscopy as well as the analytic pipeline and tools that I created to obtain high quality, and high throughput data from 3D image stacks to permit qualitative and importantly quantitative data to analyze DRG components. Further, as noted above, the DRG is densely vascularized with fenestrated blood vessels. And accordingly lies outside the BBB. This indicates a high likelihood of vascular permeability, which would also make the primary afferents susceptible to circulating agents[188]. Here we explore whether fluorescently labeled agents can make it into the DRG and use our newly developed techniques to assess the cell types and quantities of agents making it into cells. To characterize the power of this technique and along with the appreciated importance to DRG function we asked whether we could identify changes in macrophages in a model of innate immune mediated pain, I undertook to assess changes in macrophage activity induced by i) the spinal activation of TLR4 signaling through the intrathecal delivery of lipopolysaccharide (LPS), and ii) the systemic

delivery of cisplatin to produce a chemotherapy induced poly neuropathy (CIPN). Further to assess the ability to define the evoked effects on macrophage function generated in the DRG downstream to TLR 4 signaling, I examined the effects of intrathecally delivered of A1 Binding protein (A1BP) which is known to block TLR4 signaling on the changes induced by the cisplatin polyneuropathy[193]

3.2 METHODS

3.2.1 Animals

All animal experiments were carried out according to protocols approved by the Institutional Animal Care and Use Committee of UC San Diego. Mice were housed with up to 4 littermates per cage, and given food and water ad libitum, in a temperature-controlled facility with 12-hour light dark cycles. Wild type C57/Bl6 mice were purchased from Jackson Laboratory and Ccr2 KO mice, $Ccr2^{rfp/rfp}$ mice (B6.129(Cg)-*Ccr2*$^{tm2.1Ifc}$/J; stock017586), were purchased from The Jackson Laboratory (Bar Harbor, ME) and bred and maintained at UCSD. In this strain, a monomeric red fluorescent protein (RFP) sequence replaces the coding sequence of the Ccr2 gene, abolishing gene function.

.

3.2.2 Chemotherapy induced peripheral neuropathy (CIPN)

CIPN was induced using cisplatin (CIS; 2. 3 mg/kg/day; n =15) (Spectrum Chemical MFG. , Gardena, CA, USA) given intraperitoneally two times at D1 and D3. Saline (SAL; 0. 9% NaCl; n=5) was injected in control mice.

3.2.3 Intrathecal drug delivery

Mice were anaesthetized with 2-3% Isoflurane, and the respiratory rate was monitored via observation. Stock LPS (50µL aliquots at 2mg/ml stored in -20°) was diluted (10µL stock/ 90µL

saline) to a final concentration of 0. 2μg/μL, AIBP was diluted to 0. 5μg/5μ and Saline (NaCl 0. 9%) for controls. AAV9-mCherry was generously donated by Prashant Mali (UCSD) and was delivered at $1xe^{12}$ total viral particles. Injections were performed as follows: A 25μL Hamilton syringe affixed to a 30g needle via polyethylene tubing PE10 was first flushed with sterile water and then loaded with 5μL of LPS. The 30g needle was then inserted between L4-L5 intervertebral-space until a tail twitch was observed. The injection was performed slowly, during which, any compression of the air bubble within the tubing was be observed and noted as an indication of impeded flow.

3.2.4 Mouse IT AIBP

Seven days after cisplatin induced CIPN, AIBP (0. 5μg/5μl) or Saline (NaCl 0. 9%/5μl) were injected in mice by intrathecal injection performed as previously described[194]. Mice were anesthetized using 3% isoflurane for induction and 1. 5-2. 5% for maintenance of anesthesia with mixture of 50% oxygen and 50% room air. The lower back was shaved and the animal was placed in a prone posture so that the pelvis could be held between the thumb and forefinger. The L5 and L6 vertebrae were identified by palpation and a 30G needle was inserted percutaneously on midline between the L5 and L6 vertebrae. Successful entry was assessed by the observation of a brisk tail flick. Following recovery from anesthesia, mice were evaluated for normal motor coordination and muscle tone.

3.2.5 Tissue collection

Mice were deeply anesthetized with isoflurane, and then euthanized with 0. 1ml of Beuthenasia (Merck) delivered into the intraperitoneal space. Mice were then transcardially perfused with ice cold saline followed by 4% PFA and post-fixed in 4% PFA for 24 hours, then stored in PBS with 0. 02% sodium azide. The spinal cord and DRGs were exposed via laminectomy using fine bone trimmers along the entire vertebral column. L3-5 DRGs were

identified by following the sciatic nerve and DRGs were collected via using jewelers' forceps to carefully grab the peripheral nerve leaving 0. 5-1cm of both peripheral nerve and dorsal root intact. Leaving the nerves intact gives something to hold on to with the forceps when performing histology and mounting later and helps prevent grabbing the cell body rich portion of the DRG, which can cause damage that readily shows up when imaging.

3.2.6 Design and materials for imaging chambers

Imaging chambers were designed and modeled in Autodesk Fusion 360. PLA, PETG, Nylon, and Polypropylene chambers were printed on a heavily modified wanhao duplicator i3. PLA and PETG chambers were printed using a glass bed, nylon chambers were printed on a garolite bed, and polypropylene was printed onto (polypropylene) packing tape fixed to a glass bed (for all tested chamber materials and printing method see table 3-1). Resin chambers were printed on a Formlabs, Form1+ using 3Dresyn CR UHT, or ApplyLabWork Tan resin. Chambers were designed to be leakproof and safely used with a 10x air, 20x air or 63x water immersion objective on an inverted Leica SP5 confocal microscope. This was achieved by confining the specimen to within the maximum bounds the objective could move without hitting the chamber wall. These bounds were then incorporated into the chamber design such that microscope coverslips could be securely fixed to the chamber with a suction tight seal within the chambers 1mm (figure 3-1) The leakproof seal was achieved by fixing the printed chambers to glass microscope slides using low viscosity cyanoacrylate glue and sanding the coverslip resting lip smooth with increasing grit wet/dry sanding paper with 150, 250, 400, 800, and 1500 3000 fixed to a 22mm wide flat aluminum bar. The chambers were designed to be used with 22x30mm coverslips and tested for a leakproof seal by pressing on the center and sides of the coverslip with Pasteur pipette attached to a vacuum flask and aspirating any clearing medium until sealed (figure 3-1). Immediately following imaging, we remove the coverslip, and wash the mounting

medium out of the chambers/slide, wiping it with Kim Wipes, and avoiding scratching the glass. Multiple DRGs can be imaged in one chamber, but we generally only use one at a time.

3.2.7 Tissue clearing for preserving native fluorescence

DRGs from cervical, thoracic, lumbar and sacral were dissected out and immediately cleared following the RTF method outlined by Yu et al. [195]. In brief perfusion fixed DRGs were collected and washed in PBS and then immediately placed in a solution of 30% triethanolamine (TEA), 40% formamide, (F) and 30% nanopore water (H_20) for 15 minutes at room temperature on a shake plate, then transferred to a solution of 60% TEA, 25% F, and 15%H_20 for 15 minutes at room temperature on shake plate, and finally transferred to a final solution of 70%TEA, 15% F, and 15% H_20 for 15-20 minutes (until clear). DRGs were then transferred into imaging chambers mounted on glass microscope slides (Figure 3-2 B).

3.2.8 Tissue clearing for immunohistology

DRG clearing and staining were performed using a slightly modified version of the iDISCO and or fDISCO protocols. We found that DRGs are small enough that pretreatment is not always necessary, cutting the time tissue working time down significantly. The Protocol we followed when staining DRGs for Iba1 (Wacko, 1:1000), CD-31(BD Pharmigen,1:50), NeuN (1:300), mCherry(Rockland, 1:1000) DAPI(1:10,000), was as follows. All washing steps were done in 12 well plates with transfer baskets and all incubations were done in tightly sealed Eppendorf tubes or glass vials. DRGs were washed 3x 15 minutes in PTx. 2, incubated in permeabilization solution for 2 hours at 37° C on shake plate, transferred to blocking solutions for 2 hours (or o/n) at 37°C on shake plate. DRGs were then incubated with 1° antibody for 24-72 hours at 37°C on shake plate. If DRGs could be combined, this helps to save reagents, and 1. 5ml Eppendorf tubes can be used. If DRGs must be stained individually then a rack of PCR tubes with 200µls of solution works fine. DRGs were then washed 5x 15 minutes in PTwH and incubated in secondary antibody

solutions in PTwH/3% serum for 24-72 hours at 37°C on shake plate. Finally, DRGs were then washed 1x for 1-2 hours in PTwH + Dapi 1:10,000, and then washed 5x 15 minutes with PTwH prior to clearing. For tissue clearing we found that THF often works better than methanol, but is more difficult to work with, as it can't be stored in plastic vials. We therefore perform the THF dehydration steps in tightly sealed glass vials and Dehydrate in THF/H20 series as follows: 50%,70%,80%,100%, 100%, Then DCM 33%/THF 66%, 100%DCM and finally 100% DBE (Figure 3-2A). We observe quite a bit of shrinkage of DRGs cleared with DBE in this manner, but this actually helps in some cases by decreasing the volume of the DRG to be within the working distance of the higher magnification objectives. DRGs become completely invisible to the naked eye within seconds to minutes of being submerged in DBE so we found the best way to not lose DRGs, is to always add DAPI. This enables you to use a weak UV light, with UV glasses, to easily visualize the glowing DRG. DRGs can be stored long term in DBE at 4°C or shorter periods at room temperature.

3.2.9 Imaging

Imaging was done using an inverted SP5 confocal microscope with 10x air, 20x air, and 63x water objectives. The 63x water objective used is ideal for high resolution imaging of the DRG as it's working distance is roughly 400µm, which can travel the entire depth of most DRGs. In order to best control for photobleaching and loss of fluorescent intensity at deeper tissue depths, we always optimized settings for the lowest laser signal intensity that effectively gave us signal and made sure that z stacks begin at the deepest tissue first and end at the most superficial.

3.2.10 Image analysis pipeline

Our image analysis pipeline is currently composed of a docker image with GPU support, which we are making freely available to anyone who wishes to use it. The docker contains all dependencies necessary to run the analysis pipeline, which is in the form a shell script. The shell

script takes a file directory as the input and is currently designed to support up to 3 channel image stacks. The shell script first identifies the image channel containing macrophages, and runs them through either a 3D UNET[196] or 2D UNET[197]. Models we created using yapic (Image and Data Analysis Facility, DZNE). For input image training we manually labelled 5-10 macrophages as they traversed through 20-30 image stacks, as well as what we defined as noise. We then used these labels as the ground truth labels for training data. Training data was performed for at least 1000 epochs with 50 steps per epoch on a Nvidia Quadro P5000 GPU. When raw macrophage images are run through the resulting model, we get binary outputs of individual macrophages. The pipeline then performs connected component analysis using CLIJ[198] in imageJ. Blood vessels are then segmented in imageJ using a set of filters run on image stacks with CLIJ (Figure 3-4). Macrophages are then classified as either perivascular, or non-perivascular based on their proximity to blood vessels. The resulting classified macrophage ROIs are then placed into the original raw images where their volume and morphological characteristics are quantified, along with the intensity characteristics of the raw image channels. Finally all the data generated from images within the input folder is combined into one annotated spreadsheet, and some basic statistics are performed (Figure 3-4). We also analyzed each dataset using Imaris to compare our results to those generated with the commercially available software.

3.3 RESULTS

3.3.1 Best materials for 3D printed imaging chambers

Through iterative design and 3D printing I was able to test out imaging chambers made from many different materials (table 3-1). The chambers themselves are what enable us to image whole mounted DRGs on our inverted confocal, without ruining our objectives. Therefore, we first needed to find the best materials to use for making the 3D printed chambers. I was able to achieve the best results using an SLA printer using 3Dresyn CR UHT. These chambers were easily made

perfectly flat and were able to be reused, with over 100 uses they failed to degrade or to fall off the slide when glued with low viscosity cyanoacrylate (Figure 3-1). For FDM printers I initially thought that nylon would be the best material, as it is the most resistant towards chemicals, however, nylon printed chambers did not stay glued to the glass microscope slide well, and polypropylene printed chambers were concluded to be superior. Polypropylene chambers capable of 30-80 uses before they become unglued, so I recommend making sure they are securely attached to the slide before mounting tissue (Table 3-1).

3.3.2 DRG histology of native fluorescence vs IHC

When trying to analyze native fluorescence of virally transfected DRG neurons I found that many of the available clearing techniques quenched the fluorophore. I then found that the RTF method (Figure 3-2,B and Table 3-3) retained significant amounts of native fluorescence. RTF is also beneficial in that we could quickly and efficiently analyze DRGs in a high-throughput manner and was by far the fastest, and easiest of the tissue clearing methods. I could have DRGs imaged within 1 hour of collection and achieve a good depth of penetration (> 100μm) resulting in high quality images (Figure 3-3,C). Virally labeled DRG neurons could be imaged at a high resolution for stunning reconstructions of DRGs and tracing of individual axons, even to their points of bifurcation and beyond (Figure 3-3,D). RTF also diminishes the shrinkage of tissue due to dehydration. The tissue clarity with RTF, however, significantly lower than with our modified iDISCO (DBE), and we also noticed that some stains were quenched when left in RTF solutions.

For any immunohistology, and long-term storage of tissues, we used an iDISCO protocol. This yielded better quality, greater clarity, and increased signal to noise ratio over RTF, especially when staining the large L4 DRGs (Figure 3-2,A; Figure 3-3,Table 3-2). Therefore, for all immunohistology we followed our protocol outlined above and in Figure 3-2 panel A.

3.3.3 Pipeline for 3D image analysis of DRG macrophages

As mentioned above we have a great interest in macrophages and pain but found it difficult to accurately quantify their activation state using traditional methods. Even after developing our techniques we found it difficult to analyze these large 3-dimensional datasets using freely available software such as imageJ. The limiting factor lies in the difficulty of normalizing the signal and noise intensities over an entire stack of images and finding any way of thresholding so that individual cells were isolated and represented. I was able to manually segment and quantify macrophages when using Imaris (Bitplane, Belfast UK), but this software is costly and time consuming. Therefore, I turned to machine learning to accurately and effectively isolate signal from noise in imaging stacks. An expert observer sparsely labeled signal and noise from a sample of images taken from different depths, with different intensities, and under different conditions, as a representation of any macrophage images that our model might come across (Figure 3-4). I also trained a 3D model using stacks of 30 images where 5-10 macrophages were individually labeled in every image. These models were trained for up to 2000 epochs (Figure 3-4,B), and resulted in highly reproducible and accurate predictions (Figure 3-4,C).

I then wanted to create a pipeline that would be able to take our raw images, segment macrophages into meshes, and place those meshes back into the original raw images and quantify macrophages by morphological features as well as staining intensity and even classify macrophages by the cell type/structure with which they had contact. To do so I first created a series of ImageJ macros, outlined in Figure 3-5. These were strung together with a shell script, that can easily be modified to change parameters. Since the program we currently use to run our macrophage model only works on Linux, I created a docker file that contains all the necessary packages (including tensorflow-gpu, fiji, our scripts, yapic). This platform was chosen as it should be system agnostic and run on any platform with a sufficiently powerful GPU. While, these datasets are large (each image stack around 1-2gb) the speed and power of GPU was leveraged

based calculations and image manipulations to allow processing of each stack to occur on average in 2-4 minutes.

The pipeline as shown here first identifies macrophages (Figure 3-6, Top row), then classifies them as either perivascular, meaning they are in physical contact with a blood vessel, or non-perivascular (Figure 3-6, Bottom row). This classification first came from observing that macrophages riding along blood vessels had a very different morphology from those not touching blood vessels. The pipeline then outputs data tables for each cell as well as a 32-bit label map, where each cell is given a unique gray scale value. We can then set a lut such that each cell is randomly colored, which can be used after the fact to visualize the results as either 2D z projections or 3D reconstructions (Figure 3-6, Bottom). This helps to assess the quality of macrophage segmentation, and assess whether multiple cells were clumped together, or if any cells were split apart.

3.3.4 DRG macrophages activation following intrathecal LPS

To validate our methods and pipeline, we decided to use intrathecal LPS induced pain as a model where macrophage activation would likely occur. Visually we could see a difference between wild type C57/Bl6 mice with IT LPS as compared to those with IT saline (Figure 3-7,A). In order to determine if the difference we observe is due to infiltration of macrophages we injected *Ccr2*$^{-/-}$ mice with IT LPS. Lacking the CCR2 chemokine receptor renders monocytes and macrophages incapable of being recruited during immune response, thus, indicating whether an increase in macrophages is observed due to infiltration of circulating macrophages, or local proliferation. We analyzed these images using imaris and found that the percent volume of macrophages in the DRG increases following IT LPS in *both* wild type and *Ccr2*$^{-/-}$ mice (Figure 3-7, B). We validated the Imaris results with our own pipeline (Figure 3-7. C). With our pipeline, we could also determine how many macrophages were present per sample, and determined that in contrast to the vast proportion of literature, there was in fact *no increase* in the number of DRG

macrophages (Figure 3-7,D). While the percent change in volume observed is mainly driven by changes in the perivascular macrophages, we can also see that there is an increase in the volume of both individual perivascular and non-perivascular macrophages when wild type mice were given IT LPS.

3.3.5 DRG macrophage activation in CIPN

To further test our pipeline, we examined the role of DRG macrophages in CIPN using Cisplatin. Within 2-6 days following Cisplatin injection, mice exhibit a mechanical hyperalgesia (Figure 3-8,A). We performed flow cytometry on DRG macrophages isolated from Cisplatin injected, or vehicle injected mice on days 3,10, and 17, we were unable to detect any differences (Figure 3-8,B).

AIBP was able to significantly reverse hyperalgesia in Cisplatin injected mice 24 hours after AIBP injection (Figure 3-9,A). Mechanical withdrawal thresholds in mice treated with AIBP returned to normal within 72 hours of a single injection. We therefore collected DRGs from mice at day 10 and stained them for whole mount analysis. We found that perivascular macrophages in the DRG significantly increased in percent volume on day 10, in CIPN mice, while macrophages in mice treated with AIBP appear normal (Figure 3-9,B-C). Contrary to what has been described by others, we did not observe and significant change in the number of macrophages in the DRG (Figure 3-9,D) but again did observe that activated macrophages had an increase in size compared to naïve macrophages, and a single injection of AIBP either prevented, or reversed macrophage activation (Figure 3-9,E)

3.4 DISCUSSION

In assessing DRG staining and clearing protocols we set out to determine the fastest and most efficient methodologies. Our goal was to establish techniques that would enable us to perform image acquisition and data analysis in the same amount of time that it would take to cryo-

protect, section, mount, and stain DRGs. Further many of the protocols currently available claim to work for native fluorescent markers such as GFP or RFP however we often found that native fluorescent signals were greatly diminished during the dehydration and or clearing stages. This was true of all but the RTF clearing protocol, which also happens to be the fastest, and easiest. As such we recommend using this method for rapid analysis of native fluorescence.

The pipeline we have created shows the power of using machine learning to separate signal from noise and help identify individual cells. This same basic method could be used on any cell type, and indeed there has recently been a vast increase in use of AI in doing such. We initially came up with our classification of perivascular and non-perivascular through observation that perivascular macrophages had a distinctly different morphology, and were often longer and straighter, that non-perivascular macrophages which usually appear to have more of a crescent shape (likely due to surrounding a neuronal soma). We hypothesized that these may be two distinct populations of macrophages sharing a single niche, which may serve different purposes.

With our modular image analysis strategy we can easily change parameters, for instance we could explore if macrophages in contact with specific cell types are changing in response to pain-states, one would simply stain CGRP positive neurons and instead of isolating macrophages in contact with blood vessels it would isolate macrophages in contact with CGRP positive neurons and structures. We have also imagined this pipeline could be used to combine multiple stains of macrophages to get flow cytometry quality data, but also morphological characteristics and cell quantity as well. We have performed some of these analyses and have shown that we can use molecules like fluorescently labeled dextran’s, which are taken up by macrophages (not shown here).

In the work presented here, we performed some relatively simple proof of principle experiments that our pipeline is functional and found that it is extremely sensitive to treatments that perturb DRG macrophage function. First, we compared our results to those obtained using Imaris and obtained comparable results. Imaris, while useful, is both expensive, and requires

extensive user input in setting thresholds for each individual image stack. This leaves the user with the possibility of introducing bias, even when blinded. For instance, it is often easy to distinguish between LPS and Saline treated DRG macrophages just by looking at the resulting images, which is something a user must do when manually setting thresholds. Our pipeline's use of machine learning eliminates any potential user bias from the analysis, and yet obtains the same results in terms of changes in percent volume of macrophages.

The use of flow cytometry on our CIPN mice was unable to determine a difference between vehicle and CIPN treated macrophages, but using our techniques and pipeline we were able to readily observe a robust difference between vehicle and CIPN treated mice, and show that the therapeutic agent, AIBP, not only diminished hyperalgesia, but also decreased macrophage activation, or prevented it all together. It is interesting to note that in the CIPN model we observed no change whatsoever in the percent volume of non-perivascular macrophages, whereas IT LPS caused a potential trend in activation of all non-perivascular macrophages and increase in the size of individual macrophages. We hypothesize that this may be due to perivascular macrophages acting as gate keepers to the DRG and sampling the blood, which would mean they come in more contact with circulating cisplatin. This paves the way for potentially identifying a new class of DRG macrophages and warrants further research.

Often infiltration of macrophages has been described in the literature following injury [199, 200], and following paclitaxel[201] and vincristine[202] induced peripheral neuropathy. Treatment of rats with minocycline (suppressing macrophage/microglia activation) has been shown to alleviate hyperalgesia following oxaliplatin induced CIPN[203]. Many of these experiments have used traditional techniques of quantifying macrophages and often come to the conclusion that increased infiltration, and or increased numbers of macrophages are present. However, here we describe that one potential pitfall with traditional histology approaches is the amorphous organization and orientation of macrophages, which could lead to slice histology observing more cells, when in fact there may simply be larger cells with more processes. that pass in and out of

the plane of section. Thus unexpectedly, given the extant literature, in none of the experiments and quantifications performed here, did we observe significant differences in the number of macrophages in DRGs following any treatments. This also holds true in the CCR2 knockout mice, which should have no infiltration of monocytes or macrophages into the DRG. Thus, we believe that the increase in percent volume of macrophages often observed, is actually due to an increase in the size of DRG macrophages that are present.

3.5 ACKNOWLEDGEMENTS

Chapter 3 is currently in preparation for submission as: Matthew A. Hunt, Harald Lund, Lauriane Delay, Juliana Navia, Sara Hunt, Gilson Dos Santos,Tony L. Yaksh. Three dimensional study of macrophages in the DRG: Tools and techniques. The dissertation author was the primary researcher and author of this material.

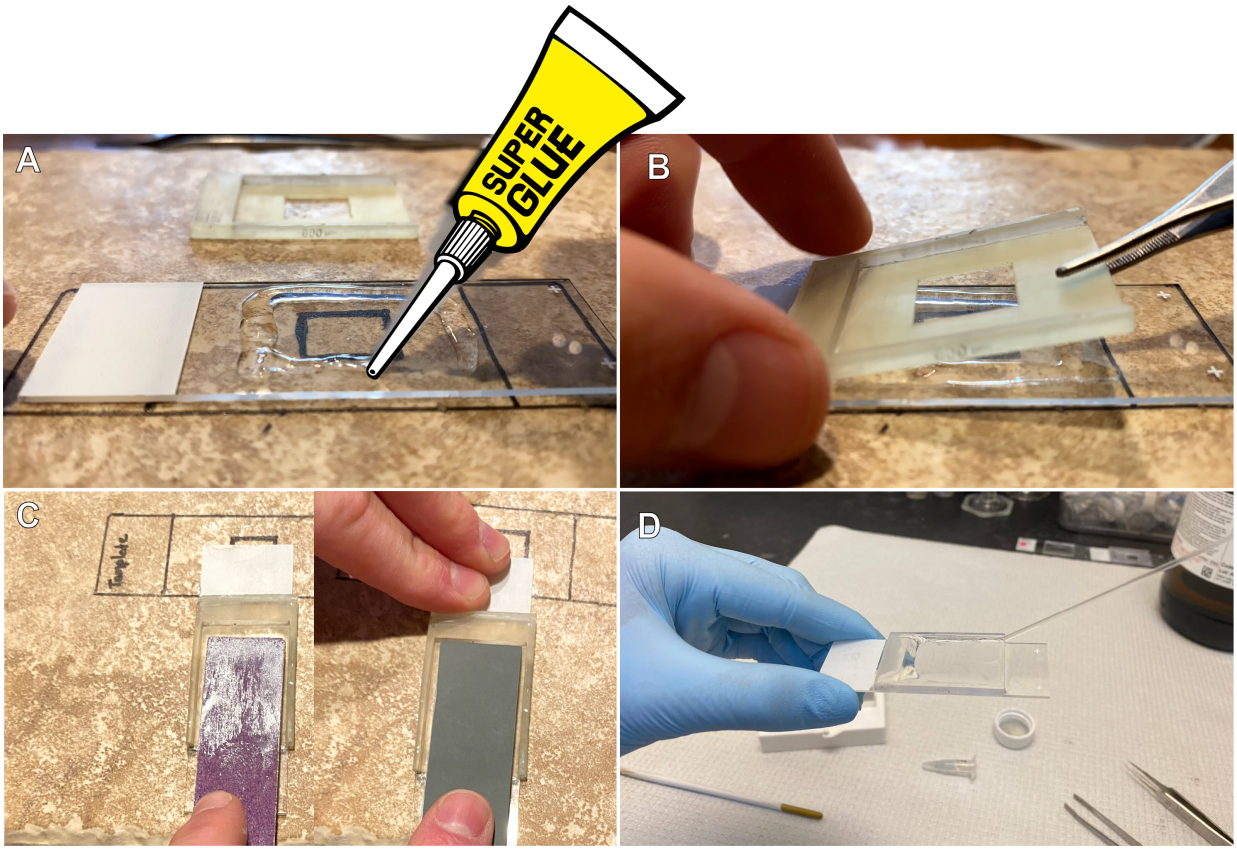

Figure 3-1 : Making DRG chambers: Chambers are printed in a resin SLA printer. Glue is placed on a microscope slide (A) and the chamber is then attached (B). Chambers are then flatted to make sure they will form a perfect seal with sandpaper grits from 200-3000 (C). Tissues are mounted in their respective clearing medium and then any additional medium is removed via aspiration with a fire polished Pasteur pipette affixed to a vacuum flask (D).

Table 3-1 : Chamber materials

Material	Bed	Printer Type	Print Temp/Setting	RTF-solutions	DBE	Notes
PLA	Glass	FDM	205-215	-	-	Colors leech and degrades quickly
clear PETG	Glass + Glustick	FDM	220-240	+	-	
Nylon	G10	FDM	240-260	-	-	nylon does not glue well to glass
PolyPropylene	Packing (PP) Tape	FDM	230	++	++	Holds up well
ApplyLabWork Tan	Alluminum	SLA	Formlabs Grey	++	+	degrades after 10-15 uses
3Dresyn CR-UHT	Alluminum	SLA	Formlabs Clear 3	+++	+++	Easiest to work with and longest lasting

Table 3-2 : Histology solutions

Histology Solutions	**PBS-Az**	100mL 10x PBS 0. 2g Sodium Azide (NaN_3) 900mL Nanopure H20
	PTx. 2	2 mL TritonX-100 998 mL PBS-Az
	PTwH	2 mL Tween-20 1 mL Heparin (10mg/ml)
	Permeabilization Solution	23g Glycine 200 mL DMSO 800 mL Ptx. 2
	Blocking Solution	3 mL Serum 5 mL DMSO 42 mL PTx. 2

Table 3-3 : Solutions for clearing DRGs to preserve native fluorescence

RTF (Native Fluorescence) Clearing Solutions	**RTF1**	Triethanolamine-30% Formamide-40% Water-30%
	RTF2	Triethanolamine-60% Formamide-25% Water-15%
	RTF3	Triethanolamine-70% Formamide-15% Water-15%

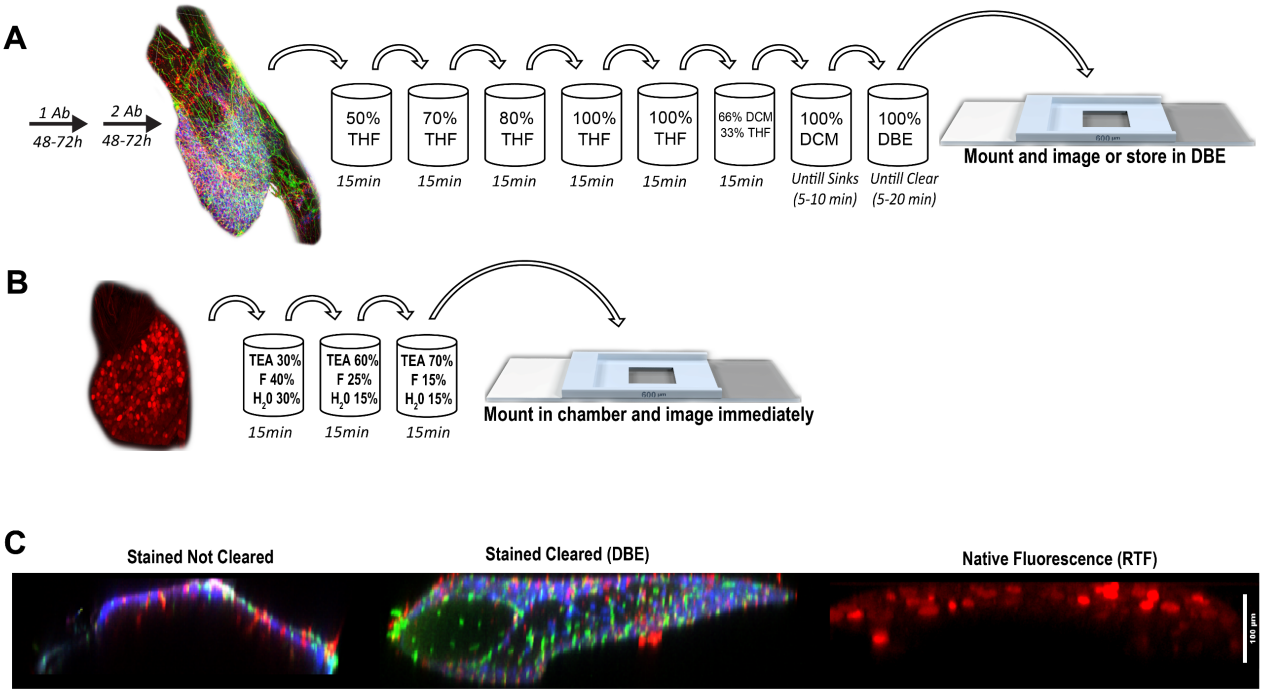

Figure 3-2 : DRG clearing protocols: A.) Process for Immunohistochmemistry showing our abbreviated version of iDISCO. B.) Process for imaging Native Fluorescence of virally transfected DRG neurons expressing RFP. C.) Comparisons between stained but not cleared DRG, a stained DRG cleared with DBE, and the native RFP fluorescence of a DRG cleared with RTF. (stained DRGs are here are stained with Iba1(red), NeuN(blue), and CD31 (green). All images were taken at 10x and displayed is the XY axis with scale bar 100µm.

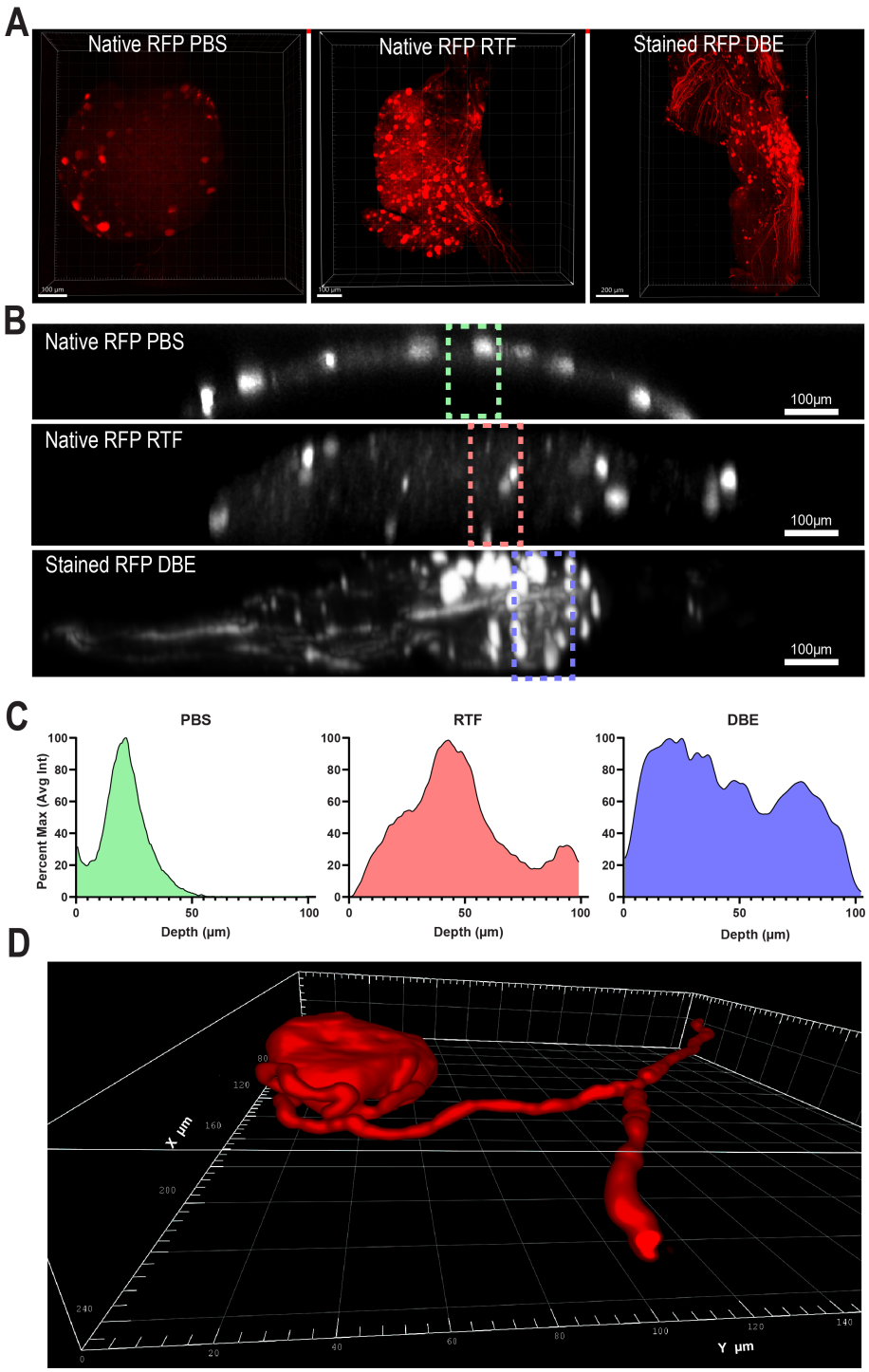

Figure 3-3 Virally transfected DRG neurons: A.) Representative images of virally transfected DRG neurons cleared with PBS, RTF, or iDISCO/DBE. B.) Representative images of showing the depth of imaging. C.) Intensity of ROIs shown in B. Average intensity from pixel rows was calculated then displayed as percent of max average intensity as a function of imaging depth. D.) Reconstruction of native fluorescence from virally transfected neuron illustrating the golumerular structure of the extending axon and tracing the axon to the point of bifurcation and beyond.

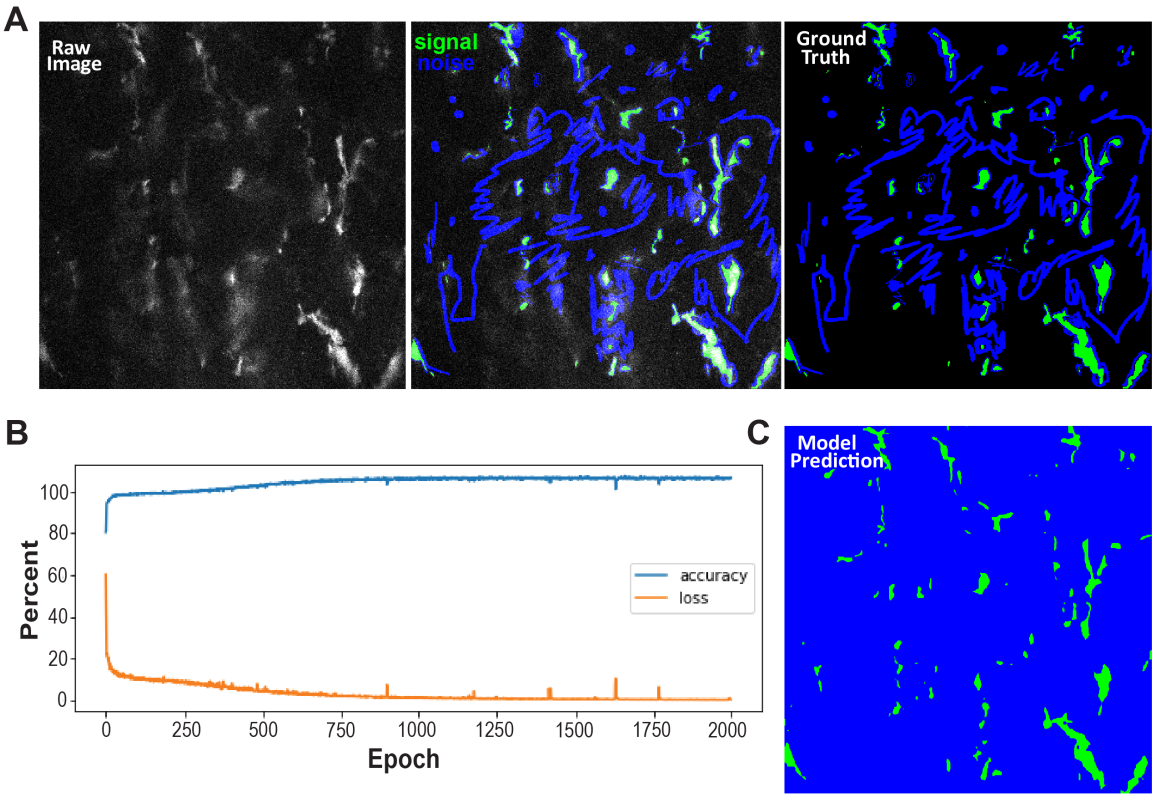

Figure 3-4 Macrophage training: A.) Sample of raw grayscale image of Iba1 stained macrophages in the DRG. Signal (green) and background is manually drawn by an expert. True signal vs noise then becomes a set of ground truth images for each raw image. B.) Training of this model was done for 2000 epochs showing accuracy increasing as loss decreases. C.) The results of running the raw image through the trained model where blue is background and green is macrophage signal.

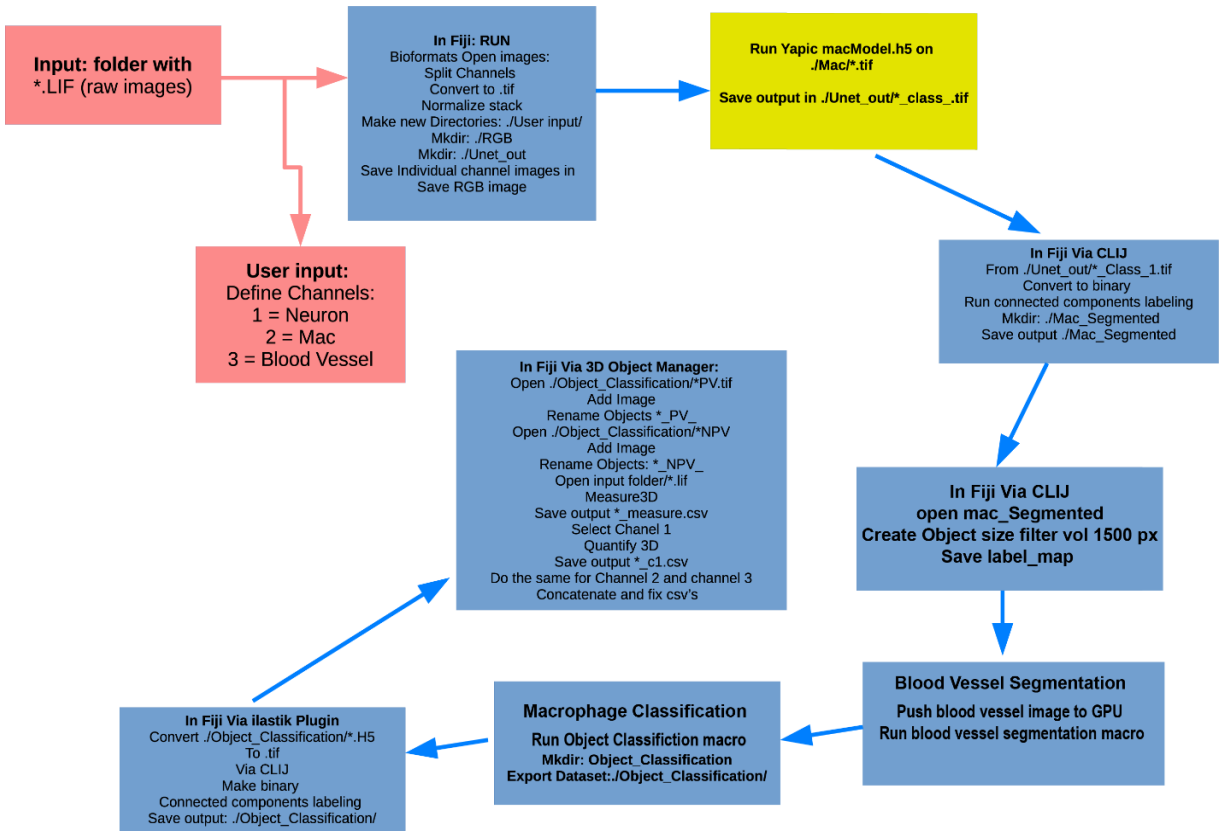

Figure 3-5 Flow chart of image analysis pipeline: Flow chart displays the paths and commands directed by the shell script. User input steps are displayed as salmon colored boxes. Fiji macros are in blue boxes and yapic is in yellow. Macros can easily be swapped out if changes to quantifications are desired.

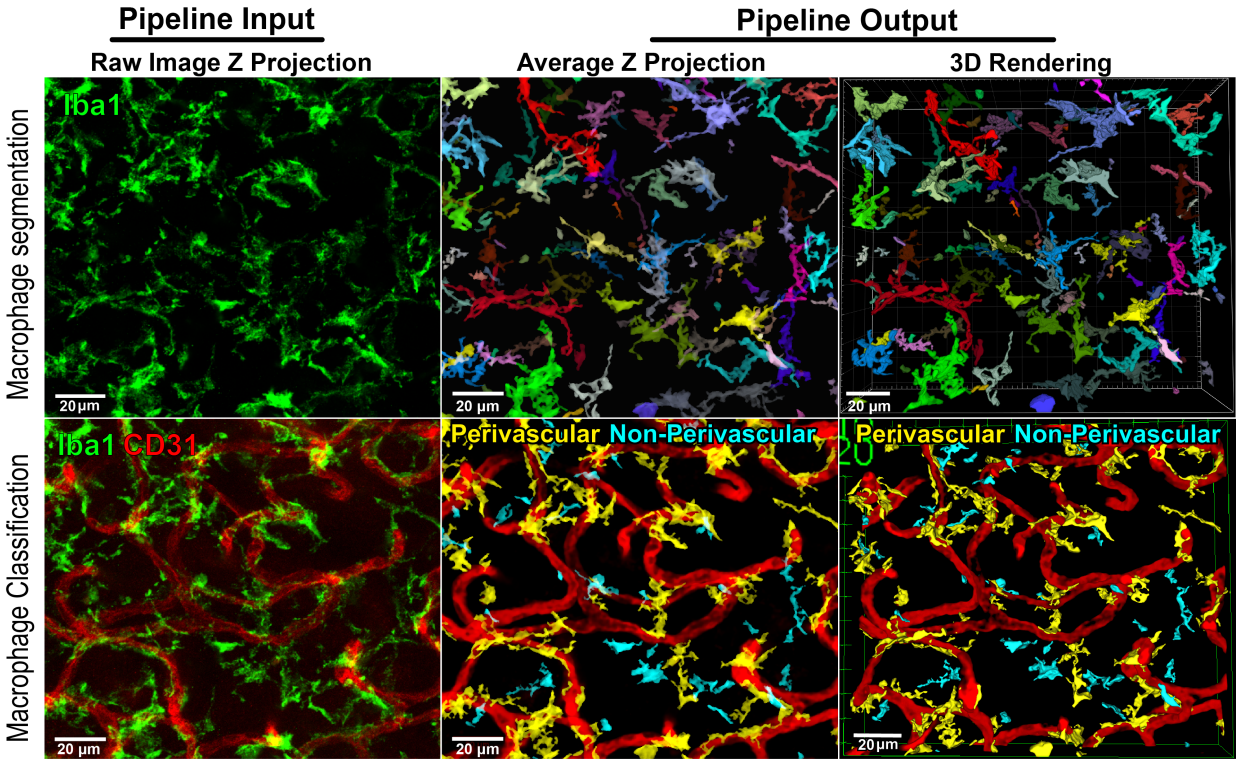

Figure 3-6 Image analysis pipeline example: Segmentation and identification of DRG macrophages Top row shows the input and output of a representative, difficult to manually threshold, iba1 stained wholemount DRG, followed by the output from our pipeline, with the average Z projection and a 3D rendering. Individually segmented macrophages are displayed as randomly colored objects, where each color representes one individual macrophage. The bottom row shows the raw iba1 positive macrophages with CD31 labelled blood vessels and the subsequent outputs of the pipelines macrophage classification as either perivascular (yellow) or non-perivascular (cyan).

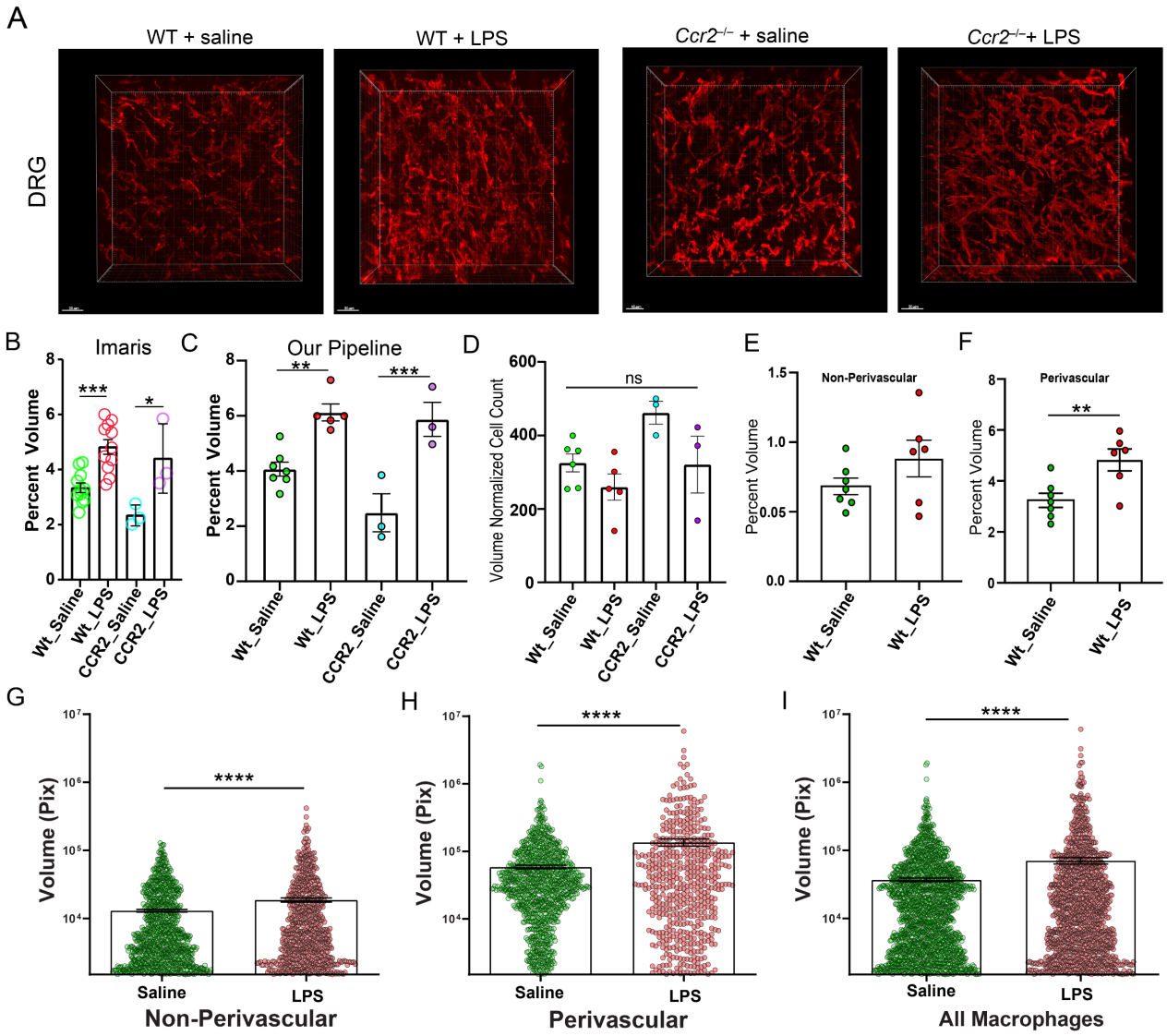

Figure 3-7 LPS induced macrophage activation our pipeline comparison: A.) Representative images of macrophages following intrathecal saline or LPS in wild type C57/Bl6 mice and Ccr2-/- mice. B.) LPS induces an increase in the volume over macrophages over total volume of the sample in both wild type and Ccr2-/- mice, Analysis performed with Imaris C.) Automated analysis with our pipeline shows consistent results with imaris. D.) no difference is observed between PV and NPV macrophages in macrophage numbers. E.) No significant change is observed in the percent volume of non-perivascular macrophages. F.) Perivascular macrophages increase in volume in response to IT LPS. G.) Both non-perivascular and perivascular macrophages increase in size following IT-LPS. * P<0. 05, ** P<0. 01, ***P<0. 001, **** P<0. 0001

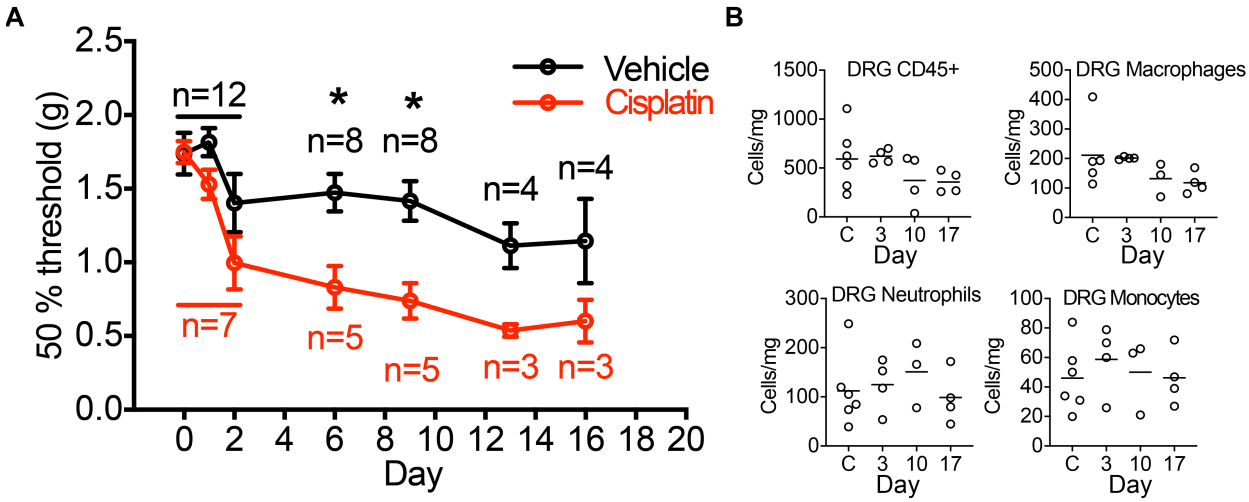

Figure 3-8 Flow cytometry of DRG in the CIPN Model: A.) Mechanical withdrawal thresholds following induction of CIPN. B.) Flow cytometry data of dissociated DRGs from control (C) and DRGs collected on days 3, 10, and 17 following induction of CIPN. * P>0. 05 2 way anova repeated measures.

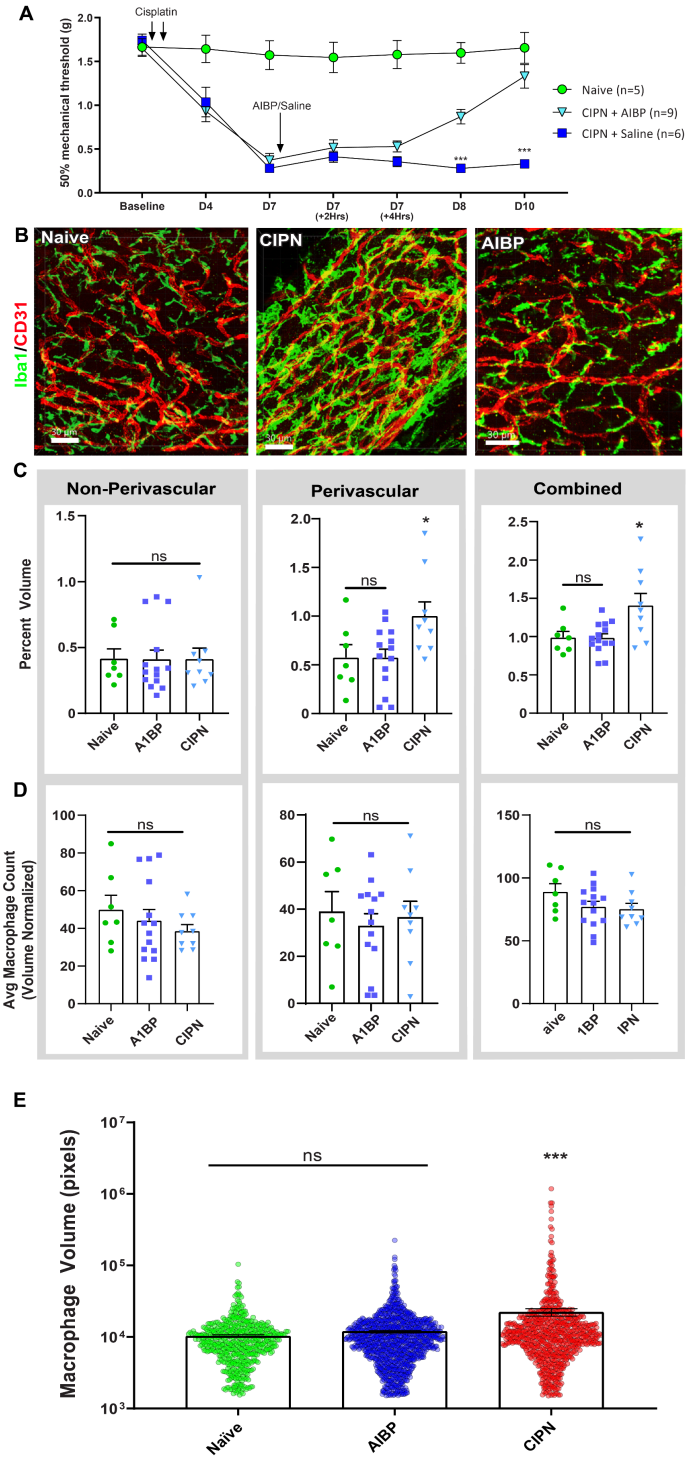

Figure 3-9 Macrophages in the DRG of CIPN mice: A.) Mechanical Withdrawal thresholds of CIPN mice treated with AIBP significantly increase 24 hours after administration of AIBP and return to normal after 72 hours (arrows indicate time and number of injections). B.) Representative Images of DRG macrophages stained with CD31 for blood vessels and Iba1 for Macrophages. C.) Percent volume of macrophages from Non-Perivascular (left) Perivascular (middle) and combined (right). D.) Macrophage count per image stack normalized by image volume. E.) Individual perivascular macrophages by volume. (* P<0. 05, **P<0. 01, ***P<0. 001)

CHAPTER 4: THE PAIRED MICRO-VALVE INTRATHECAL CATHETER

4.1 INTRODUCTION

4.1.1 Rationale

In the course of this work I had sought to develop an intrathecal intervention to knock out IRF7 using antisense oligonucleotide and/or AAV9. Development of the ASO in collaboration with IONIS failed to result in an effective ASO without neuronal toxicity, and the Yaksh lab has an ongoing collaboration with IONIS to obtain an effective candidate IRF7 targeted ASO. We turned our sights to the use of an AAV9 vector to deliver IRF7 siRNA or CRISPR deletion. This approach was in progress in collaboration with the Salk Institute's viral vector core. However, in the course of these efforts, delays arose as a result of scheduling and then were put on hold because of the COVID lock down. However, we did begin initial testing of control viral AAV8-RFP and AAV9-RFP in mice to work out effective delivery titers and methods. In collaboration with Prashant Mali (UCSD Bioengineering), we observed that intrathecal lumbar injection of 5μL of AAV at low titers in mice resulted in a dramatic drop-off in transfection efficiency of DRG neurons as distance from the injection location increased (manuscript accepted, Science Translational Medicine). In the mean while it had become clear in conversations with Dr. Yaksh, who has extensive experience with intrathecal delivery, that that one of the major problems with this route of delivery is the ability to homogeneously distribute small volumes of injectate over large areas of spinal axis. This becomes particularly important when dealing with therapeutics such as viral vectors, as large viral titers would be necessary to transfect neurons at regions distant the site of injection, which is both exceedingly expensive and high titers be associated with local toxicity. Accordingly, as we were preparing for the development of the IRF7 reagent we set out to develop a better delivery platform focusing on the catheter though which these therapeutics would be delivered. These studies were based on a catheter platform that employed micro-orifices that had some prior development by the Yaksh Lab. I was able to markedly improve on this system and characterize a catheter

platform that has become an important component of advancing the technology of intrathecal delivery of materials such as AAVs.

4.1.2 History of intrathecal delivery

Nearly 100 million people in the US alone experience chronic pain, which also inflicts a major financial burden estimated to be between $560-$635 billion[5, 204]. Chronic pain is a double edged sword in that it's also incredibly difficult to treat, as many therapeutics fail to adequately reach treatment goals, which include the ability to function in daily tasks without serious adverse effects[205]. Intrathecal administration of analgesics represents a direct approach that is effective for patients that have exhausted most other drug delivery methods. The administration of intrathecal analgesics dates to 1899 when August Bier used bolus intrathecal administration of cocaine during operations on the lower extremities[206]. The discovery of the efficacy of intrathecally delivered opioids in preclinical models to robustly alter pain states in a naloxone reversible fashion[207] was followed after several years by the demonstration of the effect in the human pain patient[208, 209]. This fueled intrathecal / epidural delivery of morphine as routine for intraoperative and postoperative regimes as well as a safe means for spinal analgesia during labor[210]. It was nearly half a century after Bier's use of bolus intrathecal cocaine when the first intrathecal catheters for continuous diffusion were developed[211], and not until 1981 were subcutaneous pumps connected to intrathecal catheters to manage chronic pain in cancer patients through the continuous intrathecal infusion of morphine [212]. In 1991 programable intrathecal pumps were approved by the FDA for treatment of chronic pain[213]. The use of chronically implanted intrathecal catheters and pumps led to the implementation of this platform in the management of chronic pain. Pairing the use of these indwelling intrathecal delivery systems with baclofen provided significant benefit in managing treatment of spasticity, as is common in patients with cerebral palsy[214], following stroke[215], brain or spinal cord injury[216], or in later stage patients with multiple sclerosis[217].

4.1.3 Rationale for intrathecal drug delivery

Intrathecal delivery allows markedly decreased doses of drugs that directly act on CNS receptors as compared to systemic delivery. Direct delivery to the CNS allows drugs to bypass first-pass metabolism and systemic dilution. Bypassing system circulation also greatly reduces off target effects as any systemic targets are less likely to be reached. Further, IT delivery avoids the difficulty of getting molecules across the blood brain barrier (BBB). The BBB is the term used to describe the unique microvasculature within the CNS. The non-fenestrated vessels composed of endothelial cells connected via tight junctions[218]. The BBB endothelial cells along with other cell types, such as pericytes and astrocytes which act in a concerted manner to tightly regulate and restrict movement of molecules into and out of the CNS[219, 220].

4.1.4 Injectate distribution issues peculiar to the intrathecal space

The spinal CSF, into which the drug is delivered, is limited in volume and poorly mixed, e. g. there is minimal CSF flow leading to a limited redistribution of an intrathecally delivered drug[221]. The limited redistribution has two important consequence which I will discuss and present relevant examples[222].

i) *Spinal drug activity:* The spinal processing of pain input and changes in spinal motor function leading to spasticity are not limited to a single spinal segment. Afferent traffic from a single nerve root (say L3) may communicate with spinal levels as much as 5-10 segments distant[223]. Accordingly, the spinal drug, which must act on the afferent terminal (such as morphine) must reach spinal levels of say T12 which, in dog and humans is as much as 5 and 10 cm respectively, distal from the level of stimulus input. So even for a drug targeted at a lower extremity input, it is necessary to achieve a substantial rostro-caudal redistribution.

ii) *Intrathecal viral vector mediated therapeutics*: It is not feasible for localized delivery of a viral vector, say AAV, to reliably achieve homogeneous transfection of target cell

populations with large rostrocaudal segmental distribution throughout the neuraxis (as in treatment of neurodegenerative disorders). Here the problem is increasing the rostrocaudal movement a drug delivered into the lumbar space, the spinal level which is most accessible for needle and catheter placement. Redistribution of the injected drug may be enhanced by greater volumes or higher rates of infusion. However, for the implanted pump with a limited reservoir size (10-20 mL), infusion rates are low and total daily volumes typically do not exceed 20μL/h. This leads to limited injectate redistribution.

4.1.5 Consequence of maldistribution

A consequence of this lack of redistribution of drug within the CSF is apparent with a bolus delivery, where in order to enhance the rostrocaudal distribution of injectate into the distal tails of the distribution curve, one must vastly increase the required infusate concentration. The absence of robust redistribution of the highly concentrated injectate leads to an enhanced likelihood of local toxicity. The effects of local anesthetics can producing neurolysis and a radiculopathy from formation of a meningeally derived space occupying mass are only two such examples[221, 224-227]. These phenomena have been shown to evolve in a concentration dependent fashion and are the results of poor redistribution compounded by the maldistribtuion of the infusate. The problem is particularly exacerbated when there is a low rate of infusion, where pooling of the injectate around the catheter leads to sustained high levels of drug that can enhance the likelihood of a local toxicity. Even with a single bolus delivered in a large volume to force redistribution, this results in a substantial increase in the total amount of drug, ASO or virus required and again increases the likelihood of unwanted detrimental effects.

A third issue is that the typical catheter has large ports that permit infusion and CSF withdrawal. While the ability withdraw is considered of interest for sampling local CSF, it bears little benefit for on-going delivery. Further the presence of these open ports can lead to ingrowth of fibroblast and other constitutively present cells in the CSF as well as local proteinaceous

deposits, which can occlude the catheter systems. This is of particular significance for chronic catheters where injectates may be delivered at long inter-injection intervals (as with ASOs or AAVs delivered neuraxially).

4.1.6 Addressing problems in neuraxial delivery.

In the course of addressing the problems outlined above, we have focused on improving catheter design as an all-in-one solution. To date catheters have been an open or close ended tube, with 1 or more side ports (lumens) proximal to the delivery end of the catheter. Typically, these delivery orifices are large, low resistance exit sites. While such multipored large orifice catheters have been said to reduce the incidence of laboring patients reporting to have inadequate analgesia[228], their utility in drug distribution in these patients may reflect upon the fact that they are employed with large volume bolus deliveries. Similarly, in preclinical studies with canine models of catheter placement, morphine induced spinal mass formation following continuous infusion of morphine commonly occurred with higher concentrations delivered at lower rates. Periodic bolusing was observed to reduce the incidence of intrathecal pathology [227, 229], which is consistent with our lab's observation that with large poly-port catheters the rate of injection greatly affected the distribution of drug. Thus, with slow delivery, as commonly used clinically (20 μL/hr e. g. 0. 3 μL/min), infusate exited through the first of 6 ports. However, when delivering the infusate by a series of sequential boluses (high rates for very short periods) the infusate exited though more distal ports as well, increasing distribution[230].

Here we aimed to address the problems outlined above through the development of a catheter with the following design considerations:

i. For a given volume, the exit velocity of the infusate will be inversely proportional to exit resistance, with the idea of maximizing exit velocity for small volume deliveries. This could be achieved via small orifices, which, by their increased exit resistance provide a gain in exit velocity. We realized that the systems could be additionally enhanced if instead of

orifice we constructed valves in the wall of the catheter. Because of the compliance of the catheter wall, these valves would remain closed until there is a transmural pressure gradient that causes the valve to open. This results in an enhanced pressure gradient upon valve opening causing, the infusate to exit at a greater velocity

ii. These sites of exit thus function as a valve that only opens under pressure provided by the infusion system.

iii. These multiple small valves provide for a closed system in the absence of any infusion pressure. The absence of constant opening, such as is provided by a port, will prevent the ingrowth of cells or proteinaceous debris.

iv. A valve system serving as a series of high resistance exit sites results in an even pressure gradient along the extent of the catheter. Meaning that the transmural pressure at any valve will be same no matter the proximity of the valve to the infusion sources. This will allow an even distribution of fluid movement from the catheter at valves distributed along the length of the catheter.

Presented here, we developed and manufactured functional prototypes of the proposed system outlined above and demonstrate the validity of our assumptions regarding the functionality of using a multi-valved system to increase lateral distribution. We then show *in-vivo* the ability to produce an enhanced rostrocaudal distribution of an injectate as compared to a single port injection system delivering the same volume and concentration of drug.

4.2 METHODS

4.2.1 Animals

All animal experiments were carried out according to protocols approved by the Institutional Animal Care and Use Committee of UC San Diego. Adult male Sprague Dawley rats (250-350g) purchased from Envigo were singly housed, and given food and water ad libitum, in a temperature-controlled facility with 12-hour light dark cycles.

4.2.2 Catheter materials

Both the Paired Multi-Valve Catheters (PMVC) and the Open Ended Catheters (OEC) were constructed using Polyethylene (PE) tubing purchased from Scientific Commodities. For OECs and PMVCs a 33-gauge wire was inserted through a 7cm length of PE10 and then through a 13cm length of PE08, then heat was used to fuse the two PE segments together, creating a 5mm bead at the point of fusion.

4.2.3 Paired multi-valve catheter design and manufacture

Microvalves oriented parallel to the catheter axis were created in pairs at an angle of 120° to 140˚ and staggered at varying distances between them in the longitudinal axis. Microvalves were made without removing any material from the catheter and thus form a fluid tight seal when closed. As an example of the technology, the microvalves are typically approximately 0. 1mm in length and staggered by 0. 3 mm between pairs (Figure 4-1). For the purposes of testing and the experiments presented here, we designed the catheters to evenly distribute through 5 pairs of evenly spaced valves. The number and spacing of the valves can easily be changed or modified. The PMVCs were made using a 30G needle fixed to a surgical stereotax with 360° circular and 180° angular rotation. The PE08 end of the OECs (described above) were first heat sealed. A 27G needle fixed to 5mL syringe filled with sterile water was then inserted into the PE10 end. Manual pressure was applied to the syringe plunger to make sure that the fused PE08 and PE10

was tightly sealed. A 30G needle was used to make a tiny relief cut in the PE08 end so that air in the catheter could be removed replaced with sterile water. The catheter was then secured to the catheter support guide (CSG). The CSG can be modified for each chosen catheter design layout. The CSG was designed using fusion 360, and printed on a Formlabs Form1+ 3D printer, using 3Dresyn CR UHT resin. In short, it is composed of a Start end and a Cut end. The PE10/PE08 fusion bead is placed in a notch at the start end and secured with polypropylene tape (scotch brand). A groove runs the longitudinal length of the guide where catheter comfortable sits within. The PE08 is pulled taut and laid into the groove. The catheter is then fixed to the guide using tape. The top 2cm of the PE08 represent about the distance from the nuchal crest to the cisterna opening where the catheters can be inserted, and thus no valves are placed in this region. The valves can then be evenly spaced depending on the desired injection locations. Here we designed the guide to be 11cm total. The first 2cm are blank, as well as the last 2cm, leaving 7cm in the middle where valve guides can be evenly spaced. Valve guides are grooves in the horizontal axis that are wide enough to allow a 30G needle to fit and expose only one lateral surface of the catheter so that the needle can create the valve. Pairs of valve guides are spaced 0. 3mm apart from one another, and evenly spaced pairs are distributed along the middle 7cm section of the CSG. A deeper horizontal groove is placed 2cm from the end of the Cut end of the CSG to allow a razor, or number 11 scalpel blade to cut the completed PE08 end to 9cm.

Once the catheter is securely in place, the CSG is then placed in the stereotactic device under a surgical microscope. The stereotax angle is set as desired (here 70°) and the first valve guide is located, pressure is applied to the syringe and the 30G needle is inserted until it penetrates the catheter up to the bevel of the needle, carefully making sure it does not puncture the lumen on the other side of the catheter (0. 2mm). When the needle is removed a bead of water from the relief on internal pressure should be observed. Keeping pressure internally enables the integrity of the catheter to be sustained while puncturing it with the needle to create the valves. The valves along one side are made, then the CSG is turned around and the valves are made

along the guides on the opposite side. This creates valve pairs at 140° angles (figure 4-1). Once all valves are made the catheter is cut at the cut end using a #11 surgical scalpel or sharp razor.

The now open end of the PE08 catheter is then threaded through a 22G needle and heat sealed. While heat sealing the catheter is pulled through the needle to create a rounded end cap instead of a flat end cap. The end cap is then observed under the surgical scope and can be cleaned up using a scalpel to remove any burrs or corners. Finally, a 0. 08mm relief valve is made using a 30G needle in the end cap so that air can escape. Once finished the PMVCs can be tested by hand to observe even bead formation by applying pressure to the sterile water plunger before use or further testing in a test chamber (Figure 4-2,). Prior to implantation the PE10 end of the catheter is cut to 5cm so that the total dead volume within the catheter holds 6μL.

4.2.4 Catheter Testing

Catheter testing was performed using chambers made from plexiglass that were 100cm long 3cm tall and either 100, 10, or 2cms wide. A drill press was used to bore a 0. 5mm hole into the bottom of one side of the chamber and a 22G needle was inserted and glued in place with super glue. The catheters were placed into the chamber through the 22G needle, pulled taut and laid on the floor of the chamber fixed with tape. The chamber could then be filled with distilled water and would not leak. A syringe could then be placed into a Motor-driven system (Harvard Apparatus) connected to PE10 tubing with a 27g needle. This system could then apply new methylene blue into the PMVCs at varying speeds, quantities and pressures. Movies of the catheters were taken using a USB 3. 0 camera generously donated from IDS (IDS UI-3360CP-M-GL, AB00242). Movies were created directly in imageJ using HF_IDS_CAM[231] to capture the video. A script was then written as an imageJ macro that took the first frame of the video, subtracted the first frame from each additional image, then ROIs over each valve pair were created and the average intensity of each ROI was plotted as a function of time.

4.2.5 Intrathecal catheter implant surgeries

All catheters used for intrathecal implant were gas sterilized prior to implant. Intrathecal implants were performed as previously described[232]. In brief, rats were anesthetized using 50% Isoflurane and 50% oxygen, and depth of anesthetization was assessed and maintained by observation of respiratory rate. The hair along the rat's neck and head were shaved, ophthalmic ointment placed over the eyes. The rat was then placed in the stereotaxic device and a 1cm incision is made in the midline of the neck, the muscles covering the occipital crest are peeled away from the bone and the cisternal membrane at the base of the skull is exposed. A small (1-2cm) incision is made in the cisternal membrane. Sterile catheters are flushed, and then inserted caudally into the cisternal incision. The catheter is then carefully fed down the spinal column, watching for any twitching, which indicates stimulation of spinal nerves. The bulb of the catheter was glued to the skull and the PE10 end was fed through hole in the skin 1cm cranial to the incision site and secured with a suture. Finally, the catheter was then plugged with a stainless steel 28G wire. Post-surgery rats were given 5mL of Lactated Ringers Solution subcutaneously and observed upon wake up for any behavioral abnormalities.

4.2.6 Intrathecal injections

IT injections were performed using a 50μL Hamilton syringe fixed to a length of PE10 tubing and 27G needle. All PMVCs were tested and analyzed prior to implant, and all catheters were gas sterilized. Rats were either given AAV-9 IT at $1xe^{12}$ (n=6) or $1xe^{10}$ (n=6) total viral genomes at the time of catheter implant. The Syringe and tubing were completely filled with water such that no air bubbles were present in the system. The plunger was retracted so that a small air gap was formed in the needle. Then 12. 5 μL of saline was pulled followed by a tiny air gap, and 7. 5 μL of drug. The 7. 5 μL of drug was then pushed along with the 12. 5 μL of saline flush so that no drug should be left in the catheter, as the total volume of the catheter was 6μL. AAV-9 RFP (generously donated by Prashant Mali) was first concentrated using Amicon Ultra 0. 5

Centrifugal filter Device (Millipore), and then diluted in sterile saline, to either $1xe^{10}$ or $1xe^{12}$ total viral genomes per 7. 5μL. Morphine (Merck) was diluted to 10, 1, or 0. 1 μg per 7. 5 μL of sterile saline. AAV injections were performed under anesthesia, at the time of catheter implant. Morphine injections were performed without anesthesia, by gently restraining the animal.

4.2.7 Behavioral testing

Rats were tested for thermal induced nociceptive hind paw withdrawal latency as described previously[233]. In brief withdrawal latency was measured using a Hargreaves type thermal escape system[234]. Rats were acclimatized for 30 minutes to standing on a 2mm thick glass floor sustained at 30°C, with an elevated floor housing a mobile radiant heat source, which is controlled by the examiner. The examiner would then apply the heat source, which reaches 41-42. 5°C to the plantar surface of each hind paw. Once the heat source is engaged a timer starts, which is turned off when the hind paw is removed, thus measuring the latency to nociceptive response. In the absence of a withdrawal, the timer and heat source automatically disengage after 20 seconds.

4.2.8 Tissue processing and clearing

4 weeks after injection of IT AAV-9, rats were transcardially perfused with ice-cold saline containing 1% heparin, followed by 4% PFA. The spinal column and brain were left intact, and the tissues were post-fixed for 24 hours. The tissue was washed in PBS prior to dissection. Laminectomies of each vertebrae were carefully performed using fine bone trimmers (Roboz, RS-8469), carefully leaving the dura intact. One DRG was carefully extracted from right and left sides at mid-cervical, mid-thoracic, Lumbar (L2-L3), and mid sacral. DRGs were washed in PBS+Az and then immediately cleared using RTF[195] as previously described (Table 3-3) and placed into 600μm chamber slides.

4.2.9 DRG analysis

DRGs were analyzed by taking 10x confocal images of native fluorescence. A representative sample of images were then labeled by hand for background, DRG soma, Neuronal Soma, and neuronal nuclei using ilastik[235]. Raw images, along with ground truth labels, were used to train a 2D UNET[236] via Yapic (Image and Data Analysis Facility, DZNE). DRG soma is was defined here as the cell dense region of the DRG, not including locations where fiber tracts were present. The model was trained for 2000 epochs with good results. Nuclei were readily distinguished as they exhibited lower intensity then the surrounding soma. The DRG soma was used to determine the volume of the DRG so that cell counts could be normalized to volume. Images output from the model were then analyzed using an image J macro that identified each neuron and placed them back into the original raw image to measure intensity. The macro output included cell count, cell size and the intensity of RFP.

4.3 RESULTS

4.3.1 Pre-implant catheter testing

PMVCs were iteratively designed and tested before in-vivo use. Parameters modified included valve vs slit designs as well as changing valve size. A sample of catheter testing is shown in figure 4-4. We found that the most consistent results were obtained from catheters with paired valves roughly 0. 1mm wide. With these small valves a large pressure is necessary to open the valve (Figure 4-4,C-D;Figure 4-5). Once open, a jet is formed with an exit velocity of 41mm/s, far greater than the exit velocity of open end catheters which we determined to be 29mm/s (Figure4-5).

4.3.2 PMVC distribution of single bolus delivery

To test initial proof of principle in-vivo we implanted 1 PMVC and 1 OEC into rats. We then quickly transcardially perfused with saline to remove any blood and performed laminectomies of every vertebra down the spinal column to expose the spinal cord, carefully using fine bone trimmers to leave the dura intact. We delivered a single bolus of 7. 5μL of new methylene blue followed by a 12. 5μL flush of saline. The injections were recorded and still images are shown in figure 4-5, along with images where the first frame was subtracted from all following frames. The bolus delivered with the PMVC is hard to see, as the catheter was implanted dorsally in the cervical region, but immediately went to the ventral and lateral sides out of view, but you can see a light, evenly distributed change along the rostral caudal axis. In contrast, the single bolus delivered form the OEC is clearly visible in the lower lumbar region, and quickly descends into the sacral, but does not ascend rostrally beyond lumbar (Figure 4-5). This can be clearly observed when the spinal column was carefully dissected out, leaving the DRGs attached when possible, where the new methylene blue dye left a nearly navy blue stain in the lumbar region (Figure 4-7,right), whereas, the PMVC left an even distribution along the spinal cord, and even resulted in a light blue coloration in the cervical DRGs and peripheral nerves (Figure 4-7, white arrows).

4.3.3 PMVC vs OEC analgesic delivery

To test whether PMVCs would alter the effect of intrathecal morphine we assessed rats thermal escape latency. 12 rats were either implanted with OECs (n=6) or PMVCs (n=6). Upon waking up from anesthesia 1 rat that was implanted with an OEC was observed to have unilateral paralysis, the catheter was removed, and the rat was able to recover motor function. We Found that there was no significant difference between PMVCs and OECs when 10μg, 1μg or 0. 1μg micrograms of morphine was delivered in 7. 5μL saline, followed by a 12. 5μL flush (Figure 4-8).

4.3.4 PMVC Vs OEC viral drug delivery

To assess PMVCs as potential drug delivery devices for transient, or repeated viral vector mediated therapeutics, we injected AAV9-RFP at the time of catheterization (the same rats from above). All PMVCs were tested and analyzed prior to implant, and all catheters were gas sterilized. Rats were either given AAV-9 IT at $1e^{12}$ (n=6) or $1e^{10}$ (n=6) total viral genomes at the time of catheter implant. 4 weeks after injection of IT AAV-9 we observed that PMVCs vastly outperformed OECs. At the low dose concentration zero RFP positive cells were observed in the cervical DRG or thoracic DRGs (Figure 4-9,A-B), while PMVCs had RFP positive cells detected at all levels. Significantly more neurons were transfected in the PMVC rats at cervical and lumbar levels for both titers of AAV (Figure 4-9, A,C). The overall distribution of small medium and large neurons, however, was no different between PMVCs and OECs (Figure 4-10), and representative 3D images can be seen in figure 4-11.

4.3.5 PMVC Vs OEC infiltration

Finally following decalcification and sectioning of the vertebral column we observed that OECs contained significant amounts of infiltration and debris within the distal portion of the catheter (Figure 4-12, A). In stark contrast we observed minimal to no infiltration or cellular debris within PMVC catheters (Figure 4-12, B).

4.4 DISCUSSION

Here we present the paired multi-valve catheter and performed 2 proof of principle experiments of its potential benefits. The paired multi-valve catheters were tested through iterative design and rapid prototype testing. We tested many designs with large valves vs small valves and multiple slit or valve designs and found that the pressure required to open the small valves led to increased exit velocity and less variability in the amount of injectate delivered.

The PMVC represents a closed system, which greatly reduces the potential of cellular or other debris from entering into and occluding the system.

The fact that PMVC worked equally as well with IT morphine, was a surprise to us, as we hypothesized that the OECs would work better, as they are targeting all of the drug to the lumbar region, which as where we were testing for analgesia. There may in fact, be a small dose range where the OECs would work better, but the PMVC should be distributing the analgesic to more locations and at equivalent doses. Assessing concurrent changes in forelimb and hind limb thresholds might be of importance in assessing the difference in the analgesic profile produced by the multi-valved platform.

The valve opening pressure can be taken advantage of in multiple ways. We envision that if a constant pump is used that delivers subthreshold instantaneous pressure, the valve opening pressure could be optimized such that transient delivery occurs from a constant pump. The time interval between valve opening, drug delivery events, could be controlled by both the valve opening pressure as well as the instantaneous pressure provided by the pump.

Clinical trials of gene modifying therapeutics utilizing engineered virus's such as AAV, as vectors are rapidly increasing. However, two major hurdles for CNS disorders are injection titer and potential neuronal loss. In order to get widespread distribution in humans, large amounts of AAV must be produced for any given treatment (2e14vg/kg). This is both extremely expensive and has the potential for detrimental side effects. High dose intrathecal delivery of Novartis's

AAV9-SMN in preclinical trials resulted in inflammation and death of DRG neurons[237]. Here we present our results that indicate that the PMVC could reduce the concentration of AAV9 necessary get widespread distribution and with sufficient titer at each spinal level to produce a uniform transfection by up to 100-fold. This would serve to both drastically reduce the amount of virus and thereby reduce the cost of the gene therapy, as well as reduce the potential for neuronal death and inflammation. We had previously performed intrathecal injections of AAV in mice and done similar quantifications and noticed that with a single lumbar injection of mice, we obtained a sharp falloff in the number of positive neurons per DRG as we moved further from the site of injection. The scale from rodent to human in terms of distance is on the order of 7-10 cm versus 50-80 cm, and we believe that there is a clear and present need for new delivery method such as the one developed and presented here in order to effectively delivery viral-vector gene therapies.

4.4.1 Other use cases of PMVCs

Treatment of centrally seeding cancers can benefit delivering the chemotherapeutic to the neuraxis (reducing systemic exposure). Here there is a need to make the drug have access to many spinal segments[238]. Producing a wide spread distribution of the agent along the spinal axis poses a problem given that intrathecal drug distribution as currently employed is noted for its lack of rostrocaudal distribution and local high drug concentrations (at the site of delivery), leading to toxicity[222, 239, 240] An important property of the spinal intrathecal space is that the cerebrospinal fluid under goes *limited* bulk movement[241, 242]. Thus, an injection into that space will typically remain proximal to the site of injection. In light of the need for the drug to move rostrally and caudally many segments, such limited redistribution impacts upon the ability of the intrathecal drug to alter the processing relevant to local pain or spasticity or the neurodegenerative/ pathological processes.

Treatment of Neurodegenerative disorders with Antisense Oligonucleotide therapy is another arena in which our catheter would likely outperform any existing drug delivery systems.

More recently there is an increasing use of the spinal route to deliver disease modifying medication, such as oligonucleotides for treating neurodegenerative disorders. Similar to AAV-based gene therapies above, there is a need to deliver the disease modifying agents to the entire neuraxis, which requires large volumes of injectate and large amounts of therapeutics[243]. Just as with viral vector mediate therapies we tested above, ASO's have also been shown to have dose, concentration, and treatment duration related toxicity[244].

In short, we believe this design modification represents an important advance in catheter technology. We would note that there is a single patent which appears to describe a simple small orifice in which they also note the use of a slit[245]. However, this description considers the orifice not as a valve and does not address the specific function of the valve function vs a simple opening in the wall of the catheter. We have submitted the current design and supporting data to UCSD as a potential patent application of this design.

4.5 ACKNOWLEDGEMENTS

Chapter 4 is currently in prepration for submission as: Matthew A. Hunt, Sara A.C. Hunt, Joanne Steinauer, Tony L. Yaksh. Characterization of a Poly Valve Catheter for Intrathecal Delivery. The dissertation author was the primary researcher and author of this material and a patent application has been preliminarily filed for the PMVC.

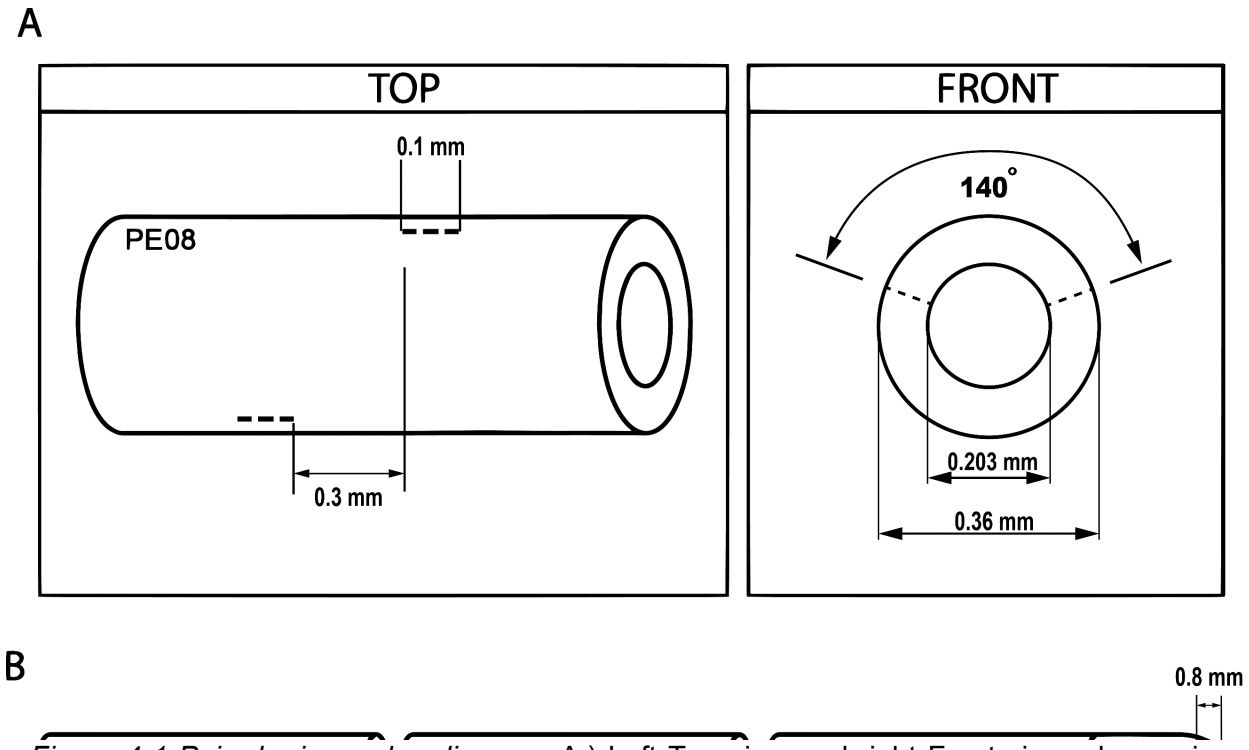

Figure 4-1 Paired micro-valve diagram: A.) Left Top view and right Front view where micro valves are represented by dashed lines created in PE08 catheters. B.) Paired micro valves are evenly distributed along the catheter at a distance determined by the target area for therapeutic agent action. The end cap (EC) is a closed portion of the catheter with a release valve that is smaller <0. 1 mm, than the rest and allows for gas and small volumes of fluid to escape.

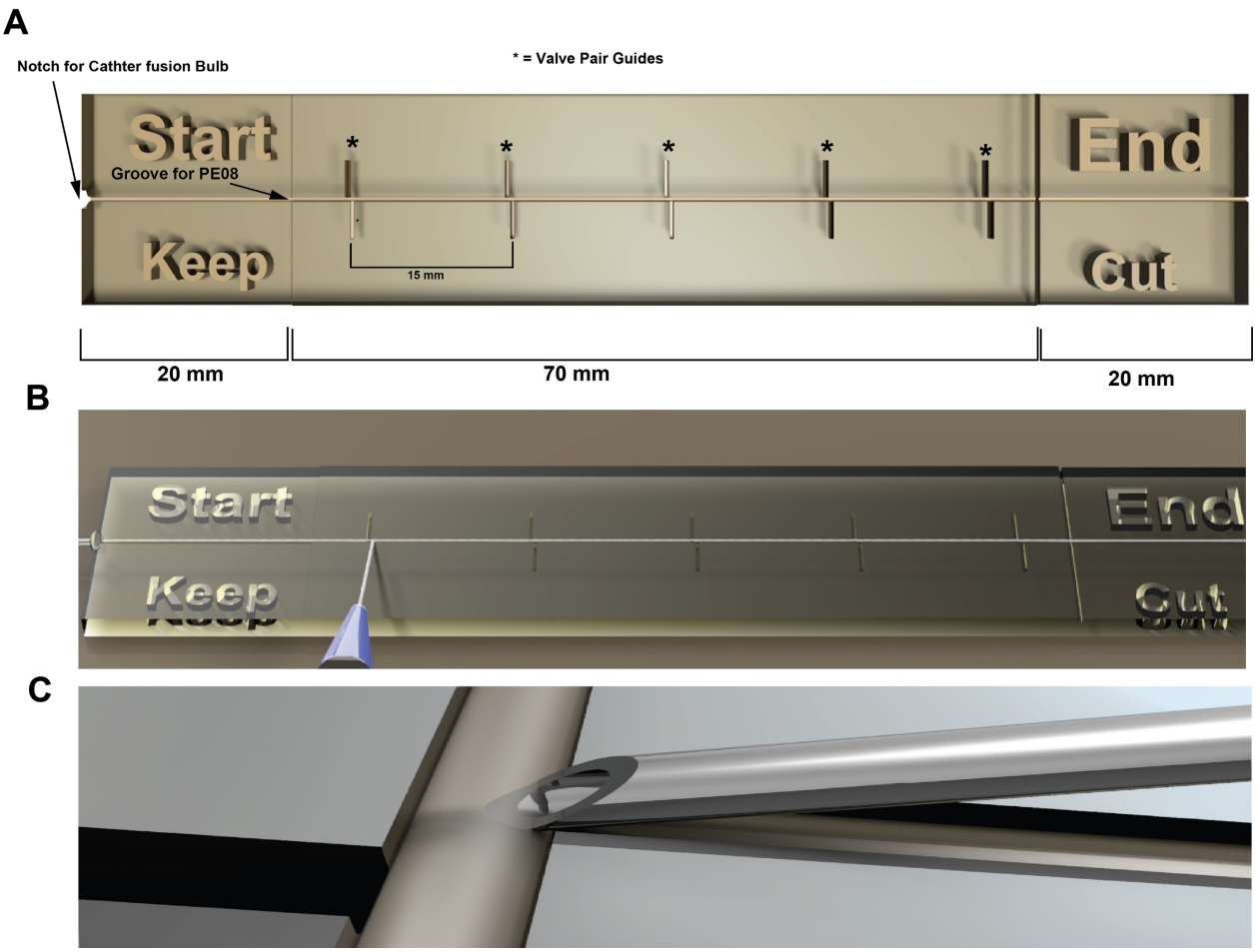

Figure 4-2 Catheter manufacturing: A.) Layout of the catheter guide, showing where the notch for the point of fusion of the PE08 and PE10, the groove that the PE08 sits in, as well as the pairs of valve guides indicated by *. B.) Rendering of catheter (white) sitting in the guide and a 30G needle in a valve guide. C.) Closeup of 30G needle puncturing the PE08 Catheter to make the valves.

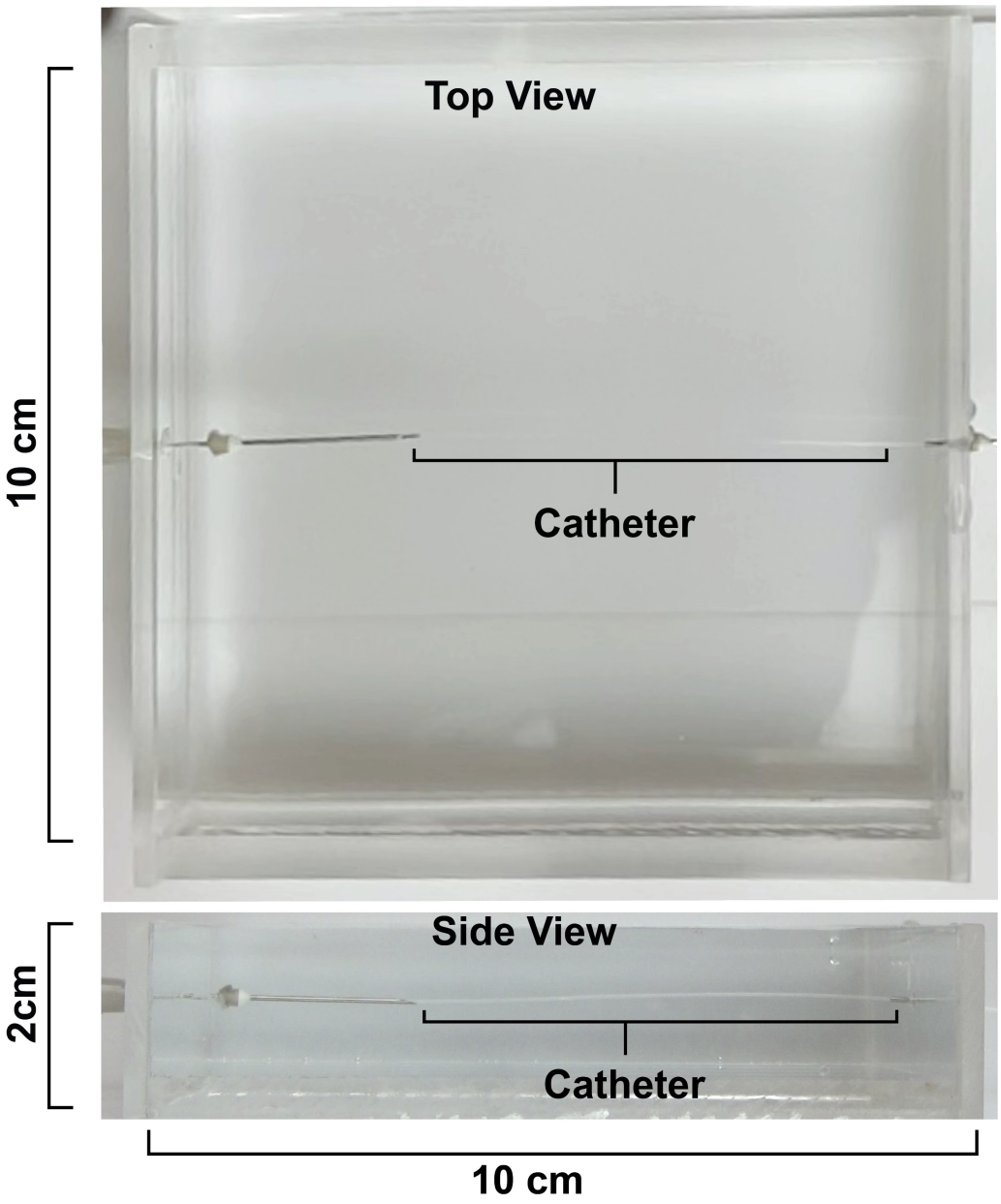

Figure 4-3 Valve testing chamber: Layout of the large testing chamber with a catheter suspended within and filled with water.

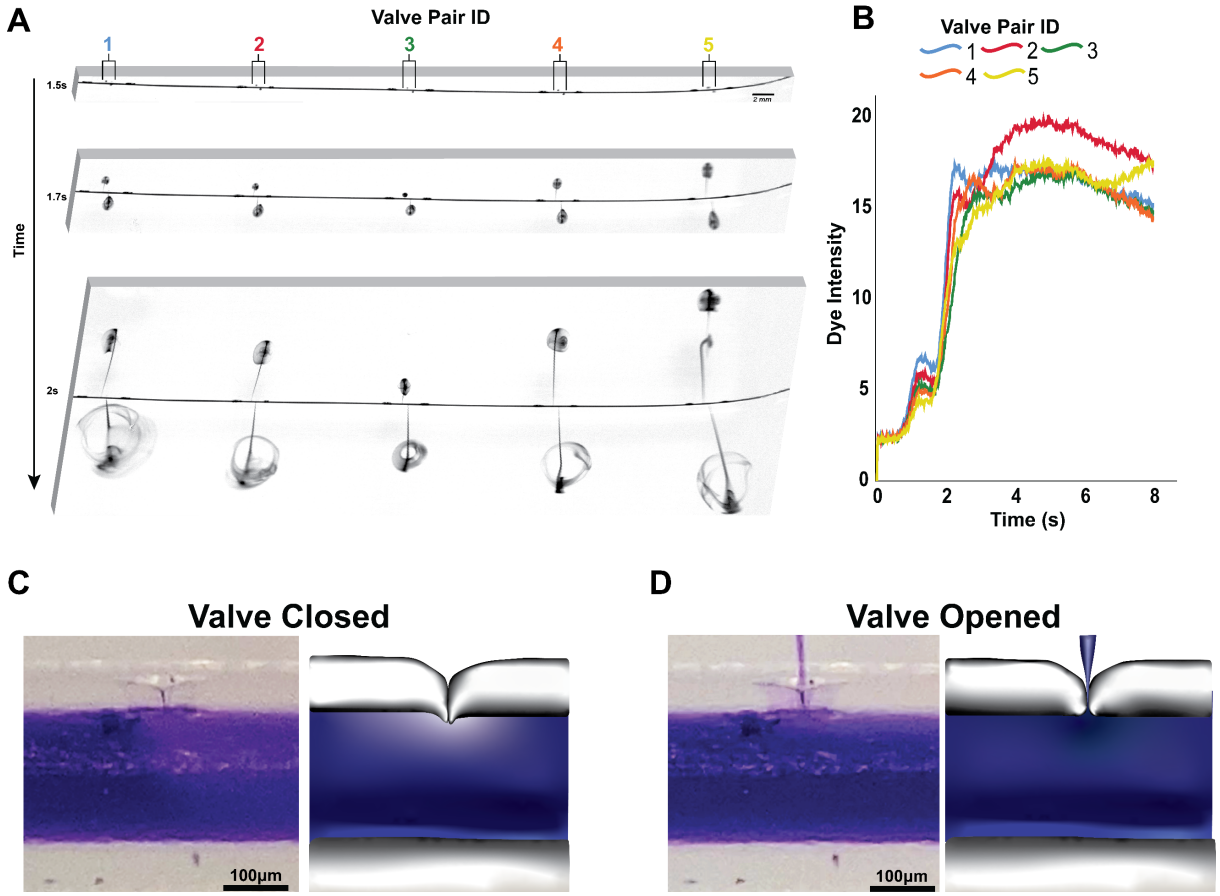

Figure 4-4 Analysis of paired valve catheter distribution of blue dye: A.) Cropped video frames analyzing 10 µL of blue dye injected at 1ml per minute, paired ports numbered 1-5 show dye exiting with high velocity in opposite directions. B.) Analysis of video at 60fps, all images are subtracted from pre-injection conditions, inverted, and the average intensity is analyzed with ROIs spanning the width of the chamber. C & D) High magnification video still shows a single microvalve (left) alongside a graphical representation (right), showing a closed valve (C) and an open valve with jet (D).

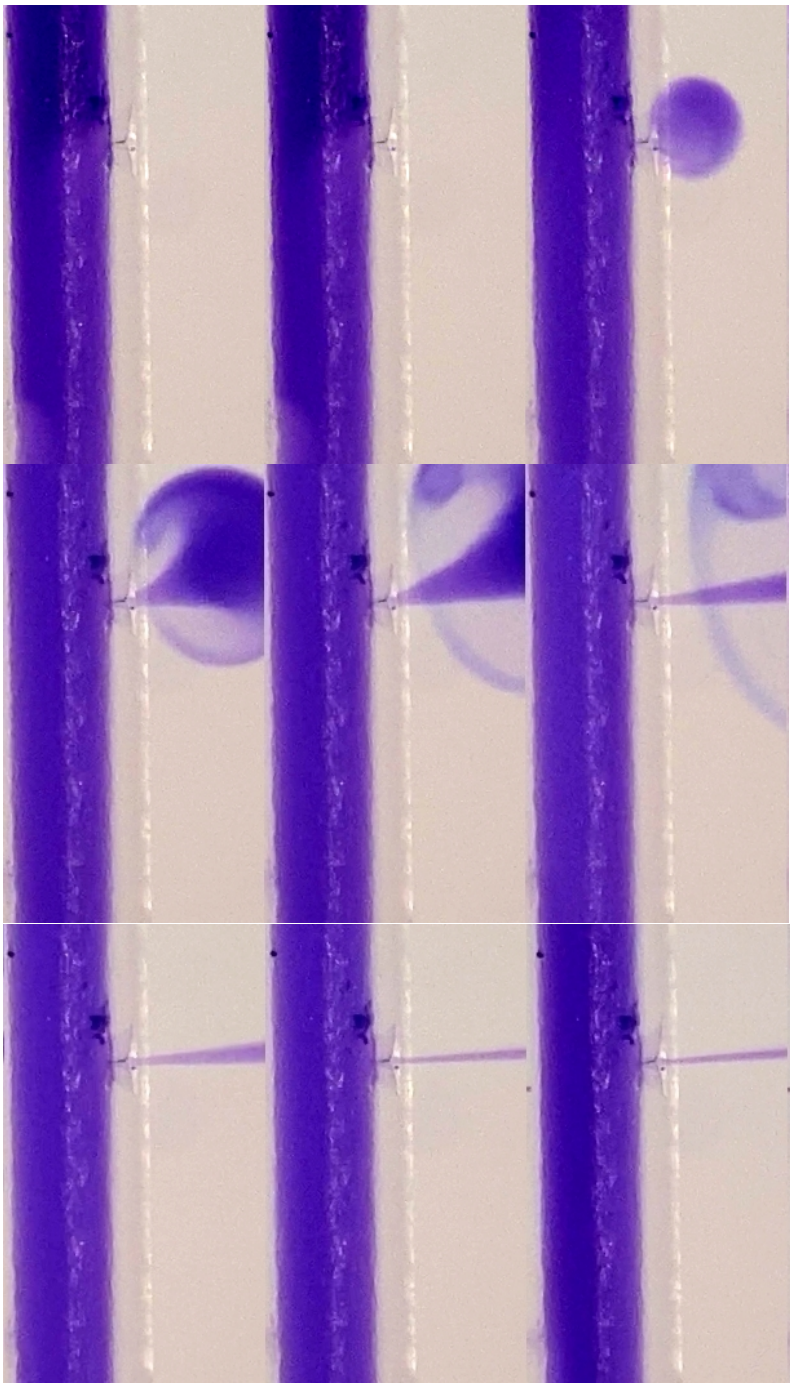

Figure 4-5 Catheter opening montage: Opening of single Valve is shown as stills from a video taken under a surgical microscope.

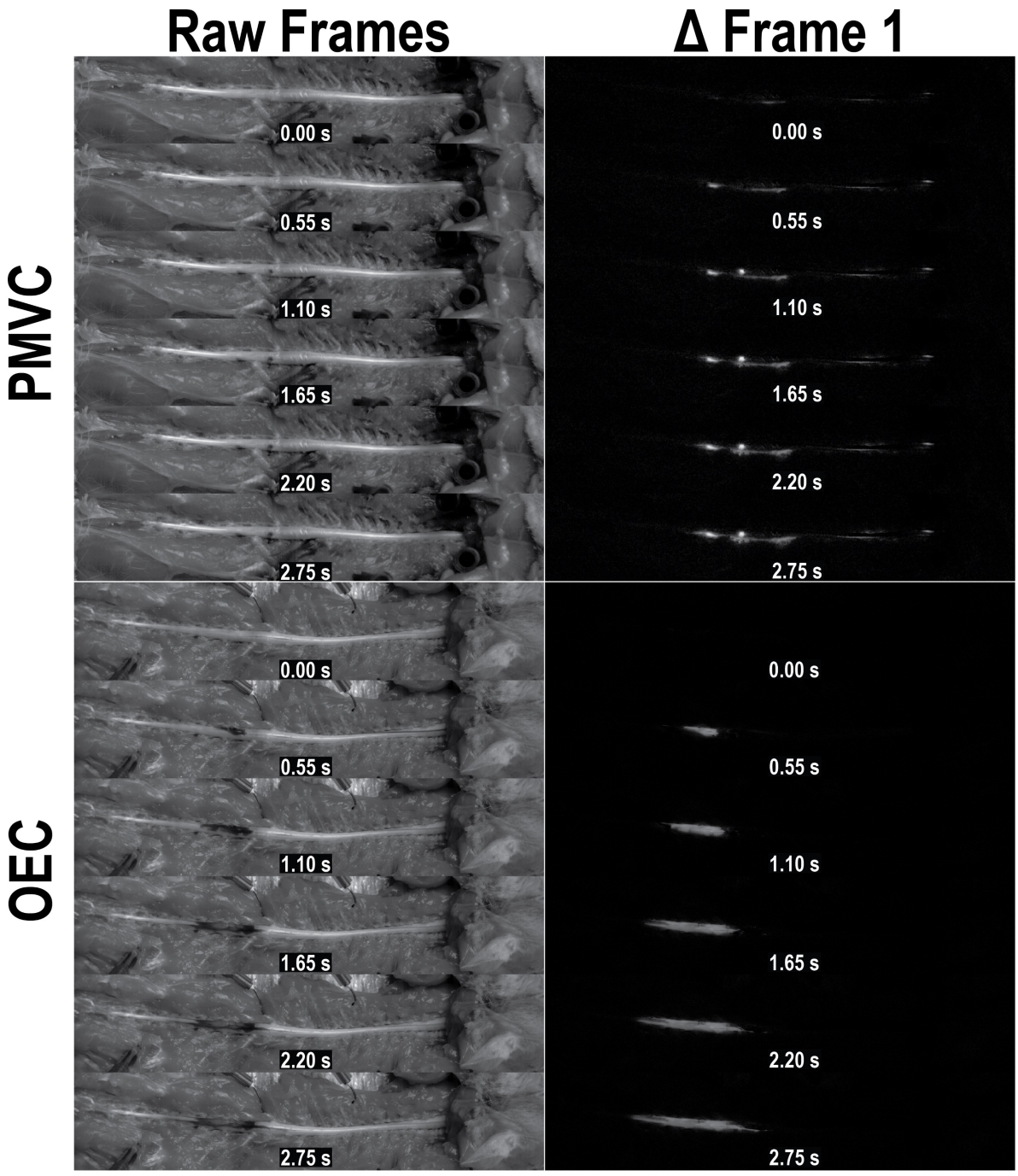

Figure 4-6: In-Vivo blue dye test: Frames from video of intrathecal methylene blue test (left) along side analysis frames (right), which show change from the frame image prior to injection. Comparison between PMVC (top row) and OEC (bottom row).

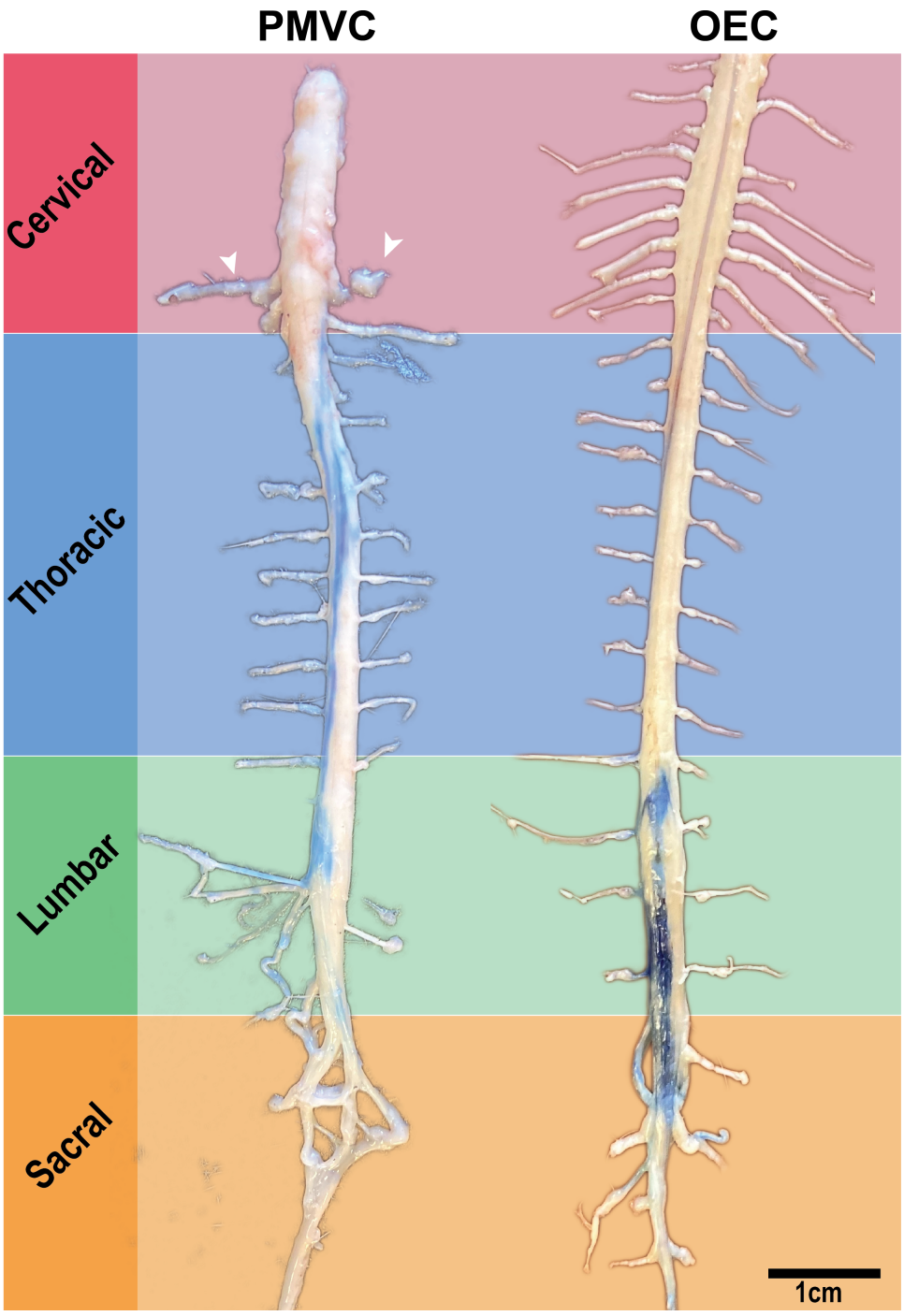

Figure 4-7: In-Vivo blue dye test: Dissected spinal columsn with DRGs attached showing comparison of 7. 5 µL of new methylene blue injection followed by 12. 5 µL saline flush using either PMVC (left) or OEC (right).

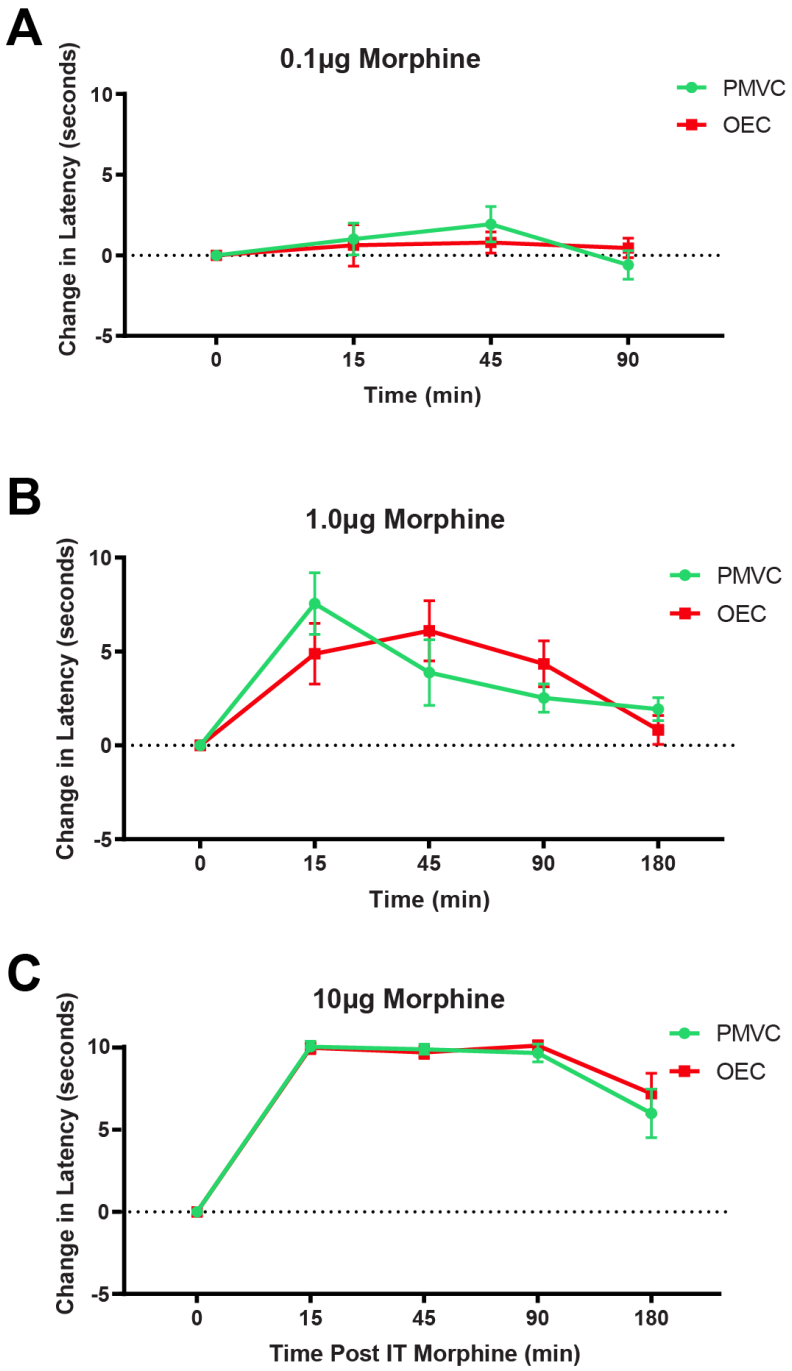

Figure 4-8: In-vivo morphine: graphs show change in latency from baseline following intrathecal injection of morphine (A) 0. 1µg (B) 1. 0 µg and (C) 10µg.

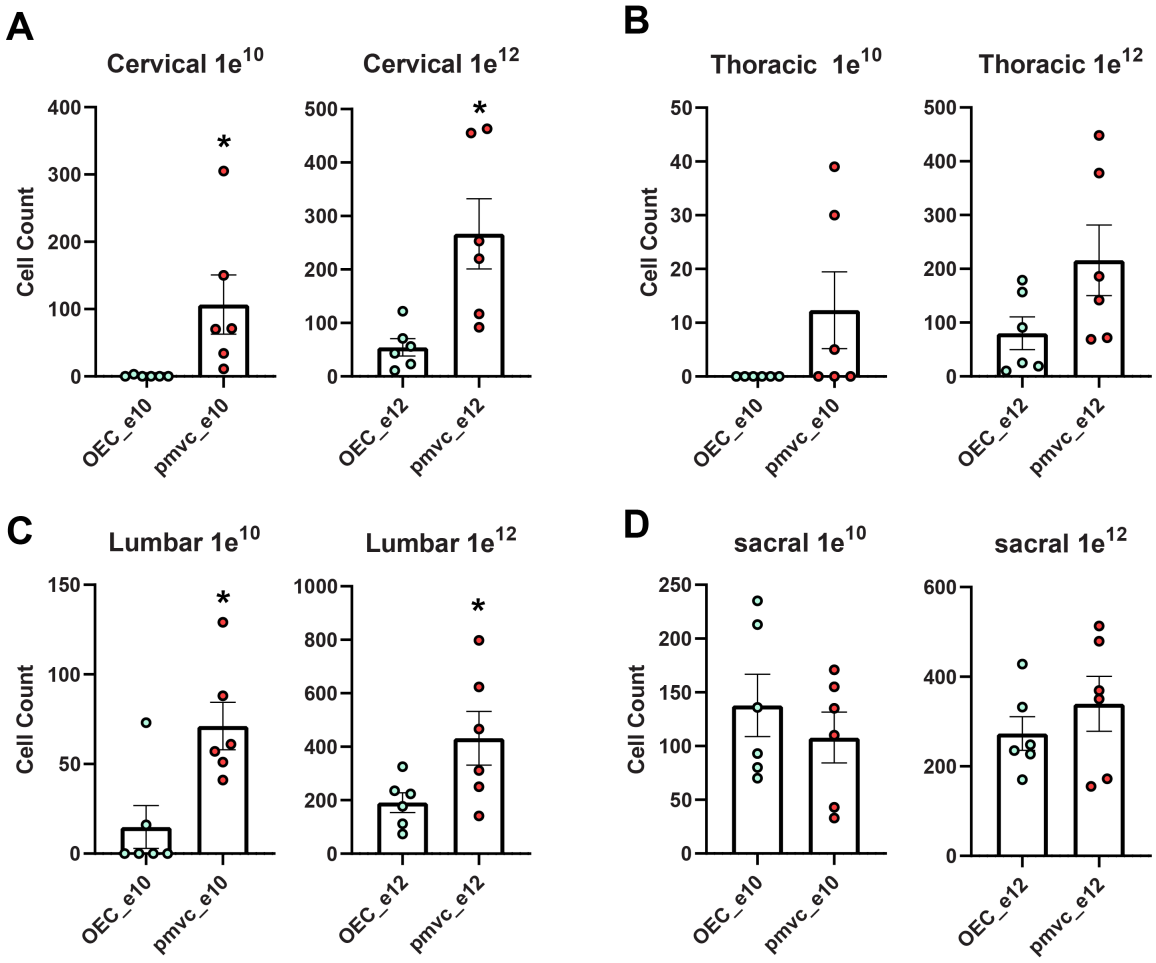

Figure 4-9: In-vivo AAV positive cell count: The count of RFP positive neurons are shown per DRG from Cervical (A), Thoracic (B), Lumbar (C) and Sacral (D) DRGs. * P<0. 05

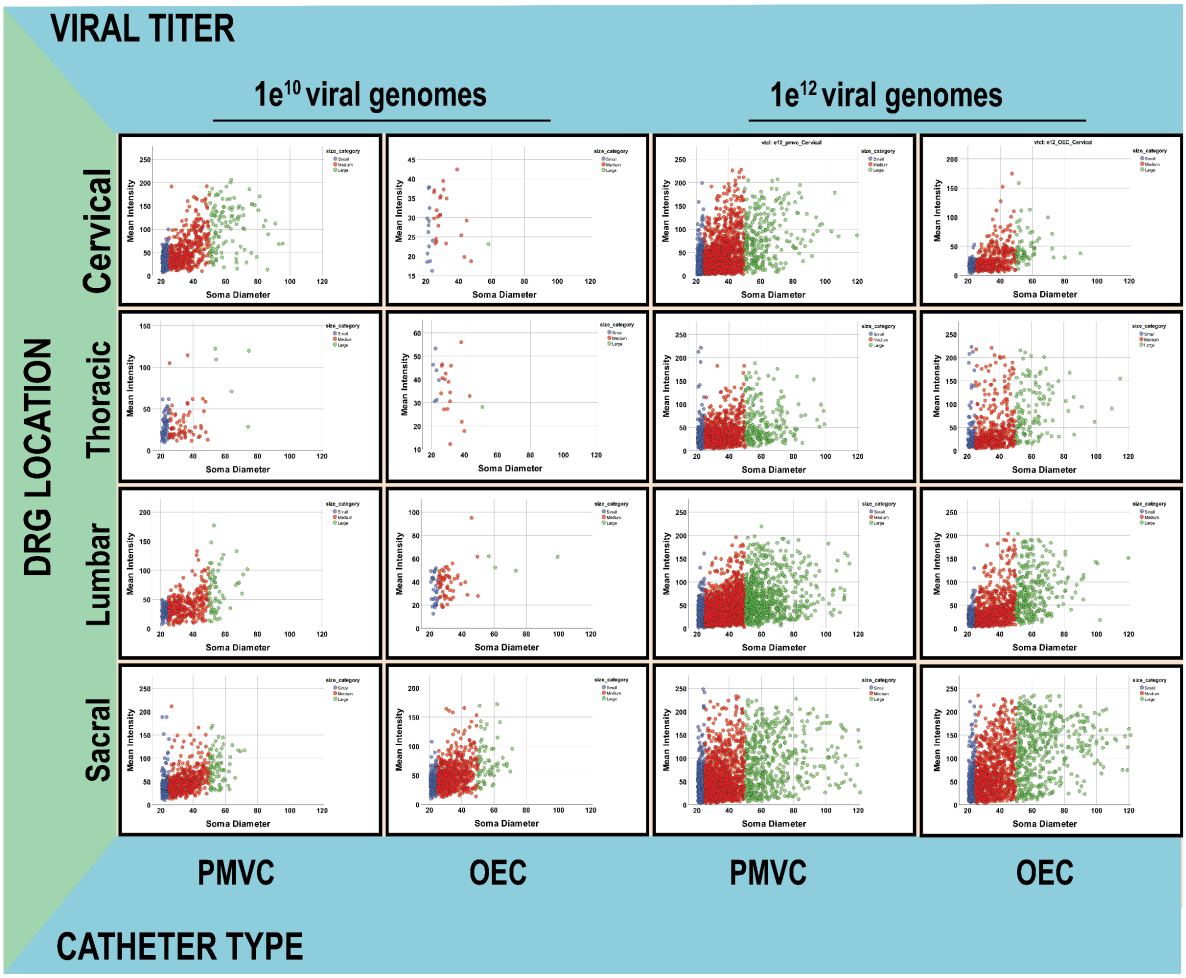

Figure 4-10: In-vivo AAV cell size distribution: Graphs display distribution of AAV positive neurons as a function of their soma size (x-axis) and their mean intensity of native RFP (y-axis). Small neurons (blue) medium neurons (red) and large neurons (green) can be visualized throughout their location in the neuraxis (rows), their viral titer (top of the columns), as well as the catheter type (bottom of the columns).

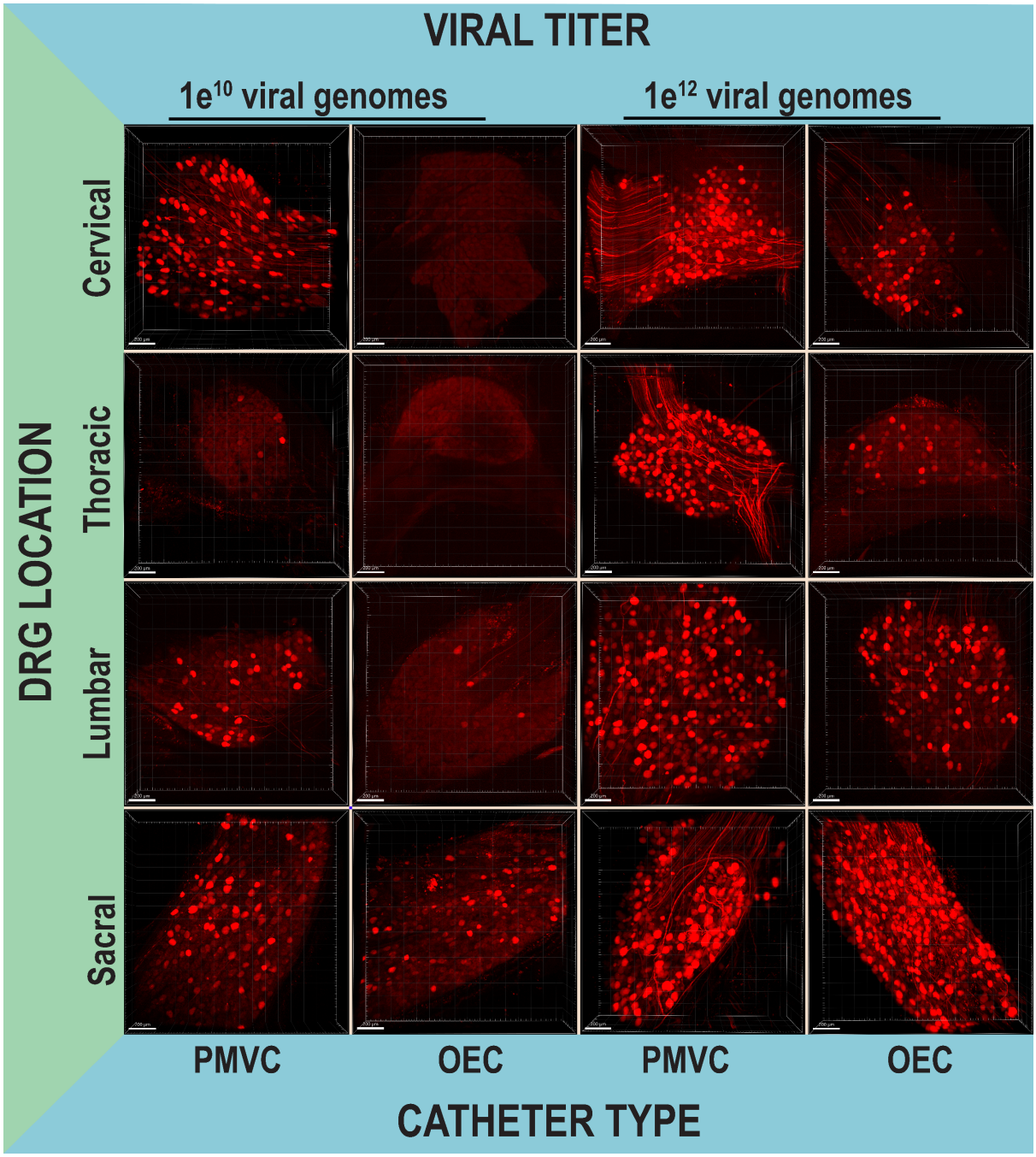

4-11: In-vivo AAV representative whole mount DRGs: representative whole mount DRGs visualized throughout their location in the neuraxis (rows), their viral titer (top of the columns), as well as the catheter type (bottom of the columns).

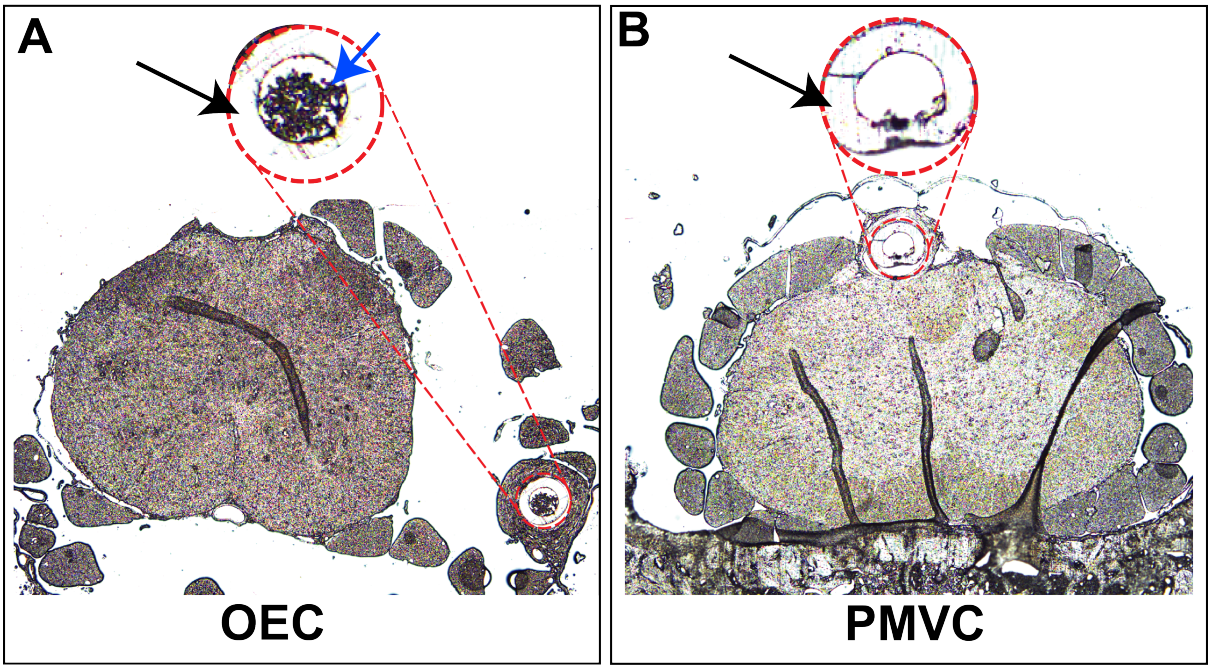

Figure 4-12: Accumulation of catheter debris. Figure presents representative lumbar sections though the spinal cord showing an OEC (A) and a PMVC (B) catheter. After a two week interval where no injection was made, harvested animals prepared with OECs show significant accumulations of debris (Blue Arrow) in contrast to the PMVCs which typically were absent of such debris. Magnified catheters are shown with the catheter wall signified by black arrows.

WORKS CITED

1. Sherrington, C., *The integrative action of the nervous system*. 1952: CUP Archive.

2. Sherrington, C.S., *Qualitative difference of spinal reflex corresponding with qualitative difference of cutaneous stimulus.* The Journal of physiology, 1903. **30**(1): p. 39.

3. Milligan, E.D. and L.R. Watkins, *Pathological and protective roles of glia in chronic pain.* Nat Rev Neurosci, 2009. **10**(1): p. 23-36.

4. Portenoy, R.K., *Report from the International Association for the Study of Pain Task Force on cancer pain.* J Pain Symptom Manage, 1996. **12**(2): p. 93-6.

5. Gaskin, D.J. and P. Richard, *The Economic Costs of Pain in the United States.* The Journal of Pain, 2012. **13**(8): p. 715-724.

6. Ojeda, B., A. Salazar, M. Dueñas, L.M. Torres, J.A. Micó, and I. Failde, *The impact of chronic pain: the perspective of patients, relatives, and caregivers.* Fam Syst Health, 2014. **32**(4): p. 399-407.

7. Dueñas, M., B. Ojeda, A. Salazar, J.A. Mico, and I. Failde, *A review of chronic pain impact on patients, their social environment and the health care system.* Journal of pain research, 2016. **9**: p. 457-467.

8. Kibaly, C., H.H. Loh, and P.Y. Law, *A Mechanistic Approach to the Development of Gene Therapy for Chronic Pain.* International Review of Cell and Molecular Biology, 2016. **327**: p. 89-161.

9. ACPA, *ACPA resource guide to chronic pain treatment an integrated guide to physical, behavioral and pharmacologic therapy* 2016, American Chronic Pain Association;: https://theacpa.org/uploads/documents/ACPA_Resource_Guide_2016.pdf.

10. Atluri, S., G. Sudarshan, and L. Manchikanti, *Assessment of the trends in medical use and misuse of opioid analgesics from 2004 to 2011.* Pain physician, 2014. **17**(2): p. E119-E128.

11. Basbaum, A.I., D.M. Bautista, G. Scherrer, and D. Julius, *Cellular and molecular mechanisms of pain.* Cell, 2009. **139**(2): p. 267-284.

12. Dubin, A.E. and A. Patapoutian, *Nociceptors: the sensors of the pain pathway.* The Journal of clinical investigation, 2010. **120**(11): p. 3760-3772.

13. Woolf, C.J. and Q. Ma, *Nociceptors--noxious stimulus detectors.* Neuron, 2007. **55**(3): p. 353-64.

14. Djouhri, L. and S.N. Lawson, *Abeta-fiber nociceptive primary afferent neurons: a review of incidence and properties in relation to other afferent A-fiber neurons in mammals.* Brain Res Brain Res Rev, 2004. **46**(2): p. 131-45.

15. Raja, S.N., R.A. Meyer, and J.N. Campbell, *Peripheral mechanisms of somatic pain.* Anesthesiology, 1988. **68**(4): p. 571-90.

16. Van Hees, J. and J. Gybels, *C nociceptor activity in human nerve during painful and non painful skin stimulation.* J Neurol Neurosurg Psychiatry, 1981. **44**(7): p. 600-7.

17. Raouf, R., K. Quick, and J.N. Wood, *Pain as a channelopathy.* J Clin Invest, 2010. **120**(11): p. 3745-52.

18. Ossipov, M.H., G.O. Dussor, and F. Porreca, *Central modulation of pain.* J Clin Invest, 2010. **120**(11): p. 3779-87.

19. Ossipov, M.H., K. Morimura, and F. Porreca, *Descending pain modulation and chronification of pain.* Curr Opin Support Palliat Care, 2014. **8**(2): p. 143-51.

20. Herrero, J.F., J.M. Laird, and J.A. López-García, *Wind-up of spinal cord neurones and pain sensation: much ado about something?* Prog Neurobiol, 2000. **61**(2): p. 169-203.

21. Wall, P.D. and C.J. Woolf, *Muscle but not cutaneous C-afferent input produces prolonged increases in the excitability of the flexion reflex in the rat.* The Journal of physiology, 1984. **356**: p. 443-458.

22. Woolf, C.J. and S.W.N. Thompson, *The induction and maintenance of central sensitization is dependent on N-methyl-d-aspartic acid receptor activation; implications for the treatment of post-injury pain hypersensitivity states.* Pain, 1991. **44**(3): p. 293-299.

23. Galan, A., J.M. Laird, and F. Cervero, *In vivo recruitment by painful stimuli of AMPA receptor subunits to the plasma membrane of spinal cord neurons.* Pain, 2004. **112**(3): p. 315-23.

24. Ji, R.R., R.W.t. Gereau, M. Malcangio, and G.R. Strichartz, *MAP kinase and pain.* Brain Res Rev, 2009. **60**(1): p. 135-48.

25. St John Smith, E., *Advances in understanding nociception and neuropathic pain.* Journal of neurology, 2018. **265**(2): p. 231-238.

26. Ronchetti, S., G. Migliorati, and D.V. Delfino, *Association of inflammatory mediators with pain perception.* Biomedicine & Pharmacotherapy, 2017. **96**: p. 1445-1452.

27. Pinho-Ribeiro, F.A., W.A. Verri, Jr., and I.M. Chiu, *Nociceptor Sensory Neuron-Immune Interactions in Pain and Inflammation.* Trends Immunol, 2017. **38**(1): p. 5-19.

28. Campbell, J.N. and R.A. Meyer, *Mechanisms of neuropathic pain.* Neuron, 2006. **52**(1): p. 77-92.

29. Opree, A. and M. Kress, *Involvement of the proinflammatory cytokines tumor necrosis factor-alpha, IL-1 beta, and IL-6 but not IL-8 in the development of heat hyperalgesia: effects on heat-evoked calcitonin gene-related peptide release from rat skin.* J Neurosci, 2000. **20**(16): p. 6289-93.

30. Puig, S. and L.S. Sorkin, *Formalin-evoked activity in identified primary afferent fibers: systemic lidocaine suppresses phase-2 activity.* Pain, 1996. **64**(2): p. 345-55.

31. Woolf, C.J. and M.W. Salter, *Neuronal plasticity: increasing the gain in pain.* Science, 2000. **288**(5472): p. 1765-9.

32. Woolf, C.J. and S.W. Thompson, *The induction and maintenance of central sensitization is dependent on N-methyl-D-aspartic acid receptor activation; implications for the treatment of post-injury pain hypersensitivity states.* Pain, 1991. **44**(3): p. 293-9.

33. Yashpal, K., K. Fisher, J.G. Chabot, and T.J. Coderre, *Differential effects of NMDA and group I mGluR antagonists on both nociception and spinal cord protein kinase C translocation in the formalin test and a model of neuropathic pain in rats.* Pain, 2001. **94**(1): p. 17-29.

34. Pezet, S., F. Marchand, R. D'Mello, J. Grist, A.K. Clark, M. Malcangio, A.H. Dickenson, R.J. Williams, and S.B. McMahon, *Phosphatidylinositol 3-kinase is a key mediator of central sensitization in painful inflammatory conditions.* J Neurosci, 2008. **28**(16): p. 4261-70.

35. Tsokas, P., T. Ma, R. Iyengar, E.M. Landau, and R.D. Blitzer, *Mitogen-activated protein kinase upregulates the dendritic translation machinery in long-term potentiation by controlling the mammalian target of rapamycin pathway.* J Neurosci, 2007. **27**(22): p. 5885-94.

36. Asante, C.O., V.C. Wallace, and A.H. Dickenson, *Formalin-induced behavioural hypersensitivity and neuronal hyperexcitability are mediated by rapid protein synthesis at the spinal level.* Mol Pain, 2009. **5**: p. 27.

37. Colloca, L., T. Ludman, D. Bouhassira, R. Baron, A.H. Dickenson, D. Yarnitsky, R. Freeman, A. Truini, N. Attal, N.B. Finnerup, C. Eccleston, E. Kalso, D.L. Bennett, R.H. Dworkin, and S.N. Raja, *Neuropathic pain.* Nature reviews. Disease primers, 2017. **3**: p. 17002-17002.

38. Park, H.J., *Chemotherapy induced peripheral neuropathic pain.* Korean journal of anesthesiology, 2014. **67**(1): p. 4-7.

39. Bouhassira, D., M. Letanoux, and A. Hartemann, *Chronic pain with neuropathic characteristics in diabetic patients: a French cross-sectional study.* PLoS One, 2013. **8**(9): p. e74195.

40. Solaro, C., G. Brichetto, M.P. Amato, E. Cocco, B. Colombo, G. D'Aleo, C. Gasperini, A. Ghezzi, V. Martinelli, C. Milanese, F. Patti, M. Trojano, E. Verdun, and G.L. Mancardi, *The prevalence of pain in multiple sclerosis: a multicenter cross-sectional study.* Neurology, 2004. **63**(5): p. 919-21.

41. Siddall, P.J., J.M. McClelland, S.B. Rutkowski, and M.J. Cousins, *A longitudinal study of the prevalence and characteristics of pain in the first 5 years following spinal cord injury.* Pain, 2003. **103**(3): p. 249-57.

42. Cohen, S.P. and J. Mao, *Neuropathic pain: mechanisms and their clinical implications.* Bmj, 2014. **348**: p. f7656.

43. Yu, X., H. Liu, K.A. Hamel, M.G. Morvan, S. Yu, J. Leff, Z. Guan, J.M. Braz, and A.I. Basbaum, *Dorsal root ganglion macrophages contribute to both the initiation and persistence of neuropathic pain.* Nat Commun, 2020. **11**(1): p. 264.

44. Hinder, L.M., P.D. Brien, J.M. Hayes, C. Backus, A.P. Solway, C. Sims-Robinson, and E.L. Feldman, *Dietary reversal of neuropathy in a murine model of prediabetes and metabolic syndrome.* Disease Models & Mechanisms, 2017. **10**(6): p. 717.

45. Pal, P.K., *Clinical and electrophysiological studies in vincristine induced neuropathy.* Electromyography and clinical neurophysiology, 1999. **39**(6): p. 323.

46. Todd, G.C., W.R. Gibson, and D.M. Morton, *Toxicology of vindesine (desacetyl vinblastine amide) in mice, rats, and dogs.* Journal of Toxicology and Environmental Health, Part A Current Issues, 1976. **1**(5): p. 843-849.

47. Xiao, W.H. and G.J. Bennett, *Chemotherapy-evoked neuropathic pain: Abnormal spontaneous discharge in A-fiber and C-fiber primary afferent neurons and its suppression by acetyl-L-carnitine.* Pain, 2008. **135**(3): p. 262-270.

48. Dalziel, R.G., S. Bingham, D. Sutton, D. Grant, J.M. Champion, S.A. Dennis, J.P. Quinn, C. Bountra, and M.A. Mark, *Allodynia in rats infected with varicella zoster virus--a small animal model for post-herpetic neuralgia.* Brain Res Brain Res Rev, 2004. **46**(2): p. 234-42.

49. Fan, X. and Y. Agid, *At the Origin of the History of Glia.* Neuroscience, 2018. **385**: p. 255-271.

50. Oberheim, N.A., X. Wang, S. Goldman, and M. Nedergaard, *Astrocytic complexity distinguishes the human brain.* Trends Neurosci, 2006. **29**(10): p. 547-53.

51. Rowitch, D.H. and A.R. Kriegstein, *Developmental genetics of vertebrate glial-cell specification.* Nature, 2010. **468**(7321): p. 214-22.

52. Nayak, D., T.L. Roth, and D.B. McGavern, *Microglia development and function.* Annual review of immunology, 2014. **32**: p. 367.

53. Lenz, K.M. and L.H. Nelson, *Microglia and Beyond: Innate Immune Cells As Regulators of Brain Development and Behavioral Function.* Front Immunol, 2018. **9**: p. 698.

54. Ji, R.R., T. Berta, and M. Nedergaard, *Glia and pain: is chronic pain a gliopathy?* Pain, 2013. **154 Suppl 1**(0 1): p. S10-28.

55. Kimelberg, H.K. and M. Nedergaard, *Functions of astrocytes and their potential as therapeutic targets.* Neurotherapeutics, 2010. **7**(4): p. 338-53.

56. Iadecola, C. and M. Nedergaard, *Glial regulation of the cerebral microvasculature.* Nat Neurosci, 2007. **10**(11): p. 1369-76.

57. Cholewinski, A.J., M.R. Hanley, and G.P. Wilkin, *A phosphoinositide-linked peptide response in astrocytes: evidence for regional heterogeneity.* Neurochem Res, 1988. **13**(4): p. 389-94.

58. Beaujouan, J.C., M.C. Daguet de Montety, Y. Torrens, M. Saffroy, M. Dietl, and J. Glowinski, *Marked regional heterogeneity of 125I-Bolton Hunter substance P binding and substance P-induced activation of phospholipase C in astrocyte cultures from the embryonic or newborn rat.* J Neurochem, 1990. **54**(2): p. 669-75.

59. Honore, P., S.D. Rogers, M.J. Schwei, J.L. Salak-Johnson, N.M. Luger, M.C. Sabino, D.R. Clohisy, and P.W. Mantyh, *Murine models of inflammatory, neuropathic and cancer pain each generates a unique set of neurochemical changes in the spinal cord and sensory neurons.* Neuroscience, 2000. **98**(3): p. 585-98.

60. Hald, A., S. Nedergaard, R.R. Hansen, M. Ding, and A.M. Heegaard, *Differential activation of spinal cord glial cells in murine models of neuropathic and cancer pain.* Eur J Pain, 2009. **13**(2): p. 138-45.

61. Garrison, C.J., P.M. Dougherty, K.C. Kajander, and S.M. Carlton, *Staining of glial fibrillary acidic protein (GFAP) in lumbar spinal cord increases following a sciatic nerve constriction injury.* Brain Res, 1991. **565**(1): p. 1-7.

62. Li, W.W., T.Z. Guo, X. Shi, Y. Sun, T. Wei, D.J. Clark, and W.S. Kingery, *Substance P spinal signaling induces glial activation and nociceptive sensitization after fracture.* Neuroscience, 2015. **310**: p. 73-90.

63. Haas, C.A., M. Reddington, and G.W. Kreutzberg, *Calcitonin Gene-related Peptide Stimulates the Induction of c-fos Gene Expression in Rat Astrocyte Cultures.* Eur J Neurosci, 1991. **3**(7): p. 708-712.

64. Ahmed, Z., C.A. Lewis, and D.S. Faber, *Glutamate stimulates release of Ca2+ from internal stores in astroglia.* Brain Res, 1990. **516**(1): p. 165-9.

65. Gu, J.G., *P2X receptor-mediated modulation of sensory transmission to the spinal cord dorsal horn.* Neuroscientist, 2003. **9**(5): p. 370-8.

66. Garrison, C.J., P.M. Dougherty, and S.M. Carlton, *GFAP expression in lumbar spinal cord of naive and neuropathic rats treated with MK-801.* Exp Neurol, 1994. **129**(2): p. 237-43.

67. Stoll, G. and S. Jander, *The role of microglia and macrophages in the pathophysiology of the CNS.* Progress in neurobiology, 1999. **58**(3): p. 233-247.

68. Tremblay, M., B. Stevens, A. Sierra, H. Wake, A. Bessis, and A. Nimmerjahn, *The role of microglia in the healthy brain.* J Neurosci, 2011. **31**(45): p. 16064-9.

69. Hanisch, U.-K. and H. Kettenmann, *Microglia: active sensor and versatile effector cells in the normal and pathologic brain.* Nature Neuroscience, 2007. **10**(11): p. 1387-1394.

70. Eriksson, N.P., J.K.E. Persson, M. Svensson, J. Arvidsson, C. Molander, and H. Aldskogius, *A quantitative analysis of the microglial cell reaction in central primary sensory projection territories following peripheral nerve injury in the adult rat.* Experimental Brain Research, 1993. **96**(1): p. 19-27.

71. Ledeboer, A., E.M. Sloane, E.D. Milligan, M.G. Frank, J.H. Mahony, S.F. Maier, and L.R. Watkins, *Minocycline attenuates mechanical allodynia and proinflammatory cytokine expression in rat models of pain facilitation.* Pain, 2005. **115**(1): p. 71-83.

72. Lin, C.-S., M.-L. Tsaur, C.-C. Chen, T.-Y. Wang, C.-F. Lin, Y.-L. Lai, T.-C. Hsu, Y.-Y. Pan, C.-H. Yang, and J.-K. Cheng, *Chronic Intrathecal Infusion of Minocycline Prevents the Development of Spinal-Nerve Ligation–Induced Pain in Rats.* Regional Anesthesia and Pain Medicine, 2007. **32**(3): p. 209-216.

73. Coyle, D.E., *Partial peripheral nerve injury leads to activation of astroglia and microglia which parallels the development of allodynic behavior.* Glia, 1998. **23**(1): p. 75-83.

74. Colburn, R.W., J.A. DeLeo, A.J. Rickman, M.P. Yeager, P. Kwon, and W.F. Hickey, *Dissociation of microglial activation and neuropathic pain behaviors following peripheral nerve injury in the rat.* Journal of Neuroimmunology, 1997. **79**(2): p. 163-175.

75. Beggs, S. and M.W. Salter, *Stereological and somatotopic analysis of the spinal microglial response to peripheral nerve injury.* Brain, Behavior, and Immunity, 2007. **21**(5): p. 624-633.

76. Daulhac, L., C. Mallet, C. Courteix, M. Etienne, E. Duroux, A.-M. Privat, A. Eschalier, and J. Fialip, *Diabetes-Induced Mechanical Hyperalgesia Involves Spinal Mitogen-Activated Protein Kinase Activation in Neurons and Microglia via N-Methyl-D-aspartate-Dependent Mechanisms.* Molecular Pharmacology, 2006. **70**(4): p. 1246.

77. Zhang, R.X., B. Liu, L. Wang, K. Ren, J.T. Qiao, B.M. Berman, and L. Lao, *Spinal glial activation in a new rat model of bone cancer pain produced by prostate cancer cell inoculation of the tibia.* Pain, 2005. **118**(1-2): p. 125-36.

78. Milligan, E.D., K.A. O'Connor, K.T. Nguyen, C.B. Armstrong, C. Twining, R.P. Gaykema, A. Holguin, D. Martin, S.F. Maier, and L.R. Watkins, *Intrathecal HIV-1 envelope glycoprotein gp120 induces enhanced pain states mediated by spinal cord proinflammatory cytokines.* J Neurosci, 2001. **21**(8): p. 2808-19.

79. Zheng, F.Y., W.H. Xiao, and G.J. Bennett, *The response of spinal microglia to chemotherapy-evoked painful peripheral neuropathies is distinct from that evoked by traumatic nerve injuries.* Neuroscience, 2011. **176**: p. 447-54.

80. Hu, P. and E.M. McLachlan, *Distinct functional types of macrophage in dorsal root ganglia and spinal nerves proximal to sciatic and spinal nerve transections in the rat.* Exp Neurol, 2003. **184**(2): p. 590-605.

81. Simeoli, R., K. Montague, H.R. Jones, L. Castaldi, D. Chambers, J.H. Kelleher, V. Vacca, T. Pitcher, J. Grist, H. Al-Ahdal, L.F. Wong, M. Perretti, J. Lai, P. Mouritzen, P. Heppenstall, and M. Malcangio, *Exosomal cargo including microRNA regulates sensory neuron to macrophage communication after nerve trauma.* Nat Commun, 2017. **8**(1): p. 1778.

82. Douarin, N.L., C. Dulac, E. Dupin, and P. Cameron-Curry, *Glial cell lineages in the neural crest.* Glia, 1991. **4**(2): p. 175-184.

83. Serbedzija, G.N., S.E. Fraser, and M. Bronner-Fraser, *Pathways of trunk neural crest cell migration in the mouse embryo as revealed by vital dye labelling.* Development, 1990. **108**(4): p. 605-612.

84. Ma, Q., C. Fode, F. Guillemot, and D.J. Anderson, *Neurogenin1 and neurogenin2 control two distinct waves of neurogenesis in developing dorsal root ganglia.* Genes & development, 1999. **13**(13): p. 1717-1728.

85. Maro, G.S., M. Vermeren, O. Voiculescu, L. Melton, J. Cohen, P. Charnay, and P. Topilko, *Neural crest boundary cap cells constitute a source of neuronal and glial cells of the PNS.* Nature neuroscience, 2004. **7**(9): p. 930-938.

86. Gresset, A., F. Coulpier, G. Gerschenfeld, A. Jourdon, G. Matesic, L. Richard, J.-M. Vallat, P. Charnay, and P. Topilko, *Boundary caps give rise to neurogenic stem cells and terminal glia in the skin.* Stem Cell Reports, 2015. **5**(2): p. 278-290.

87. Jacob, C., P. Lötscher, S. Engler, A. Baggiolini, S.V. Tavares, V. Brügger, N. John, S. Büchmann-Møller, P.L. Snider, and S.J. Conway, *HDAC1 and HDAC2 control the specification of neural crest cells into peripheral glia.* Journal of Neuroscience, 2014. **34**(17): p. 6112-6122.

88. Ahimsadasan, N., V. Reddy, and A. Kumar, *Neuroanatomy, Dorsal Root Ganglion*, in *StatPearls*. 2020, StatPearls Publishing

89. Hoeffel, G. and F. Ginhoux, *Ontogeny of Tissue-Resident Macrophages.* Front Immunol, 2015. **6**: p. 486.

90. Rigato, C., R. Buckinx, H. Le-Corronc, J.M. Rigo, and P. Legendre, *Pattern of invasion of the embryonic mouse spinal cord by microglial cells at the time of the onset of functional neuronal networks.* Glia, 2011. **59**(4): p. 675-95.

91. Fan, W., X. Zhu, Y. He, M. Zhu, Z. Wu, F. Huang, and H. He, *The role of satellite glial cells in orofacial pain.* J Neurosci Res, 2019. **97**(4): p. 393-401.

92. Pannese, E., *The satellite cells of the sensory ganglia*. Vol. 65. 2013: Springer Science & Business Media.

93. Li, J., C.V. Vause, and P.L. Durham, *Calcitonin gene-related peptide stimulation of nitric oxide synthesis and release from trigeminal ganglion glial cells.* Brain research, 2008. **1196**: p. 22-32.

94. Ceruti, S., M. Fumagalli, G. Villa, C. Verderio, and M.P. Abbracchio, *Purinoceptor-mediated calcium signaling in primary neuron-glia trigeminal cultures.* Cell calcium, 2008. **43**(6): p. 576-590.

95. Zhang, X., Y. Chen, C. Wang, and L.-Y. Huang, *Neuronal somatic ATP release triggers neuron–satellite glial cell communication in dorsal root ganglia.* Proceedings of the National Academy of Sciences, 2007. **104**(23): p. 9864-9869.

96. Takeda, M., M. Takahashi, and S. Matsumoto, *Contribution of the activation of satellite glia in sensory ganglia to pathological pain.* Neuroscience & Biobehavioral Reviews, 2009. **33**(6): p. 784-792.

97. Dubový, P., R. Jančálek, I. Klusáková, I. Svíženská, and K. Pejchalová, *Intra-and extraneuronal changes of immunofluorescence staining for TNF-and TNFR1 in the dorsal root ganglia of rat peripheral neuropathic pain models.* Cellular and molecular neurobiology, 2006. **26**(7-8): p. 1203-1215.

98. Li, M., J. Shi, J.r. TANG, D. Chen, B. Ai, J. Chen, L.n. WANG, F.y. CAO, L.I. LI, and C.y. LIN, *Effects of complete Freund's adjuvant on immunohistochemical distribution of IL-1β and IL-1R I in neurons and glia cells of dorsal root ganglion 1.* Acta pharmacologica Sinica, 2005. **26**(2): p. 192-198.

99. Pomonis, J.D., S.D. Rogers, C.M. Peters, J.R. Ghilardi, and P.W. Mantyh, *Expression and localization of endothelin receptors: implications for the involvement of peripheral glia in nociception.* Journal of Neuroscience, 2001. **21**(3): p. 999-1006.

100. Castillo, C., M. Norcini, L.M. Hernandez, G. Correa, T. Blanck, and E. Recio-Pinto, *Satellite glia cells in dorsal root ganglia express functional NMDA receptors.* Neuroscience, 2013. **240**: p. 135-146.

101. Gu, Y., Y. Chen, X. Zhang, G. Li, C.Y. Wang, and L.-Y.M. Huang, *Neuronal soma-satellite glial cell interactions in sensory ganglia and the participation of purinergic receptors.* Neuron glia biology, 2010. **6**(1): p. 53.

102. Huang, L.Y., Y. Gu, and Y. Chen, *Communication between neuronal somata and satellite glial cells in sensory ganglia.* Glia, 2013. **61**(10): p. 1571-81.

103. Waller, A.V., *XX. Experiments on the section of the glossopharyngeal and hypoglossal nerves of the frog, and observations of the alterations produced thereby in the structure of their primitive fibres.* Philosophical transactions of the Royal society of London, 1850(140): p. 423-429.

104. Brown, M.C., V.H. Perry, E.R. Lunn, S. Gordon, and R. Heumann, *Macrophage dependence of peripheral sensory nerve regeneration: possible involvement of nerve growth factor.* Neuron, 1991. **6**(3): p. 359-70.

105. Miller, R.J., H. Jung, S.K. Bhangoo, and F.A. White, *Cytokine and chemokine regulation of sensory neuron function.* Handbook of experimental pharmacology, 2009(194): p. 417-449.

106. Chiu, I.M., C.A. von Hehn, and C.J. Woolf, *Neurogenic inflammation and the peripheral nervous system in host defense and immunopathology.* Nature neuroscience, 2012. **15**(8): p. 1063-1067.

107. Brain, S.D. and T.J. Williams, *Interactions between the tachykinins and calcitonin gene-related peptide lead to the modulation of oedema formation and blood flow in rat skin.* Br J Pharmacol, 1989. **97**(1): p. 77-82.

108. Edvinsson, L., R. Ekman, I. Jansen, J. McCulloch, and R. Uddman, *Calcitonin gene-related peptide and cerebral blood vessels: distribution and vasomotor effects.* J Cereb Blood Flow Metab, 1987. **7**(6): p. 720-8.

109. McCormack, D.G., J.C. Mak, M.O. Coupe, and P.J. Barnes, *Calcitonin gene-related peptide vasodilation of human pulmonary vessels.* J Appl Physiol (1985), 1989. **67**(3): p. 1265-70.

110. Lotze, M.T., H.J. Zeh, A. Rubartelli, L.J. Sparvero, A.A. Amoscato, N.R. Washburn, M.E. DeVera, X. Liang, M. Tör, and T. Billiar, *The grateful dead: damage-associated molecular pattern molecules and reduction/oxidation regulate immunity.* Immunological Reviews, 2007. **220**(1): p. 60-81.

111. Bianchi, M.E., *DAMPs, PAMPs and alarmins: all we need to know about danger.* Journal of leukocyte biology, 2007. **81**(1): p. 1-5.

112. Akira, S., S. Uematsu, and O. Takeuchi, *Pathogen recognition and innate immunity.* Cell, 2006. **124**(4): p. 783-801.

113. Scaffidi, P., T. Misteli, and M.E. Bianchi, *Release of chromatin protein HMGB1 by necrotic cells triggers inflammation.* Nature, 2002. **418**(6894): p. 191-195.

114. Quintana, F.J. and I.R. Cohen, *Heat shock proteins as endogenous adjuvants in sterile and septic inflammation.* The Journal of Immunology, 2005. **175**(5): p. 2777-2782.

115. Hofmann, M.A., S. Drury, C. Fu, W. Qu, A. Taguchi, Y. Lu, C. Avila, N. Kambham, A. Bierhaus, and P. Nawroth, *RAGE mediates a novel proinflammatory axis: a central cell surface receptor for S100/calgranulin polypeptides.* Cell, 1999. **97**(7): p. 889-901.

116. Bours, M., E. Swennen, F. Di Virgilio, B. Cronstein, and P. Dagnelie, *Adenosine 5'-triphosphate and adenosine as endogenous signaling molecules in immunity and inflammation.* Pharmacology & therapeutics, 2006. **112**(2): p. 358-404.

117. Kawasaki, T. and T. Kawai, *Toll-Like Receptor Signaling Pathways.* Frontiers in Immunology, 2014. **5**(461).

118. Janeway Jr, C.A. and R. Medzhitov, *Innate immune recognition.* Annual review of immunology, 2002. **20**(1): p. 197-216.

119. Satoh, T. and S. Akira, *Toll-Like Receptor Signaling and Its Inducible Proteins.* Microbiol Spectr, 2016. **4**(6).

120. Lin, S.C., Y.C. Lo, and H. Wu, *Helical assembly in the MyD88-IRAK4-IRAK2 complex in TLR/IL-1R signalling.* Nature, 2010. **465**(7300): p. 885-90.

121. Kawai, T. and S. Akira, *The role of pattern-recognition receptors in innate immunity: update on Toll-like receptors.* Nat Immunol, 2010. **11**(5): p. 373-84.

122. Kawai, T., O. Takeuchi, T. Fujita, J. Inoue, P.F. Mühlradt, S. Sato, K. Hoshino, and S. Akira, *Lipopolysaccharide stimulates the MyD88-independent pathway and results in activation of IFN-regulatory factor 3 and the expression of a subset of lipopolysaccharide-inducible genes.* J Immunol, 2001. **167**(10): p. 5887-94.

123. Doyle, S., S. Vaidya, R. O'Connell, H. Dadgostar, P. Dempsey, T. Wu, G. Rao, R. Sun, M. Haberland, R. Modlin, and G. Cheng, *IRF3 mediates a TLR3/TLR4-specific antiviral gene program.* Immunity, 2002. **17**(3): p. 251-63.

124. Hoshino, K., T. Kaisho, T. Iwabe, O. Takeuchi, and S. Akira, *Differential involvement of IFN-beta in Toll-like receptor-stimulated dendritic cell activation.* Int Immunol, 2002. **14**(10): p. 1225-31.

125. Janeway, C.A., Jr. and R. Medzhitov, *Innate immune recognition.* Annu Rev Immunol, 2002. **20**: p. 197-216.

126. Xu, Z.Z., Y.H. Kim, S. Bang, Y. Zhang, T. Berta, F. Wang, S.B. Oh, and R.R. Ji, *Inhibition of mechanical allodynia in neuropathic pain by TLR5-mediated A-fiber blockade.* Nat Med, 2015. **21**(11): p. 1326-31.

127. Liu, T., T. Berta, Z.Z. Xu, C.K. Park, L. Zhang, N. Lü, Q. Liu, Y. Liu, Y.J. Gao, Y.C. Liu, Q. Ma, X. Dong, and R.R. Ji, *TLR3 deficiency impairs spinal cord synaptic transmission, central sensitization, and pruritus in mice.* J Clin Invest, 2012. **122**(6): p. 2195-207.

128. Wigerblad, G., D.B. Bas, C. Fernades-Cerqueira, A. Krishnamurthy, K.S. Nandakumar, K. Rogoz, J. Kato, K. Sandor, J. Su, and J.M. Jimenez–Andrade, *Autoantibodies to citrullinated proteins may induce joint pain independent of inflammation.* Annals of the rheumatic diseases, 2016. **75**(4): p. 730-738.

129. Tékus, V., Z. Hajna, É. Borbély, A. Markovics, T. Bagoly, J. Szolcsányi, V. Thompson, Á. Kemény, Z. Helyes, and A. Goebel, *A CRPS-IgG-transfer-trauma model reproducing inflammatory and positive sensory signs associated with complex regional pain syndrome.* PAIN®, 2014. **155**(2): p. 299-308.

130. Doppler, K., L. Appeltshauser, C. Villmann, C. Martin, E. Peles, H.H. Krämer, A. Haarmann, M. Buttmann, and C. Sommer, *Auto-antibodies to contactin-associated protein 1 (Caspr) in two patients with painful inflammatory neuropathy.* Brain, 2016. **139**(Pt 10): p. 2617-2630.

131. Hunt, M.A., D.S.M. Nascimento, A. Bersellini Farinotti, and C.I. Svensson, *Autoantibodies Hurt: Transfer of Patient-Derived CASPR2 Antibodies Induces Neuropathic Pain in Mice.* Neuron, 2018. **97**(4): p. 729-731.

132. Dawes, J.M., G.A. Weir, S.J. Middleton, R. Patel, K.I. Chisholm, P. Pettingill, L.J. Peck, J. Sheridan, A. Shakir, and L. Jacobson, *Immune or genetic-mediated disruption of CASPR2 causes pain hypersensitivity due to enhanced primary afferent excitability.* Neuron, 2018. **97**(4): p. 806-822. e10.

133. Bersellini Farinotti, A., G. Wigerblad, D. Nascimento, D.B. Bas, C. Morado Urbina, K.S. Nandakumar, K. Sandor, B. Xu, S. Abdelmoaty, M.A. Hunt, K. Ängeby Möller, A. Baharpoor, J. Sinclair, K. Jardemark, J.T. Lanner, I. Khmaladze, L.E. Borm, L. Zhang, F. Wermeling, M.S. Cragg, J. Lengqvist, A.-J. Chabot-Doré, L. Diatchenko, I. Belfer, M. Collin, K. Kultima, B. Heyman, J.M. Jimenez-Andrade, S. Codeluppi, R. Holmdahl, and C.I. Svensson, *Cartilage-binding antibodies induce pain through immune complex–mediated activation of neurons.* The Journal of Experimental Medicine, 2019. **216**(8): p. 1904-1924.

134. Wang, L., X. Jiang, Q. Zheng, S.M. Jeon, T. Chen, Y. Liu, H. Kulaga, R. Reed, X. Dong, M.J. Caterina, and L. Qu, *Neuronal FcγRI mediates acute and chronic joint pain.* J Clin Invest, 2019. **129**(9): p. 3754-3769.

135. Myasoedova, E., C.S. Crowson, H.M. Kremers, T.M. Therneau, and S.E. Gabriel, *Is the incidence of rheumatoid arthritis rising?: results from Olmsted County, Minnesota, 1955–2007.* Arthritis & Rheumatism, 2010. **62**(6): p. 1576-1582.

136. Cross, M., E. Smith, D. Hoy, L. Carmona, F. Wolfe, T. Vos, B. Williams, S. Gabriel, M. Lassere, and N. Johns, *The global burden of rheumatoid arthritis: estimates from the global burden of disease 2010 study.* Annals of the rheumatic diseases, 2014. **73**(7): p. 1316-1322.

137. Barra, L., J. Pope, L. Bessette, B. Haraoui, and V. Bykerk, *Lack of seroconversion of rheumatoid factor and anti-cyclic citrullinated peptide in patients with early inflammatory arthritis: a systematic literature review.* Rheumatology, 2011. **50**(2): p. 311-316.

138. Nell-Duxneuner, V., K. Machold, T. Stamm, G. Eberl, H. Heinzl, E. Hoefler, J.S. Smolen, and G. Steiner, *Autoantibody profiling in patients with very early rheumatoid arthritis: a follow-up study.* Annals of the rheumatic diseases, 2010. **69**(01): p. 169-174.

139. Aletaha, D., F. Alasti, and J.S. Smolen, *Rheumatoid factor, not antibodies against citrullinated proteins, is associated with baseline disease activity in rheumatoid arthritis clinical trials.* Arthritis research & therapy, 2015. **17**(1): p. 229.

140. Gonzalez, A., M. Icen, H.M. Kremers, C.S. Crowson, J.M. Davis, T.M. Therneau, V.L. Roger, and S.E. Gabriel, *Mortality trends in rheumatoid arthritis: the role of rheumatoid factor.* The Journal of rheumatology, 2008. **35**(6): p. 1009-1014.

141. Van Gaalen, F.A., J. Van Aken, T.W.J. Huizinga, G.M.T. Schreuder, F.C. Breedveld, E. Zanelli, W.J. Van Venrooij, C.L. Verweij, R.E.M. Toes, and R.R.P. De Vries, *Association between HLA class II genes and autoantibodies to cyclic citrullinated peptides (CCPs) influences the severity of rheumatoid arthritis.* Arthritis & Rheumatism: Official Journal of the American College of Rheumatology, 2004. **50**(7): p. 2113-2121.

142. Jiang, X., T. Frisell, J. Askling, E.W. Karlson, L. Klareskog, L. Alfredsson, and H. Källberg, *To what extent is the familial risk of rheumatoid arthritis explained by established rheumatoid arthritis risk factors?* Arthritis & Rheumatology, 2015. **67**(2): p. 352-362.

143. Okada, Y., D. Wu, G. Trynka, T. Raj, C. Terao, K. Ikari, Y. Kochi, K. Ohmura, A. Suzuki, and S. Yoshida, *Genetics of rheumatoid arthritis contributes to biology and drug discovery.* Nature, 2014. **506**(7488): p. 376-381.

144. Smolen, J.S., D. Aletaha, and I.B. McInnes, *Rheumatoid arthritis.* The Lancet, 2016. **388**(10055): p. 2023-2038.

145. Sparks, J.A., *Rheumatoid Arthritis.* Annals of Internal Medicine, 2019. **170**(1): p. ITC1-ITC16.

146. Walsh, D.A. and D.F. McWilliams, *Mechanisms, impact and management of pain in rheumatoid arthritis.* Nat Rev Rheumatol, 2014. **10**(10): p. 581-92.

147. Heiberg, T. and T.K. Kvien, *Preferences for improved health examined in 1,024 patients with rheumatoid arthritis: pain has highest priority.* Arthritis Care & Research, 2002. **47**(4): p. 391-397.

148. McWilliams, D.F., W. Zhang, J.S. Mansell, P.D.W. Kiely, A. Young, and D.A. Walsh, *Predictors of change in bodily pain in early rheumatoid arthritis: an inception cohort study.* Arthritis care & research, 2012. **64**(10): p. 1505-1513.

149. Nielen, M.M., D. van Schaardenburg, H.W. Reesink, R.J. Van de Stadt, I.E. van der Horst-Bruinsma, M.H. de Koning, M.R. Habibuw, J.P. Vandenbroucke, and B.A. Dijkmans, *Specific autoantibodies precede the symptoms of rheumatoid arthritis: a study of serial measurements in blood donors.* Arthritis & Rheumatism: Official Journal of the American College of Rheumatology, 2004. **50**(2): p. 380-386.

150. Van Gaalen, F.A., J. Van Aken, T.W. Huizinga, G.M.T. Schreuder, F.C. Breedveld, E. Zanelli, W.J. Van Venrooij, C.L. Verweij, R.E. Toes, and R.R. De Vries, *Association between HLA class II genes and autoantibodies to cyclic citrullinated peptides (CCPs) influences the severity of rheumatoid arthritis.* Arthritis & Rheumatism: Official Journal of the American College of Rheumatology, 2004. **50**(7): p. 2113-2121.

151. Lillegraven, S., D. van der Heijde, T. Uhlig, T.K. Kvien, and E.A. Haavardsholm, *What is the clinical relevance of erosions and joint space narrowing in RA?* Nat Rev Rheumatol, 2012. **8**(2): p. 117-20.

152. Rombouts, Y., A. Willemze, J.J. van Beers, J. Shi, P.F. Kerkman, L. van Toorn, G.M. Janssen, A. Zaldumbide, R.C. Hoeben, and G.J. Pruijn, *Extensive glycosylation of ACPA-IgG variable domains modulates binding to citrullinated antigens in rheumatoid arthritis.* Annals of the rheumatic diseases, 2016. **75**(3): p. 578-585.

153. Rombouts, Y., E. Ewing, L.A. van de Stadt, M.H. Selman, L.A. Trouw, A.M. Deelder, T.W. Huizinga, M. Wuhrer, D. van Schaardenburg, and R.E. Toes, *Anti-citrullinated protein antibodies acquire a pro-inflammatory Fc glycosylation phenotype prior to the onset of rheumatoid arthritis.* Annals of the rheumatic diseases, 2015. **74**(1): p. 234-241.

154. Harre, U., D. Georgess, H. Bang, A. Bozec, R. Axmann, E. Ossipova, P.-J. Jakobsson, W. Baum, F. Nimmerjahn, and E. Szarka, *Induction of osteoclastogenesis and bone loss by human autoantibodies against citrullinated vimentin.* The Journal of clinical investigation, 2012. **122**(5): p. 1791-1802.

155. McInnes, I.B. and G. Schett, *The pathogenesis of rheumatoid arthritis.* New England Journal of Medicine, 2011. **365**(23): p. 2205-2219.

156. McInnes, I.B. and G. Schett, *Cytokines in the pathogenesis of rheumatoid arthritis.* Nature Reviews Immunology, 2007. **7**(6): p. 429-442.

157. Brentano, F., D. Kyburz, O. Schorr, R. Gay, and S. Gay, *The role of Toll-like receptor signalling in the pathogenesis of arthritis.* Cellular immunology, 2005. **233**(2): p. 90-96.

158. Seibl, R., T. Birchler, S. Loeliger, J.P. Hossle, R.E. Gay, T. Saurenmann, B.A. Michel, R.A. Seger, S. Gay, and R.P. Lauener, *Expression and regulation of Toll-like receptor 2 in rheumatoid arthritis synovium.* The American journal of pathology, 2003. **162**(4): p. 1221-1227.

159. Feldmann, M. and S.R.N. Maini, *Role of cytokines in rheumatoid arthritis: an education in pathophysiology and therapeutics.* Immunological reviews, 2008. **223**(1): p. 7-19.

160. Pettit, A.R., H. Ji, D. von Stechow, R. Müller, S.R. Goldring, Y. Choi, C. Benoist, and E.M. Gravallese, *TRANCE/RANKL knockout mice are protected from bone erosion in a serum transfer model of arthritis.* The American journal of pathology, 2001. **159**(5): p. 1689-1699.

161. Redlich, K., S. Hayer, R. Ricci, J.-P. David, M. Tohidast-Akrad, G. Kollias, G. Steiner, J.S. Smolen, E.F. Wagner, and G. Schett, *Osteoclasts are essential for TNF-α–mediated joint destruction.* The Journal of clinical investigation, 2002. **110**(10): p. 1419-1427.

162. Martel-Pelletier, J., D.J. Welsch, and J.-P. Pelletier, *Metalloproteases and inhibitors in arthritic diseases.* Best practice & research Clinical rheumatology, 2001. **15**(5): p. 805-829.

163. Trentham, D.E., A.S. Townes, and A.H. Kang, *Autoimmunity to type II collagen an experimental model of arthritis.* The Journal of experimental medicine, 1977. **146**(3): p. 857-868.

164. Courtenay, J.S., M.J. Dallman, A.D. Dayan, A. Martin, and B. Mosedale, *Immunisation against heterologous type II collagen induces arthritis in mice.* Nature, 1980. **283**(5748): p. 666-8.

165. Holmdahl, R., L. Jansson, A. Larsson, and R. Jonsson, *Arthritis in DBA/1 mice induced with passively transferred type II collagen immune serum. Immunohistopathology and serum levels of anti-type II collagen auto-antibodies.* Scand J Immunol, 1990. **31**(2): p. 147-57.

166. Mauri, C., R.O. Williams, M. Walmsley, and M. Feldmann, *Relationship between Th1/Th2 cytokine patterns and the arthritogenic response in collagen-induced arthritis.* European journal of immunology, 1996. **26**(7): p. 1511-1518.

167. Holmdahl, R., K. Rubin, L. Klareskog, E. Larsson, and H. Wigzell, *Characterization of the antibody response in mice with type II collagen–induced arthritis, using monoclonal anti–type II collagen antibodies.* Arthritis & Rheumatism: Official Journal of the American College of Rheumatology, 1986. **29**(3): p. 400-410.

168. Stuart, J.M. and F.J. Dixon, *Serum transfer of collagen-induced arthritis in mice.* J Exp Med, 1983. **158**(2): p. 378-92.

169. Nandakumar, K.S. and R. Holmdahl, *Efficient promotion of collagen antibody induced arthritis (CAIA) using four monoclonal antibodies specific for the major epitopes recognized in both collagen induced arthritis and rheumatoid arthritis.* Journal of immunological methods, 2005. **304**(1-2): p. 126-136.

170. Kouskoff, V., A.S. Korganow, V. Duchatelle, C. Degott, C. Benoist, and D. Mathis, *Organ-specific disease provoked by systemic autoimmunity.* Cell, 1996. **87**(5): p. 811-22.

171. Christensen, A.D., C. Haase, A.D. Cook, and J.A. Hamilton, *K/BxN Serum-Transfer Arthritis as a Model for Human Inflammatory Arthritis.* Frontiers in immunology, 2016. **7**: p. 213-213.

172. Wipke, B.T., Z. Wang, W. Nagengast, D.E. Reichert, and P.M. Allen, *Staging the initiation of autoantibody-induced arthritis: a critical role for immune complexes.* J Immunol, 2004. **172**(12): p. 7694-702.

173. Corr, M. and B. Crain, *The role of FcgammaR signaling in the K/B x N serum transfer model of arthritis.* J Immunol, 2002. **169**(11): p. 6604-9.

174. Klein, C.J., V.A. Lennon, P.A. Aston, A. McKeon, and S.J. Pittock, *Chronic pain as a manifestation of potassium channel-complex autoimmunity.* Neurology, 2012. **79**(11): p. 1136.

175. Klein, C.J., V.A. Lennon, P.A. Aston, A. McKeon, and S.J. Pittock, *Chronic pain as a manifestation of potassium channel-complex autoimmunity.* Neurology, 2012. **79**(11): p. 1136-44.

176. Dawes, J.M., G.A. Weir, S.J. Middleton, R. Patel, K.I. Chisholm, P. Pettingill, L.J. Peck, J. Sheridan, A. Shakir, L. Jacobson, M. Gutierrez-Mecinas, J. Galino, J. Walcher, J. Kühnemund, H. Kuehn, M.D. Sanna, B. Lang, A.J. Clark, A.C. Themistocleous, N. Iwagaki, S.J. West, K. Werynska, L. Carroll, T. Trendafilova, D.A. Menassa, M.P. Giannoccaro, E. Coutinho, I. Cervellini, D. Tewari, C. Buckley, M.I. Leite, H. Wildner, H.U. Zeilhofer, E. Peles, A.J. Todd, S.B. McMahon, A.H. Dickenson, G.R. Lewin, A. Vincent, and D.L. Bennett, *Immune or Genetic-Mediated Disruption of CASPR2 Causes Pain Hypersensitivity Due to Enhanced Primary Afferent Excitability.* Neuron, 2018. **97**(4): p. 806-822.e10.

177. de Hair, M.J., M.G. van de Sande, T.H. Ramwadhdoebe, M. Hansson, R. Landewé, C. van der Leij, M. Maas, G. Serre, D. van Schaardenburg, L. Klareskog, D.M. Gerlag, L.G. van Baarsen, and P.P. Tak, *Features of the synovium of individuals at risk of developing rheumatoid arthritis: implications for understanding preclinical rheumatoid arthritis.* Arthritis Rheumatol, 2014. **66**(3): p. 513-22.

178. Rantapää-Dahlqvist, S., B.A. de Jong, E. Berglin, G. Hallmans, G. Wadell, H. Stenlund, U. Sundin, and W.J. van Venrooij, *Antibodies against cyclic citrullinated peptide and IgA rheumatoid factor predict the development of rheumatoid arthritis.* Arthritis Rheum, 2003. **48**(10): p. 2741-9.

179. Honda, K., H. Yanai, H. Negishi, M. Asagiri, M. Sato, T. Mizutani, N. Shimada, Y. Ohba, A. Takaoka, N. Yoshida, and T. Taniguchi, *IRF-7 is the master regulator of type-I interferon-dependent immune responses.* Nature, 2005. **434**(7034): p. 772-7.

180. Dixon, W.J., *Efficient Analysis of Experimental Observations.* Annual Review of Pharmacology and Toxicology, 1980. **20**(1): p. 441-462.

181. Chaplan, S.R., F.W. Bach, J.W. Pogrel, J.M. Chung, and T.L. Yaksh, *Quantitative assessment of tactile allodynia in the rat paw.* J Neurosci Methods, 1994. **53**(1): p. 55-63.

182. Terato, K., D.S. Harper, M.M. Griffiths, D.L. Hasty, X.J. Ye, M.A. Cremer, and J.M. Seyer, *Collagen-induced arthritis in mice: synergistic effect of E. coli lipopolysaccharide bypasses epitope specificity in the induction of arthritis with monoclonal antibodies to type II collagen.* Autoimmunity, 1995. **22**(3): p. 137-47.

183. Bersellini Farinotti, A., G. Wigerblad, D. Nascimento, D.B. Bas, C. Morado Urbina, K.S. Nandakumar, K. Sandor, B. Xu, S. Abdelmoaty, M.A. Hunt, K. Ängeby Möller, A. Baharpoor, J. Sinclair, K. Jardemark, J.T. Lanner, I. Khmaladze, L.E. Borm, L. Zhang, F. Wermeling, M.S. Cragg, J. Lengqvist, A.J. Chabot-Doré, L. Diatchenko, I. Belfer, M. Collin, K. Kultima, B. Heyman, J.M. Jimenez-Andrade, S. Codeluppi, R. Holmdahl, and C.I. Svensson, *Cartilage-binding antibodies induce pain through immune complex-mediated activation of neurons.* J Exp Med, 2019. **216**(8): p. 1904-1924.

184. Hutchinson, M.R., A.L. Northcutt, T. Hiranita, X. Wang, S.S. Lewis, J. Thomas, K. van Steeg, T.A. Kopajtic, L.C. Loram, C. Sfregola, E. Galer, N.E. Miles, S.T. Bland, J. Amat, R.R. Rozeske, T. Maslanik, T.R. Chapman, K.A. Strand, M. Fleshner, R.K. Bachtell, A.A. Somogyi, H. Yin, J.L. Katz, K.C. Rice, S.F. Maier, and L.R. Watkins, *Opioid activation of toll-like receptor 4 contributes to drug reinforcement.* The Journal of neuroscience : the official journal of the Society for Neuroscience, 2012. **32**(33): p. 11187-11200.

185. Al-Ofi, E.A. and B.S. Al-Ghamdi, *High-Mobility Group Box 1 (HMGB1), an Endogenous Ligand of Toll-Like Receptors 2 and 4, Induces Astroglial Inflammation via NF-κβ Pathway.* Folia Morphol (Warsz), 2018.

186. Sorge, R.E., M.L. LaCroix-Fralish, A.H. Tuttle, S.G. Sotocinal, J.-S. Austin, J. Ritchie, M.L. Chanda, A.C. Graham, L. Topham, S. Beggs, M.W. Salter, and J.S. Mogil, *Spinal cord Toll-like receptor 4 mediates inflammatory and neuropathic hypersensitivity in male but not female mice.* The Journal of neuroscience : the official journal of the Society for Neuroscience, 2011. **31**(43): p. 15450-15454.

187. Abram, S.E., J. Yi, A. Fuchs, and Q.H. Hogan, *Permeability of injured and intact peripheral nerves and dorsal root ganglia.* Anesthesiology, 2006. **105**(1): p. 146-53.

188. Jimenez-Andrade, J.M., M.B. Herrera, J.R. Ghilardi, M. Vardanyan, O.K. Melemedjian, and P.W. Mantyh, *Vascularization of the dorsal root ganglia and peripheral nerve of the mouse: implications for chemical-induced peripheral sensory neuropathies.* Mol Pain, 2008. **4**: p. 10.

189. Xie, W., J.A. Strong, and J.M. Zhang, *Increased excitability and spontaneous activity of rat sensory neurons following in vitro stimulation of sympathetic fiber sprouts in the isolated dorsal root ganglion.* Pain, 2010. **151**(2): p. 447-59.

190. Hanani, M. and D.C. Spray, *Emerging importance of satellite glia in nervous system function and dysfunction.* Nature Reviews Neuroscience, 2020. **21**(9): p. 485-498.

191. Ruscheweyh, R., L. Forsthuber, D. Schoffnegger, and J. Sandkühler, *Modification of classical neurochemical markers in identified primary afferent neurons with Abeta-, Adelta-, and C-fibers after chronic constriction injury in mice.* J Comp Neurol, 2007. **502**(2): p. 325-36.

192. Yu, X., H. Liu, K.A. Hamel, M.G. Morvan, S. Yu, J. Leff, Z. Guan, J.M. Braz, and A.I. Basbaum, *Dorsal root ganglion macrophages contribute to both the initiation and persistence of neuropathic pain.* Nature Communications, 2020. **11**(1): p. 264.

193. Woller, S.A., S.H. Choi, E.J. An, H. Low, D.A. Schneider, R. Ramachandran, J. Kim, Y.S. Bae, D. Sviridov, M. Corr, T.L. Yaksh, and Y.I. Miller, *Inhibition of Neuroinflammation by AIBP: Spinal Effects upon Facilitated Pain States.* Cell Rep, 2018. **23**(9): p. 2667-2677.

194. Hylden, J.L. and G.L. Wilcox, *Intrathecal morphine in mice: a new technique.* Eur J Pharmacol, 1980. **67**(2-3): p. 313-6.

195. Yu, T., J. Zhu, Y. Li, Y. Ma, J. Wang, X. Cheng, S. Jin, Q. Sun, X. Li, H. Gong, Q. Luo, F. Xu, S. Zhao, and D. Zhu, *RTF: a rapid and versatile tissue optical clearing method.* Sci Rep, 2018. **8**(1): p. 1964.

196. Çiçek, Ö., A. Abdulkadir, S. Lienkamp, T. Brox, and O. Ronneberger. *3D U-Net: Learning Dense Volumetric Segmentation from Sparse Annotation*. in *MICCAI*. 2016.

197. Ronneberger, O., P. Fischer, and T. Brox. *U-Net: Convolutional Networks for Biomedical Image Segmentation*. in *MICCAI*. 2015.

198. Haase, R., L.A. Royer, P. Steinbach, D. Schmidt, A. Dibrov, U. Schmidt, M. Weigert, N. Maghelli, P. Tomancak, F. Jug, and E.W. Myers, *CLIJ: GPU-accelerated image processing for everyone.* Nature Methods, 2020. **17**(1): p. 5-6.

199. Hu, P. and E.M. McLachlan, *Distinct functional types of macrophage in dorsal root ganglia and spinal nerves proximal to sciatic and spinal nerve transections in the rat.* Experimental Neurology, 2003. **184**(2): p. 590-605.

200. Simeoli, R., K. Montague, H.R. Jones, L. Castaldi, D. Chambers, J.H. Kelleher, V. Vacca, T. Pitcher, J. Grist, H. Al-Ahdal, L.-F. Wong, M. Perretti, J. Lai, P. Mouritzen, P. Heppenstall, and M. Malcangio, *Exosomal cargo including microRNA regulates sensory neuron to macrophage communication after nerve trauma.* Nature communications, 2017. **8**(1): p. 1778-1778.

201. Zhang, H., Y. Li, M. de Carvalho-Barbosa, A. Kavelaars, C.J. Heijnen, P.J. Albrecht, and P.M. Dougherty, *Dorsal Root Ganglion Infiltration by Macrophages Contributes to Paclitaxel Chemotherapy-Induced Peripheral Neuropathy.* J Pain, 2016. **17**(7): p. 775-86.

202. Peters, C.M., J.M. Jimenez-Andrade, B.M. Jonas, M.A. Sevcik, N.J. Koewler, J.R. Ghilardi, G.Y. Wong, and P.W. Mantyh, *Intravenous paclitaxel administration in the rat induces a peripheral sensory neuropathy characterized by macrophage infiltration and injury to sensory neurons and their supporting cells.* Experimental neurology, 2007. **203**(1): p. 42-54.

203. Boyette-Davis, J. and P.M. Dougherty, *Protection against oxaliplatin-induced mechanical hyperalgesia and intraepidermal nerve fiber loss by minocycline.* Exp Neurol, 2011. **229**(2): p. 353-7.

204. Institute of Medicine Committee on Advancing Pain Research, C. and Education, *The National Academies Collection: Reports funded by National Institutes of Health*, in *Relieving Pain in America: A Blueprint for Transforming Prevention, Care, Education, and Research*. 2011, National Academies Press (US)
Copyright © 2011, National Academy of Sciences.: Washington (DC).

205. Vos, T., A.D. Flaxman, M. Naghavi, R. Lozano, C. Michaud, M. Ezzati, K. Shibuya, J.A. Salomon, S. Abdalla, V. Aboyans, J. Abraham, I. Ackerman, R. Aggarwal, S.Y. Ahn, M.K. Ali, M. Alvarado, H.R. Anderson, L.M. Anderson, K.G. Andrews, C. Atkinson, L.M. Baddour, A.N. Bahalim, S. Barker-Collo, L.H. Barrero, D.H. Bartels, M.-G. Basáñez, A. Baxter, M.L. Bell, E.J. Benjamin, D. Bennett, E. Bernabé, K. Bhalla, B. Bhandari, B. Bikbov, A. Bin Abdulhak, G. Birbeck, J.A. Black, H. Blencowe, J.D. Blore, F. Blyth, I. Bolliger, A. Bonaventure, S. Boufous, R. Bourne, M. Boussinesq, T. Braithwaite, C. Brayne, L. Bridgett, S. Brooker, P. Brooks, T.S. Brugha, C. Bryan-Hancock, C. Bucello, R. Buchbinder, G. Buckle, C.M. Budke, M. Burch, P. Burney, R. Burstein, B. Calabria, B. Campbell, C.E. Canter, H. Carabin, J. Carapetis, L. Carmona, C. Cella, F. Charlson, H. Chen, A.T.-A. Cheng, D. Chou, S.S. Chugh, L.E. Coffeng, S.D. Colan, S. Colquhoun, K.E. Colson, J. Condon, M.D. Connor, L.T. Cooper, M. Corriere, M. Cortinovis, K.C. de Vaccaro, W. Couser, B.C. Cowie, M.H. Criqui, M. Cross, K.C. Dabhadkar, M. Dahiya, N. Dahodwala, J. Damsere-Derry, G. Danaei, A. Davis, D. De Leo, L. Degenhardt, R.

Dellavalle, A. Delossantos, J. Denenberg, S. Derrett, D.C. Des Jarlais, S.D. Dharmaratne, M. Dherani, C. Diaz-Torne, H. Dolk, E.R. Dorsey, T. Driscoll, H. Duber, B. Ebel, K. Edmond, A. Elbaz, S.E. Ali, H. Erskine, P.J. Erwin, P. Espindola, S.E. Ewoigbokhan, F. Farzadfar, V. Feigin, D.T. Felson, A. Ferrari, C.P. Ferri, E.M. Fèvre, M.M. Finucane, S. Flaxman, L. Flood, K. Foreman, M.H. Forouzanfar, F.G.R. Fowkes, R. Franklin, M. Fransen, M.K. Freeman, B.J. Gabbe, S.E. Gabriel, E. Gakidou, H.A. Ganatra, B. Garcia, F. Gaspari, R.F. Gillum, G. Gmel, R. Gosselin, R. Grainger, J. Groeger, F. Guillemin, D. Gunnell, R. Gupta, J. Haagsma, H. Hagan, Y.A. Halasa, W. Hall, D. Haring, J.M. Haro, J.E. Harrison, R. Havmoeller, R.J. Hay, H. Higashi, C. Hill, B. Hoen, H. Hoffman, P.J. Hotez, D. Hoy, J.J. Huang, S.E. Ibeanusi, K.H. Jacobsen, S.L. James, D. Jarvis, R. Jasrasaria, S. Jayaraman, N. Johns, J.B. Jonas, G. Karthikeyan, N. Kassebaum, N. Kawakami, A. Keren, J.-P. Khoo, C.H. King, L.M. Knowlton, O. Kobusingye, A. Koranteng, R. Krishnamurthi, R. Lalloo, L.L. Laslett, T. Lathlean, J.L. Leasher, Y.Y. Lee, J. Leigh, S.S. Lim, E. Limb, J.K. Lin, M. Lipnick, S.E. Lipshultz, W. Liu, M. Loane, S.L. Ohno, R. Lyons, J. Ma, J. Mabweijano, M.F. MacIntyre, R. Malekzadeh, L. Mallinger, S. Manivannan, W. Marcenes, L. March, D.J. Margolis, G.B. Marks, R. Marks, A. Matsumori, R. Matzopoulos, B.M. Mayosi, J.H. McAnulty, M.M. McDermott, N. McGill, J. McGrath, M.E. Medina-Mora, M. Meltzer, G.A. Mensah, T.R. Merriman, A.-C. Meyer, V. Miglioli, M. Miller, T.R. Miller, P.B. Mitchell, A.O. Mocumbi, T.E. Moffitt, A.A. Mokdad, L. Monasta, M. Montico, M. Moradi-Lakeh, A. Moran, L. Morawska, R. Mori, M.E. Murdoch, M.K. Mwaniki, K. Naidoo, M.N. Nair, L. Naldi, K.M.V. Narayan, P.K. Nelson, R.G. Nelson, M.C. Nevitt, C.R. Newton, S. Nolte, P. Norman, R. Norman, M. O'Donnell, S. O'Hanlon, C. Olives, S.B. Omer, K. Ortblad, R. Osborne, D. Ozgediz, A. Page, B. Pahari, J.D. Pandian, A.P. Rivero, S.B. Patten, N. Pearce, R.P. Padilla, F. Perez-Ruiz, N. Perico, K. Pesudovs, D. Phillips, M.R. Phillips, K. Pierce, S. Pion, G.V. Polanczyk, S. Polinder, C.A. Pope, 3rd, S. Popova, E. Porrini, F. Pourmalek, M. Prince, R.L. Pullan, K.D. Ramaiah, D. Ranganathan, H. Razavi, M. Regan, J.T. Rehm, D.B. Rein, G. Remuzzi, K. Richardson, F.P. Rivara, T. Roberts, C. Robinson, F.R. De Leòn, L. Ronfani, R. Room, L.C. Rosenfeld, L. Rushton, R.L. Sacco, S. Saha, U. Sampson, L. Sanchez-Riera, E. Sanman, D.C. Schwebel, J.G. Scott, M. Segui-Gomez, S. Shahraz, D.S. Shepard, H. Shin, R. Shivakoti, D. Singh, G.M. Singh, J.A. Singh, J. Singleton, D.A. Sleet, K. Sliwa, E. Smith, J.L. Smith, N.J.C. Stapelberg, A. Steer, T. Steiner, W.A. Stolk, L.J. Stovner, C. Sudfeld, S. Syed, G. Tamburlini, M. Tavakkoli, H.R. Taylor, J.A. Taylor, W.J. Taylor, B. Thomas, W.M. Thomson, G.D. Thurston, I.M. Tleyjeh, M. Tonelli, J.A. Towbin, T. Truelsen, M.K. Tsilimbaris, C. Ubeda, E.A. Undurraga, M.J. van der Werf, J. van Os, M.S. Vavilala, N. Venketasubramanian, M. Wang, W. Wang, K. Watt, D.J. Weatherall, M.A. Weinstock, R. Weintraub, M.G. Weisskopf, M.M. Weissman, R.A. White, H. Whiteford, S.T. Wiersma, J.D. Wilkinson, H.C. Williams, S.R.M. Williams, E. Witt, F. Wolfe, A.D. Woolf, S. Wulf, P.-H. Yeh, A.K.M. Zaidi, Z.-J. Zheng, D. Zonies, A.D. Lopez, C.J.L. Murray, M.A. AlMazroa and Z.A. Memish, *Years lived with disability (YLDs) for 1160 sequelae of 289 diseases and injuries 1990-2010: a systematic analysis for the Global Burden of Disease Study 2010.* Lancet (London, England), 2012. **380**(9859): p. 2163-2196.

206. Bier, A., *Versuche über Cocainisirung des Rückenmarkes.* Langenbeck's Archives of Surgery, 1899. **51**(3): p. 361-369.

207. Yaksh, T.L. and T.A. Rudy, *Analgesia mediated by a direct spinal action of narcotics.* Science, 1976. **192**(4246): p. 1357-1358.

208. Jones, R.D. and J.G. Jones, *Intrathecal morphine: naloxone reverses respiratory depression but not analgesia.* Br Med J, 1980. **281**(6241): p. 645-6.

209. Cousins, M.J., L.E. Mather, C.J. Glynn, P.R. Wilson, and J.R. Graham, *Selective spinal analgesia.* Lancet, 1979. **1**(8126): p. 1141-2.

210. DeBalli, P. and T.W. Breen, *Intrathecal opioids for combined spinal-epidural analgesia during labour.* CNS Drugs, 2003. **17**(12): p. 889-904.

211. TUOHY, E.B., *THE USE OF CONTINUOUS SPINAL ANESTHESIA: UTILIZING THE URETERAL CATHETER TECHNIC.* Journal of the American Medical Association, 1945. **128**(4): p. 262-264.

212. Onofrio, B.M., T.L. Yaksh, and P.G. Arnold, *Continuous low-dose intrathecal morphine administration in the treatment of chronic pain of malignant origin.* Mayo Clin Proc, 1981. **56**(8): p. 516-20.

213. Brill, S., G.M. Gurman, and A. Fisher, *A history of neuraxial administration of local analgesics and opioids.* Eur J Anaesthesiol, 2003. **20**(9): p. 682-9.

214. Albright, A.L., A. Cervi, and J. Singletary, *Intrathecal baclofen for spasticity in cerebral palsy.* Jama, 1991. **265**(11): p. 1418-22.

215. Creamer, M., G. Cloud, P. Kossmehl, M. Yochelson, G.E. Francisco, A.B. Ward, J. Wissel, M. Zampolini, A. Abouihia, A. Calabrese, and L. Saltuari, *Effect of Intrathecal Baclofen on Pain and Quality of Life in Poststroke Spasticity.* Stroke, 2018. **49**(9): p. 2129-2137.

216. Albright, A.L., R. Gilmartin, D. Swift, L.E. Krach, C.B. Ivanhoe, and J.F. McLaughlin, *Long-term intrathecal baclofen therapy for severe spasticity of cerebral origin.* J Neurosurg, 2003. **98**(2): p. 291-5.

217. Sammaraiee, Y., M. Yardley, L. Keenan, K. Buchanan, V. Stevenson, and R. Farrell, *Intrathecal baclofen for multiple sclerosis related spasticity: A twenty year experience.* Multiple Sclerosis and Related Disorders, 2019. **27**: p. 95-100.

218. Brightman, M.W., *Morphology of blood-brain interfaces.* Exp Eye Res, 1977. **25 Suppl**: p. 1-25.

219. Daneman, R. and A. Prat, *The blood-brain barrier.* Cold Spring Harb Perspect Biol, 2015. **7**(1): p. a020412.

220. Abbott, N.J., L. Rönnbäck, and E. Hansson, *Astrocyte-endothelial interactions at the blood-brain barrier.* Nat Rev Neurosci, 2006. **7**(1): p. 41-53.

221. Yaksh, T.L., K.A. Horais, N.A. Tozier, J.W. Allen, M. Rathbun, S.S. Rossi, C. Sommer, C. Meschter, P.J. Richter, and K.R. Hildebrand, *Chronically infused intrathecal morphine in dogs.* Anesthesiology, 2003. **99**(1): p. 174-87.

222. Yaksh, T.L., C.J. Fisher, T.M. Hockman, and A.J. Wiese, *Current and Future Issues in the Development of Spinal Agents for the Management of Pain.* Curr Neuropharmacol, 2017. **15**(2): p. 232-259.

223. Wall, P.D. and P. Shortland, *Long-range afferents in the rat spinal cord. 1. Numbers, distances and conduction velocities.* Philos Trans R Soc Lond B Biol Sci, 1991. **334**(1269): p. 85-93.

224. Yaksh, T.L., J.W. Allen, S.L. Veesart, K.A. Horais, S.A. Malkmus, M. Scadeng, J.J. Steinauer, and S.S. Rossi, *Role of meningeal mast cells in intrathecal morphine-evoked granuloma formation.* Anesthesiology, 2013. **118**(3): p. 664-78.

225. Drasner, K., *Local anesthetic systemic toxicity: a historical perspective.* Reg Anesth Pain Med, 2010. **35**(2): p. 162-6.

226. North, R.B., P.N. Cutchis, J.A. Epstein, and D.M. Long, *Spinal cord compression complicating subarachnoid infusion of morphine: case report and laboratory experience.* Neurosurgery, 1991. **29**(5): p. 778-84.

227. Yaksh, T.L., S. Hassenbusch, K. Burchiel, K.R. Hildebrand, L.M. Page, and R.J. Coffey, *Inflammatory masses associated with intrathecal drug infusion: a review of preclinical evidence and human data.* Pain Med, 2002. **3**(4): p. 300-12.

228. D'Angelo, R., M.L. Foss, and C.H. Livesay, *A comparison of multiport and uniport epidural catheters in laboring patients.* Anesth Analg, 1997. **84**(6): p. 1276-9.

229. Sabbe, M.B., M.R. Grafe, E. Mjanger, P.J. Tiseo, H.F. Hill, and T.L. Yaksh, *Spinal delivery of sufentanil, alfentanil, and morphine in dogs. Physiologic and toxicologic investigations.* Anesthesiology, 1994. **81**(4): p. 899-920.

230. Hildebrand, K.R., L.M. Page, T.M. Billstrom, J.J. Steinauer, K.A. Eddinger, S. Arjomand, and T.L. Yaksh, *Characterization of Effect of Repeated Bolus or Continuous Intrathecal Infusion of Morphine on Spinal Mass Formation in the Dog.* Neuromodulation: Technology at the Neural Interface, 2019. **22**(7): p. 790-798.

231. Pasqualin, C., F. Gannier, P. Bredeloux, and V. Maupoil, *HF_IDS_Cam: Fast Video Capture with ImageJ for Real-Time Analysis.* Journal of Imaging, 2018. **44**(2).

232. Malkmus, S.A. and T.L. Yaksh, *Intrathecal catheterization and drug delivery in the rat.* Methods Mol Med, 2004. **99**: p. 109-21.

233. Dirig, D.M., A. Salami, M.L. Rathbun, G.T. Ozaki, and T.L. Yaksh, *Characterization of variables defining hindpaw withdrawal latency evoked by radiant thermal stimuli.* J Neurosci Methods, 1997. **76**(2): p. 183-91.

234. Hargreaves, K., R. Dubner, F. Brown, C. Flores, and J. Joris, *A new and sensitive method for measuring thermal nociception in cutaneous hyperalgesia.* Pain, 1988. **32**(1): p. 77-88.

235. Berg, S., D. Kutra, T. Kroeger, C.N. Straehle, B.X. Kausler, C. Haubold, M. Schiegg, J. Ales, T. Beier, M. Rudy, K. Eren, J.I. Cervantes, B. Xu, F. Beuttenmueller, A. Wolny, C. Zhang, U. Koethe, F.A. Hamprecht, and A. Kreshuk, *ilastik: interactive machine learning for (bio)image analysis.* Nature Methods, 2019. **16**(12): p. 1226-1232.

236. Ronneberger, O., P. Fischer, and T. Brox. *U-net: Convolutional networks for biomedical image segmentation*. in *International Conference on Medical image computing and computer-assisted intervention*. 2015. Springer.

237. Pattali, R., Y. Mou, and X.-J. Li, *AAV9 Vector: a Novel modality in gene therapy for spinal muscular atrophy.* Gene Therapy, 2019. **26**(7): p. 287-295.

238. Meng, Z., Q. Zhang, K. Hong, W. Han, Z. Zhao, Y. Liu, J. He, and H. Bu, *Clinical outcome and prognostic analysis of meningeal carcinomatosis treated by intrathecal chemotherapy.* Expert Rev Pharmacoecon Outcomes Res, 2018. **18**(4): p. 455-460.

239. Enzmann, D.R. and N.J. Pelc, *Cerebrospinal fluid flow measured by phase-contrast cine MR.* AJNR Am J Neuroradiol, 1993. **14**(6): p. 1301-7; discussion 1309-10.

240. Yaksh, T.L., J.W. Allen, S.L. Veesart, K.A. Horais, S.A. Malkmus, M. Scadeng, J.J. Steinauer, and S.S. Rossi, *Role of meningeal mast cells in intrathecal morphine-evoked granuloma formation.* Anesthesiology, 2013. **118**(3): p. 664-678.

241. Ummenhofer, W.C., R.H. Arends, D.D. Shen, and C.M. Bernards, *Comparative spinal distribution and clearance kinetics of intrathecally administered morphine, fentanyl, alfentanil, and sufentanil.* Anesthesiology, 2000. **92**(3): p. 739-53.

242. Bernards, C.M., *Cerebrospinal fluid and spinal cord distribution of baclofen and bupivacaine during slow intrathecal infusion in pigs.* Anesthesiology, 2006. **105**(1): p. 169-78.

243. Evers, M.M., L.J. Toonen, and W.M. van Roon-Mom, *Antisense oligonucleotides in therapy for neurodegenerative disorders.* Adv Drug Deliv Rev, 2015. **87**: p. 90-103.

244. Evers, M.M., L.J.A. Toonen, and W.M.C. van Roon-Mom, *Antisense oligonucleotides in therapy for neurodegenerative disorders.* Advanced Drug Delivery Reviews, 2015. **87**: p. 90-103.

245. Sorenson, J.L.S.L.C., UT, US), Haight, Levoy Golden (West Jordan, UT, US), *Apparatus and method for specific interstitial or subcutaneous diffusion and dispersion of medication*. 2007, Sorenson Development, Inc. (Salt Lake City, UT, US): United States.